Lecture notes on

Atoms & Clusters

(Theory Part)

D. Bauer

January 20, 2012

Prof. Dr. Dieter Bauer
AG Quantentheorie und
Vielteilchensysteme
Institut für Physik
Universität Rostock
18051 Rostock
Germany

dieter.bauer@uni-rostock.de
www.physik.uni-rostock.de/qtmps

Contents

1 Matter in an electromagnetic field **1**
1.1 Electromagnetic field . . . 1
1.2 Coupling to a charged particle . . . 3
1.3 One-electron atoms in an electromagnetic field . . . 4
1.3.1 Single-photon absorption and emission . . . 5
1.3.2 Absorption . . . 6
1.3.3 Stimulated emission . . . 8
1.3.4 Spontaneous emission . . . 8
1.3.5 Dipole approximation . . . 10
1.3.6 Gauge transformations in dipole approximation . . . 10
1.3.7 Einstein coefficients . . . 12
1.3.8 Spontaneous emission from the 2p level . . . 13
1.3.9 Atomic lifetimes . . . 16
1.3.10 Selection rules . . . 16
1.3.11 Helicity of the photon . . . 19
1.3.12 Spectrum of one-electron atoms . . . 20
1.3.13 Oscillator strengths . . . 21
1.3.14 Spectral lines . . . 23
1.3.15 Photoelectric effect . . . 27
1.3.16 Scattering of radiation . . . 31
1.4 Mechanical effects of light . . . 37
1.4.1 Ponderomotive force . . . 38
1.4.2 *Relativistic dynamics in an electromagnetic wave . . . 45
1.4.3 *Relativistic ponderomotive force . . . 52
1.4.4 Optical Bloch equations . . . 56

2 Condensates, superfluids, and clusters **69**
2.1 Bose-Einstein condensation . . . 69
2.1.1 Reminder: Bose-Einstein statistics . . . 69
2.1.2 Phase transition . . . 71
2.1.3 BEC in ultra-cold atomic gases . . . 74
2.1.4 Macroscopic wave function . . . 77
2.2 Superfluids . . . 79

2.2.1 Quantum fluids 79
2.2.2 Macroscopic wavefunction reloaded 82
2.2.3 Properties of He II 83
2.2.4 Flow quantization 84
2.3 Clusters 86
2.3.1 Magic numbers 87
2.3.2 Theoretical approaches to the cluster many-body problem . . 97
2.3.3 Optical properties of clusters 110

3 Laser plasmas **117**
3.1 Plasma generation 117
3.1.1 *Landau tunneling rate 119
3.1.2 *Tunneling *vs* multiphoton ionization 125

A Atomic units **127**

Chapter 1

Matter in an electromagnetic field

1.1 Electromagnetic field

We introduce a scalar and a vector potential such that the electric field is given by

$$\boldsymbol{E}(\boldsymbol{r},t) = -\boldsymbol{\nabla}\phi(\boldsymbol{r},t) - \frac{\partial}{\partial t}\boldsymbol{A}(\boldsymbol{r},t) \tag{1.1}$$

and the magnetic field by

$$\boldsymbol{B}(\boldsymbol{r},t) = \boldsymbol{\nabla} \times \boldsymbol{A}(\boldsymbol{r},t). \tag{1.2}$$

Electric and magnetic field do not change under the *gauge transformation*

$$\boldsymbol{A}(\boldsymbol{r},t) \to \boldsymbol{A}(\boldsymbol{r},t) + \boldsymbol{\nabla}\chi(\boldsymbol{r},t), \tag{1.3}$$

$$\phi(\boldsymbol{r},t) \to \phi(\boldsymbol{r},t) - \frac{\partial}{\partial t}\chi(\boldsymbol{r},t). \tag{1.4}$$

The freedom of choosing χ may be employed to fulfill the *Coulomb gauge* condition

$$\boldsymbol{\nabla} \cdot \boldsymbol{A} = 0 \tag{1.5}$$

so that Maxwell's equations in vacuum (i.e., no charges and currents) boil down to the wave equation

$$\nabla^2 \boldsymbol{A} - \frac{1}{c^2}\frac{\partial^2 \boldsymbol{A}}{\partial t^2} = 0 \tag{1.6}$$

with c the speed of light in vacuum. Plane wave solutions of (1.6) read

$$\boldsymbol{A}(\boldsymbol{r},t) = \hat{A}\boldsymbol{\varepsilon}\cos(\boldsymbol{k}\cdot\boldsymbol{r} - \omega t + \delta_\omega), \tag{1.7}$$

and angular frequency ω and wave number $k = |\boldsymbol{k}|$ satisfy the simple dispersion relation

$$\omega = kc. \tag{1.8}$$

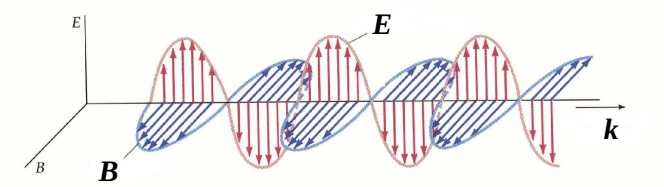

Figure 1.1: Electromagnetic wave.

The vector $\boldsymbol{\varepsilon}$ defines the polarization direction. In the Coulomb gauge (1.5)

$$\boldsymbol{k} \cdot \boldsymbol{\varepsilon} = 0 \tag{1.9}$$

follows. For $\phi = 0$ the fields read

$$\boldsymbol{E}(\boldsymbol{r}, t) = \hat{E}\boldsymbol{\varepsilon} \sin(\boldsymbol{k} \cdot \boldsymbol{r} - \omega t + \delta_\omega), \tag{1.10}$$

$$\boldsymbol{B}(\boldsymbol{r}, t) = \frac{\hat{E}}{\omega}(\boldsymbol{k} \times \boldsymbol{\varepsilon}) \sin(\boldsymbol{k} \cdot \boldsymbol{r} - \omega t + \delta_\omega), \tag{1.11}$$

where

$$\hat{E} = -\omega \hat{A}. \tag{1.12}$$

$\boldsymbol{E}$, $\boldsymbol{B}$, and $\boldsymbol{k}$ are mutually perpendicular (cf. Fig. 1.1). A general, elliptically polarized electromagnetic wave can be constructed as a superposition of two solutions with polarization vectors $\boldsymbol{\varepsilon}_\lambda$, $\lambda = 1, 2$.

The energy density of the electromagnetic field is given by

$$\frac{1}{2}\left(\varepsilon_0 |\boldsymbol{E}|^2 + \mu_0^{-1} |\boldsymbol{B}|^2\right) = \varepsilon_0 \hat{E}^2 \sin^2(\boldsymbol{k} \cdot \boldsymbol{r} - \omega t + \delta_\omega) \tag{1.13}$$

with $\varepsilon_0 \mu_0 = c^{-2}$. The time-averaged energy density is[1]

$$\rho = \frac{1}{2}\varepsilon_0 \hat{E}^2 = \frac{1}{2}\varepsilon_0 \omega^2 \hat{A}^2. \tag{1.14}$$

On the other hand, thinking in terms of photons yields an energy density

$$\rho = \frac{\hbar \omega N}{V} \tag{1.15}$$

with N the number of photons of energy $\hbar\omega$ and V is the quantization volume. The relation between classical electric field amplitude and number of photons thus reads

$$|\hat{E}| = \sqrt{\frac{2\rho}{\varepsilon_0}} = \sqrt{\frac{2\hbar\omega N}{\varepsilon_0 V}}. \tag{1.16}$$

[1]Note that the time-average of the $\sin^2$ in (1.13) is 1/2.

The intensity I is typically defined as the time-average Poynting vector $\langle \boldsymbol{S} \rangle_t$,

$$\boldsymbol{S} = \frac{1}{\mu_0}(\boldsymbol{E} \times \boldsymbol{B}), \tag{1.17}$$

leading to

$$I = \rho c = \frac{1}{2}\varepsilon_0 c \hat{E}^2 = \frac{\hbar \omega N c}{V}. \tag{1.18}$$

The intensity is the field energy transported per time perpendicularly through an unit area (i.e., parallel to the normal vector of the area).

If the phase δ_ω fluctuates randomly, as, e.g., in the case of radiation from a hot gas, the radiation is *incoherent*.

1.2 Coupling to a charged particle

Maxwell's equations do tell us how charges and currents generate electric and magnetic fields. The electromagnetic waves discussed in the previous Section are even supported without any charges and currents because we ignored the fact that they have been generated somewhere sufficiently far away. However, Maxwell's equations do not tell us how charges q move under the influence of electric and magnetic fields. At that point the Lorentz force comes into play:

$$\boldsymbol{F} = q(\boldsymbol{E} + \boldsymbol{v} \times \boldsymbol{B}). \tag{1.19}$$

In terms of potentials it reads

$$\boldsymbol{F} = q\left(-\boldsymbol{\nabla}\phi - \frac{\partial}{\partial t}\boldsymbol{A} + \boldsymbol{v} \times (\boldsymbol{\nabla} \times \boldsymbol{A})\right). \tag{1.20}$$

It can be easily shown ($\rightarrow$ exercise) that the Lagrangian

$$L = \frac{1}{2}mv^2 - q\phi + q\boldsymbol{v} \cdot \boldsymbol{A} \tag{1.21}$$

yields the equation of motion

$$m\ddot{\boldsymbol{r}} = \boldsymbol{F}. \tag{1.22}$$

The so-called *minimum coupling* Hamiltonian corresponding to the Lagrangian (1.21) reads

$$H = \frac{1}{2m}\left(\boldsymbol{p} - q\boldsymbol{A}\right)^2 + q\phi \tag{1.23}$$

where the canonical momentum $\boldsymbol{p}$ is

$$\boldsymbol{p} = m\boldsymbol{v} + q\boldsymbol{A}. \tag{1.24}$$

So far everything was classical. We assume that the classical Hamiltonian can be used as the corresponding Hamilton operator in a quantum mechanical treatment. As the latter must be Hermitian we assume

$$H = \frac{p^2}{2m} - \frac{q}{2m}(\boldsymbol{A}\cdot\boldsymbol{p} + \boldsymbol{p}\cdot\boldsymbol{A}) + \frac{q^2}{2m}A^2 + q\phi \tag{1.25}$$

(we omit indicating operators explicitly). The time-dependent Schrödinger equation (TDSE)

$$\mathrm{i}\hbar\frac{\partial}{\partial t}\Psi(\boldsymbol{r},t) = H\Psi(\boldsymbol{r},t) \tag{1.26}$$

with H according (1.25) is invariant under the gauge transformation (1.3), (1.4) as long as we also transform the wave function in the proper way:

$$\boldsymbol{A} = \boldsymbol{A}' + \boldsymbol{\nabla}\chi, \tag{1.27}$$

$$\phi = \phi' - \frac{\partial}{\partial t}\chi, \tag{1.28}$$

$$\Psi = \mathrm{e}^{\mathrm{i}q\chi/\hbar}\Psi'. \tag{1.29}$$

We can use the gauge freedom to describe the radiation field entirely by the vector potential so that $\phi = 0$, and using the fact that in Coulomb gauge

$$\boldsymbol{\nabla}\cdot(\boldsymbol{A}\Psi) = \boldsymbol{A}\cdot(\boldsymbol{\nabla}\Psi) + (\boldsymbol{\nabla}\cdot\boldsymbol{A})\Psi = \boldsymbol{A}\cdot(\boldsymbol{\nabla}\Psi) \tag{1.30}$$

the TDSE for a free charge in an electromagnetic field reads

$$\mathrm{i}\hbar\frac{\partial}{\partial t}\Psi = \left(-\frac{\hbar^2}{2m}\nabla^2 + \mathrm{i}\hbar\frac{q}{m}\boldsymbol{A}\cdot\boldsymbol{\nabla} + \frac{q^2}{2m}A^2\right)\Psi. \tag{1.31}$$

1.3 One-electron atoms in an electromagnetic field

In order to describe one-electron atoms we have to allow at least for one additional positive charge besides the electron (proton, deuteron, positron ...). Assuming that the positive charge has a much bigger mass than the electron $M \gg m$, as, e.g., in H, He^+ ... we can disregard the difference between reduced mass and electron mass as well as recoil effects. Hence, the interaction with the nucleus is simply described by an external Coulomb potential

$$V_{\mathrm{C}}(r) = -\frac{Ze^2}{4\pi\varepsilon_0 r} \tag{1.32}$$

with e the absolute value of the electron charge ($q = -e$) and Ze the nuclear charge. This external potential is added to the Coulomb-gauge Hamiltonian:

$$H = -\frac{\hbar^2}{2m}\nabla^2 - \mathrm{i}\hbar\frac{e}{m}\boldsymbol{A}\cdot\boldsymbol{\nabla} + \frac{e^2}{2m}A^2 + V_{\mathrm{C}}. \tag{1.33}$$

In the perturbative regime we partition the Hamiltonian in the form

$$H = H_0 + H_{\rm int}(t) \tag{1.34}$$

with H_0 describing the unperturbed atom,

$$H_0 = -\frac{\hbar^2}{2m}\nabla^2 + V_{\rm C} \tag{1.35}$$

and

$$H_{\rm int}(t) = -{\rm i}\hbar\frac{e}{m}\boldsymbol{A}\cdot\boldsymbol{\nabla} + \frac{e^2}{2m}A^2 \simeq -{\rm i}\hbar\frac{e}{m}\boldsymbol{A}\cdot\boldsymbol{\nabla} \tag{1.36}$$

where in the last step we made use of the fact that A^2 is of higher order.[2]

1.3.1 Single-photon absorption and emission

For weak electromagnetic fields we can apply time-dependent perturbation theory. The wave function is expanded in eigenstates ψ_j,

$$E_j\psi_j(\boldsymbol{r}) = H_0\psi_j(\boldsymbol{r}), \tag{1.37}$$

$$\Psi(\boldsymbol{r},t) = \sum_j c_j(t)\psi_j(\boldsymbol{r}){\rm e}^{-{\rm i}E_jt/\hbar}. \tag{1.38}$$

Inserting this into the TDSE one obtains a coupled set of equations for the coefficients $c_j(t)$. We are interested in transitions between two discrete bound states a, b. We obtain for the change in time of the amplitude $c_b(t)$

$$\dot{c}_b(t) = \frac{1}{{\rm i}\hbar}\sum_j \underbrace{\langle\psi_b|H_{\rm int}(t)\,|\psi_j\rangle}_{H_{\rm int}^{(bj)}(t)}\, c_j(t){\rm e}^{{\rm i}\omega_{bj}t} \tag{1.39}$$

with $\omega_{bj} = (E_b - E_j)/\hbar$. If the system is for $t \le 0$ is in the state $|\psi_a\rangle$, i.e.,

$$c_j(t \le 0) = \delta_{ja}, \tag{1.40}$$

we obtain in first order perturbation theory

$$c_b(t) = \frac{1}{{\rm i}\hbar}\int_0^t H_{\rm int}^{(ba)}(t'){\rm e}^{{\rm i}\omega_{ba}t'}\,{\rm d}t' = -\frac{e}{m}\int_0^t \langle\psi_b|\boldsymbol{A}(\boldsymbol{r},t')\cdot\boldsymbol{\nabla}\,|\psi_a\rangle\,{\rm e}^{{\rm i}\omega_{ba}t'}\,{\rm d}t'. \tag{1.41}$$

Inserting a vector potential of the form

$$\boldsymbol{A}(\boldsymbol{r},t) = \hat{A}\boldsymbol{\varepsilon}\cos(\boldsymbol{k}\cdot\boldsymbol{r} - \omega t + \delta_\omega) \tag{1.42}$$

[2] We will see later that in dipole approximation the term $\sim A^2$ is purely time-dependent and can be transformed away anyhow.

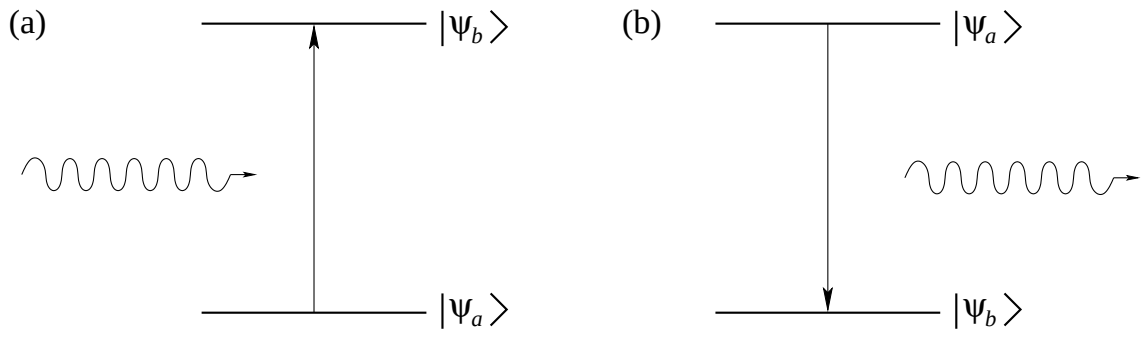

Figure 1.2: Absorption (a) and emission (b) of a photon, involving a transition to a higher (a) or lower (b) atomic level, ensuring energy conservation.

where $\hat{A}$ includes a slowly-varying pulse envelope we obtain

$$c_b(t) = -\frac{e}{2m}\hat{A}\left[\mathrm{e}^{\mathrm{i}\delta_\omega}\langle\psi_b|\mathrm{e}^{\mathrm{i}\boldsymbol{k}\cdot\boldsymbol{r}}\boldsymbol{\varepsilon}\cdot\boldsymbol{\nabla}\,|\psi_a\rangle\int_0^t \mathrm{d}t'\,\mathrm{e}^{\mathrm{i}(\omega_{ba}-\omega)t'}\right. \tag{1.43}$$
$$\left. + \mathrm{e}^{-\mathrm{i}\delta_\omega}\langle\psi_b|\mathrm{e}^{-\mathrm{i}\boldsymbol{k}\cdot\boldsymbol{r}}\boldsymbol{\varepsilon}\cdot\boldsymbol{\nabla}\,|\psi_a\rangle\int_0^t \mathrm{d}t'\,\mathrm{e}^{\mathrm{i}(\omega_{ba}+\omega)t'}\right].$$

As the pulse duration is much longer than $2\pi/\omega_{ba}$, the time integrals mainly contribute when $\omega_{ba} = \pm\omega$ for the first and the second term, respectively. Obviously the first term describes absorption of a photon, as

$$\omega_{ba} = \omega \qquad \Rightarrow \qquad E_b = E_a + \hbar\omega \tag{1.44}$$

while the second term describes emission of a photon,

$$\omega_{ba} = -\omega \qquad \Rightarrow \qquad E_b = E_a - \hbar\omega \tag{1.45}$$

(see Fig. 1.2).

1.3.2 Absorption

With

$$M_{ba}(\omega) = \langle\psi_b|\mathrm{e}^{\mathrm{i}\boldsymbol{k}\cdot\boldsymbol{r}}\boldsymbol{\varepsilon}\cdot\boldsymbol{\nabla}\,|\psi_a\rangle \tag{1.46}$$

we find for the case of absorption[3]

$$|c_b(t)|^2 = \left|-\frac{e}{2m\mathrm{i}}\hat{A}\mathrm{e}^{\mathrm{i}\delta_\omega}M_{ba}(\omega)\frac{\mathrm{e}^{\mathrm{i}(\omega_{ba}-\omega)t}-1}{\omega_{ba}-\omega}\right|^2 \tag{1.47}$$
$$= \frac{1}{2}\left(\frac{e}{m}\right)^2\hat{A}^2|M_{ba}(\omega)|^2F(t,\tilde{\omega}) \tag{1.48}$$

[3]The interference term can be neglected (→ exercise).

with

$$F(t,\tilde{\omega}) = \frac{1-\cos\tilde{\omega}t}{\tilde{\omega}^2}, \qquad \tilde{\omega} = \omega - \omega_{ba}. \tag{1.49}$$

Using

$$F(t,\tilde{\omega}) \to \pi t\,\delta(\tilde{\omega}) \qquad \text{for} \qquad t \to \infty \tag{1.50}$$

we obtain for the rate for times $t \gg 2\pi/\omega_{ba}$

$$W_{ba} = \frac{\mathrm{d}}{\mathrm{d}t}|c_b(t)|^2 = \frac{\pi}{2}\left(\frac{e}{m}\right)^2 \hat{A}^2 |M_{ba}(\omega_{ba})|^2 \delta(\omega-\omega_{ba}). \tag{1.51}$$

Since

$$\hat{A}^2 = \frac{2I}{\varepsilon_0 c\omega^2} \tag{1.52}$$

this can be written in terms of the intensity I as

$$W_{ba} = \frac{4\pi^2}{m^2 c}\left(\frac{e^2}{4\pi\varepsilon_0}\right)\frac{I}{\omega_{ba}^2}|M_{ba}(\omega_{ba})|^2\delta(\omega-\omega_{ba}). \tag{1.53}$$

The *absorption cross section* is found by noting that

$$\hbar\omega_{ba} W_{ba} = I\sigma_{ba} \tag{1.54}$$

from which

$$\sigma_{ba} = \frac{4\pi^2}{m^2 c}\left(\frac{e^2}{4\pi\varepsilon_0}\right)\frac{\hbar}{\omega_{ba}}|M_{ba}(\omega_{ba})|^2\delta(\omega-\omega_{ba}) = \frac{4\pi^2\alpha\hbar^2}{m^2\omega_{ba}}|M_{ba}(\omega_{ba})|^2\delta(\omega-\omega_{ba}) \tag{1.55}$$

follows, and

$$\alpha = \frac{e^2}{4\pi\varepsilon_0\hbar c} \simeq \frac{1}{137} \tag{1.56}$$

is the *fine structure constant*.

A radiation pulse has a finite bandwidth so that the intensity is actually distributed over frequencies,

$$I = \int_0^\infty u(\omega) c\,\mathrm{d}\omega \tag{1.57}$$

where $u(\omega)$ is the *spectral energy density*. As a consequence, not all incoming energy flux interacts resonantly with the atom, and (1.54) is to be replaced by

$$\hbar\omega_{ba} W_{ba} = \int_0^\infty u(\omega) c\,\sigma_{ba}\,\mathrm{d}\omega, \tag{1.58}$$

leading to

$$W_{ba} = \frac{4\pi^2}{m^2}\left(\frac{e^2}{4\pi\varepsilon_0}\right)\frac{u(\omega_{ba})}{\omega_{ba}^2}|M_{ba}(\omega_{ba})|^2. \tag{1.59}$$

1.3.3 Stimulated emission

We have noted already that the second term in (1.43) describes emission, where the electron drops from level a with energy $E_a > E_b$ down to level b. Interchanging the labels a and b (so that level b is again the higher one) we find for the stimulated emission rate $\bar{W}_{ab}$

$$\bar{W}_{ab} = W_{ba}, \qquad \bar{\sigma}_{ab} = \sigma_{ba}. \tag{1.60}$$

The fact that the rates for absorption and stimulated emission are equal is called the *principle of detailed balancing*. However, how frequently a process occurs also depends on the population of the levels involved. In equilibrium the upper level is less populated according to the Boltzmann factor $\exp(-\hbar\omega_{ba}/k_{\mathrm{B}}T)$ (see also Sec. 1.3.7 below).

1.3.4 Spontaneous emission

So far we have not quantized the electromagnetic field. If we did we would have obtained for the absorption rate

$$W_{ba} = \frac{4\pi^2}{m^2}\left(\frac{e^2}{4\pi\varepsilon_0}\right)\frac{N(\omega_{ba})\hbar}{V\omega_{ba}}|M_{ba}(\omega_{ba})|^2\delta(\omega-\omega_{ba}), \tag{1.61}$$

where $N(\omega_{ba})$ is the (expectation) number of photons of energy $\hbar\omega_{ba}$. This expression, because of (1.18)

$$I = \frac{\hbar\omega N c}{V},$$

is the same as (1.53).

However, because of the property of the creation operator (when acting on a Fock state)

$$a^\dagger\,|n\rangle = \sqrt{n+1}\,|n+1\rangle \tag{1.62}$$

the emission rate is different from the one without quantization of the electromagnetic field:

$$\bar{W}_{ab} = \frac{4\pi^2}{m^2}\left(\frac{e^2}{4\pi\varepsilon_0}\right)\frac{[N(\omega_{ba})+1]\hbar}{V\omega_{ba}}|M_{ba}(\omega_{ba})|^2\delta(\omega-\omega_{ba}). \tag{1.63}$$

Without quantization of the electromagnetic field there is no emission unless there are already photons in the respective mode. In a quantized field an atom in an excited state can also emit a photon into an empty mode, thanks to the 1 in $N(\omega_{ba})+1$ in the numerator on the right hand side of (1.63). For $N(\omega_{ba}) \gg 1$ the extra 1 can be neglected. Instead, for $N(\omega_{ba}) = 0$ *only* spontaneous emission contributes:

$$W^{\mathrm{s}}_{ab} = \frac{4\pi^2}{m^2}\left(\frac{e^2}{4\pi\varepsilon_0}\right)\frac{\hbar}{V\omega_{ba}}|M_{ba}(\omega_{ba})|^2\delta(\omega-\omega_{ba}). \tag{1.64}$$

Getting rid of the quantization volume via the density of states

Which photons can be emitted in the process of spontaneous emission depends on the boundary conditions. If the atom is placed into a cavity, the electromagnetic field must fit into this cavity. In our case we are interested in radiation propagating in free space. The quantization volume is just introduced as a mathematical trick to identify discrete modes of the radiation field before the continuum limit is taken, but has no physical significance. In all observables the quantization volume cancels out, e.g., by multiplication with the density of states, as we will see now. We impose periodic boundary conditions[4] and thus find for the wave vector components

$$k_x = \frac{2\pi}{L} n_x, \qquad k_y = \frac{2\pi}{L} n_y, \qquad k_z = \frac{2\pi}{L} n_z, \tag{1.65}$$

with n_x, n_y, n_z being positive or negative integers. In the continuum limit

$$\mathrm{d}^3 n = \mathrm{d}n_x \, \mathrm{d}n_y \, \mathrm{d}n_z = \left(\frac{L}{2\pi}\right)^3 \mathrm{d}k_x \, \mathrm{d}k_y \, \mathrm{d}k_z = \left(\frac{L}{2\pi}\right)^3 k^2 \, \mathrm{d}k \, \mathrm{d}\Omega = \frac{V}{(2\pi)^3} \frac{\omega^2}{c^3} \, \mathrm{d}\omega \, \mathrm{d}\Omega, \tag{1.66}$$

using $k = \omega/c$ in the last step. The density of states $\varrho_a(\omega)$ follows from

$$\mathrm{d}^3 n = \varrho_a(\omega) \, \mathrm{d}\omega \, \mathrm{d}\Omega, \tag{1.67}$$

leading to

$$\varrho_a(\omega) = \frac{V}{(2\pi)^3} \frac{\omega^2}{c^3}. \tag{1.68}$$

Multiplying $\varrho_a(\omega) \, \mathrm{d}\omega \, \mathrm{d}\Omega$ to the right hand side of (1.64) and integrating out ω yields the rate at which linearly polarized photons are emitted under an angle (θ, ϕ) into a solid angle element $\mathrm{d}\Omega$:[5]

$$W^{\mathrm{s}}_{ab} \, \mathrm{d}\Omega = \frac{\hbar}{2\pi m^2 c^3} \left(\frac{e^2}{4\pi\varepsilon_0}\right) \omega_{ba} |M_{ba}(\omega_{ba})|^2 \, \mathrm{d}\Omega. \tag{1.69}$$

The quantization volume V canceled, as required. Integration over all emission angles and summation over the two linearly independent polarizations $\boldsymbol{\varepsilon}_\lambda$, $\lambda = 1, 2$ leads to the total rate

$$W^{\mathrm{s}}_{ab} = \frac{\hbar}{2\pi m^2 c^3} \left(\frac{e^2}{4\pi\varepsilon_0}\right) \int \mathrm{d}\Omega \sum_{\lambda=1}^{2} \omega_{ba} |M^{(\lambda)}_{ba}(\omega_{ba})|^2 \tag{1.70}$$

with

$$M^{(\lambda)}_{ba}(\omega) = \langle \psi_b | \mathrm{e}^{\mathrm{i}\boldsymbol{k}\cdot\boldsymbol{r}} \boldsymbol{\varepsilon}_\lambda \cdot \boldsymbol{\nabla} \, | \psi_a \rangle \, . \tag{1.71}$$

[4] As it was done in the derivation of (1.61) and (1.63).

[5] In the following, we keep the notation W^{s}_{ab} for what actually is $\int W^{\mathrm{s}}_{ab} \, \varrho_a(\omega) \, \mathrm{d}\omega$.

1.3.5 Dipole approximation

If the wavelength is much greater than the relevant atomic length scale one may cut the expansion

$$\mathrm{e}^{\mathrm{i}\boldsymbol{k}\cdot\boldsymbol{r}} = 1 + \mathrm{i}\boldsymbol{k}\cdot\boldsymbol{r} + \frac{1}{2!}(\mathrm{i}\boldsymbol{k}\cdot\boldsymbol{r})^2 + \cdots \tag{1.72}$$

already after the first term. As the vector potential then looses its spatial dependence, the magnetic field $\boldsymbol{B} = \boldsymbol{\nabla}\times\boldsymbol{A}(t) = \boldsymbol{0}$ vanishes. The electric field is considered uniform on the atomic length scale so that also retardation effects are neglected. This approximation is called the *dipole approximation*.

In dipole approximation

$$M_{ba} \to M_{ba}^{\mathrm{D}} = \boldsymbol{\varepsilon}\cdot\langle\psi_b|\boldsymbol{\nabla}\,|\psi_a\rangle = \frac{\mathrm{i}}{\hbar}\boldsymbol{\varepsilon}\cdot\langle\psi_b|\boldsymbol{p}\,|\psi_a\rangle \tag{1.73}$$

where in the last step we used the fact that $\boldsymbol{p} = -\mathrm{i}\hbar\boldsymbol{\nabla}$ in position space representation.

1.3.6 Gauge transformations in dipole approximation

As in dipole approximation the A^2-term in (1.33)[6] is purely time-dependent, it can be transformed away by a contact transformation. Substituting

$$\psi = \exp\left(-\frac{\mathrm{i}e^2}{2m\hbar}\int^t A^2(t')\,\mathrm{d}t'\right)\psi' \tag{1.74}$$

one obtains the time-dependent Schrödinger equation in so-called *velocity gauge*,

$$\mathrm{i}\hbar\frac{\partial}{\partial t}\psi' = \left(H_0 + \frac{e}{m}\boldsymbol{A}(t)\cdot\boldsymbol{p}\right)\psi' \tag{1.75}$$

with H_0 given in (1.35). Another option is

$$\psi = \exp\left(-\frac{\mathrm{i}e}{\hbar}\boldsymbol{A}(t)\cdot\boldsymbol{r}\right)\psi'', \tag{1.76}$$

leading to the *length gauge* Schrödinger equation

$$\mathrm{i}\hbar\frac{\partial}{\partial t}\psi'' = (H_0 + e\boldsymbol{E}(t)\cdot\boldsymbol{r})\,\psi''. \tag{1.77}$$

Here, the electric field of the electromagnetic wave is $\boldsymbol{E}(t) = -\partial_t\boldsymbol{A}(t)$. Assuming a linearly polarized vector potential (1.42) the polarization vector $\boldsymbol{\varepsilon}$ is the same for $\boldsymbol{E}$

[6] Repeated here for convenience:

$$H = -\frac{\hbar^2}{2m}\nabla^2 - \mathrm{i}\hbar\frac{e}{m}\boldsymbol{A}\cdot\boldsymbol{\nabla} + \frac{e^2}{2m}A^2 + V_{\mathrm{C}}.$$

and $\boldsymbol{A}$. Note that the transformation (1.76) can be interpreted as a translation in momentum space.

If we perform the perturbative treatment of Sec. 1.3.1 in dipole approximation and length gauge we have

$$H_{\mathrm{int}}(t) = e\boldsymbol{E}(t)\cdot\boldsymbol{r} \tag{1.78}$$

and

$$M_{ba}^{\mathrm{D}} = \frac{m\omega_{ba}}{\hbar e}\boldsymbol{\varepsilon}\cdot\boldsymbol{D}_{ba}, \qquad \boldsymbol{D}_{ba} = -e\langle\psi_b|\boldsymbol{r}\,|\psi_a\rangle = -e\boldsymbol{r}_{ba} \tag{1.79}$$

so that, inserted in (1.59),

$$W_{ba}^{\mathrm{D}} = \frac{4\pi^2}{\hbar^2}\left(\frac{1}{4\pi\varepsilon_0}\right)u(\omega_{ba})|\boldsymbol{\varepsilon}\cdot\boldsymbol{D}_{ba}|^2 = \frac{4\pi^2}{\hbar^2}\left(\frac{e^2}{4\pi\varepsilon_0}\right)u(\omega_{ba})|\boldsymbol{\varepsilon}\cdot\boldsymbol{r}_{ba}|^2 \tag{1.80}$$

follows. The dipole transition matrix element $\boldsymbol{D}_{ba}$ or $\boldsymbol{r}_{ba}$ are atomic properties, the polarization vector $\boldsymbol{\varepsilon}$ is a property of the external field. Their orientation with respect to each other is crucial for the probability that a transition takes place in dipole approximation.

If the matrix element M_{ba} vanishes the corresponding transition is forbidden in first-order perturbation theory. If M_{ba}^{D} vanishes, the transition is called "E1 dipole-forbidden". The next-order term in the expansion (1.72) $\mathrm{i}\boldsymbol{k}\cdot\boldsymbol{r}$ may give rise to magnetic dipole (M1) or electric quadrupole (E2) transitions.

The last expression in (1.80) can be written as

$$W_{ba}^{\mathrm{D}} = \frac{4\pi^2}{\hbar^2}\left(\frac{e^2}{4\pi\varepsilon_0}\right)u(\omega_{ba})|\boldsymbol{r}_{ba}|^2\cos^2\theta \tag{1.81}$$

with θ being the angle between $\boldsymbol{\varepsilon}$ and $\boldsymbol{r}_{ba}$. If the radiation is unpolarized one has to average $\cos^2\theta$ over all solid angles,

$$\frac{1}{4\pi}\int_0^{2\pi}\mathrm{d}\phi\int_{-1}^{1}\mathrm{d}(\cos\theta)\,\cos^2\theta = \frac{1}{3}, \tag{1.82}$$

leading to

$$\tilde{W}_{ba}^{\mathrm{D}} = \frac{4\pi^2}{3\hbar^2}\left(\frac{1}{4\pi\varepsilon_0}\right)u(\omega_{ba})|\boldsymbol{D}_{ba}|^2 = \frac{4\pi^2}{3\hbar^2}\left(\frac{e^2}{4\pi\varepsilon_0}\right)u(\omega_{ba})|\boldsymbol{r}_{ba}|^2. \tag{1.83}$$

We know already that the rate for stimulated emission equals that of absorption. The rate for spontaneous emission (1.69) in dipole approximation and length form becomes

$$W_{ab}^{\mathrm{sD}}\,\mathrm{d}\Omega = \frac{1}{2\pi\hbar c^3}\left(\frac{1}{4\pi\varepsilon_0}\right)\omega_{ba}^3|\boldsymbol{\varepsilon}\cdot\boldsymbol{D}_{ba}|^2\,\mathrm{d}\Omega = \frac{1}{2\pi\hbar c^3}\left(\frac{e^2}{4\pi\varepsilon_0}\right)\omega_{ba}^3|\boldsymbol{\varepsilon}\cdot\boldsymbol{r}_{ba}|^2\,\mathrm{d}\Omega. \tag{1.84}$$

Summation over the two polarization directions and integration over the angles yields the total rate ($\rightarrow$ exercise)

$$\tilde{W}_{ab}^{\mathrm{sD}} = \frac{4}{3\hbar c^3}\left(\frac{1}{4\pi\varepsilon_0}\right)\omega_{ba}^3|\boldsymbol{D}_{ba}|^2 = \frac{4\alpha}{3c^2}\omega_{ba}^3|\boldsymbol{r}_{ba}|^2. \tag{1.85}$$

1.3.7 Einstein coefficients

Consider an ensemble of atoms in a container. Only two nondegenerate levels $E_b > E_a$ are assumed to be relevant, and the ensemble is supposed to be in thermal equilibrium at temperature T.

The number of atoms undergoing a transition $a \to b$ per unit time is governed by

$$\dot{N}_{ba} = W_{ba} N_a \tag{1.86}$$

where N_a is the number of atoms in state a. Einstein introduced a coefficient B_{ba} which relates the spectral energy density $u(\omega)$ with the absorption rate according

$$B_{ba} = \frac{\tilde{W}^{\mathrm{D}}_{ba}}{u(\omega)} = \frac{4\pi^2}{3\hbar^2} \left(\frac{1}{4\pi\varepsilon_0} \right) |\boldsymbol{D}_{ba}|^2. \tag{1.87}$$

Hence,

$$\dot{N}_{ba} = B_{ba} N_a u(\omega_{ba}). \tag{1.88}$$

The number of transitions $b \to a$ per unit time, accompanied by the emission of a photon, reads

$$\dot{N}_{ab} = A_{ab} N_b + B_{ab} N_b u(\omega_{ba}). \tag{1.89}$$

A_{ab} is the Einstein coefficient for spontaneous emission, B_{ab} is the Einstein coefficient for stimulated emission. At equilibrium there must be as many "upward" as "downward" transitions, $\dot{N}_{ba} = \dot{N}_{ab}$ so that

$$\frac{N_a}{N_b} = \frac{A_{ab} + B_{ab} u}{B_{ba} u}. \tag{1.90}$$

On the other hand we know that

$$\frac{N_a}{N_b} = \mathrm{e}^{\hbar\omega_{ba}/k_{\mathrm{B}}T}. \tag{1.91}$$

As a consequence, the spectral energy density is

$$u(\omega_{ba}) = \frac{A_{ab}}{B_{ba}\mathrm{e}^{\hbar\omega_{ba}/k_{\mathrm{B}}T} - B_{ab}}. \tag{1.92}$$

Comparing this with Planck's distribution

$$u(\omega_{ba}) = \frac{\hbar\omega_{ba}^3}{\pi^2 c^3} \frac{1}{\mathrm{e}^{\hbar\omega_{ba}/k_{\mathrm{B}}T} - 1} \tag{1.93}$$

yields the detailed balance and a relation between spontaneous emission and absorption:

$$B_{ba} = B_{ab}, \tag{1.94}$$

$$A_{ab} = \frac{\hbar\omega_{ba}^3}{\pi^2 c^3} B_{ab}. \tag{1.95}$$

It is easily verified that the latter equation agrees with the above derived result (1.85), i.e.,

$$A_{ab} = \tilde{W}_{ab}^{\mathrm{sD}}. \tag{1.96}$$

In the case of degenerate levels (degeneracies g_a, g_b) one obtains

$$g_a B_{ba} = g_b B_{ab} \tag{1.97}$$

whereas Eq. (1.95) remains valid ($\rightarrow$ exercise).

1.3.8 Spontaneous emission from the 2p level

As a concrete example we want to evaluate the rate of spontaneous emission (1.85) for the 2p $\rightarrow$ 1s-transition in hydrogen-like atoms or ions. First we remind ourselves that the energy levels are given by[7]

$$E_n = -\frac{e^2}{4\pi\varepsilon_0 a_0}\frac{Z^2}{2n^2} = -\frac{1}{2}mc^2\frac{(Z\alpha)^2}{n^2}, \qquad n = 1, 2, 3, \ldots \tag{1.98}$$

where

$$a_0 = \frac{4\pi\varepsilon_0\hbar^2}{me^2} \tag{1.99}$$

is the Bohr radius and n is the principal quantum number. The transition frequency ω_{ba} that appears in (1.85) thus is

$$\omega_{\mathrm{2p,1s}} = -\frac{1}{2}\frac{mc^2}{\hbar}(Z\alpha)^2\left(\frac{1}{4} - 1\right) = \frac{3}{8}\frac{mc^2}{\hbar}(Z\alpha)^2. \tag{1.100}$$

The matrix element $\boldsymbol{r}_{21m,100}$ (where the indices indicate the $n\ell m$-quantum numbers of the 2p and 1s state involved) needs to be evaluated with the corresponding hydrogenic eigenfunctions. We remember that the hydrogenic eigenfunctions separate into a radial and an angular part,

$$\Psi_{n\ell m}(r, \theta, \phi) = R_{n\ell}(r)Y_\ell^m(\theta, \phi) \tag{1.101}$$

with $Y_\ell^m(\theta, \phi)$ being the spherical harmonics, and the orbital angular momentum and magnetic quantum numbers obey

$$\ell = 0, 1, \ldots, n-1, \qquad m = -\ell, -\ell+1, \ldots, \ell, \tag{1.102}$$

respectively. The bound-state radial wave functions $R_{n\ell}(r)$ are normalized according to

$$\int_0^\infty |R_{n\ell}|^2 r^2 \,\mathrm{d}r = 1 \tag{1.103}$$

[7]Here, we neglect spin-orbit coupling and other corrections.

and can be expressed in terms of Laguerre polynomials. We give explicitly the first three of them:

$$R_{10}(r) = 2\left(\frac{Z}{a_0}\right)^{3/2} \mathrm{e}^{-Zr/a_0}, \tag{1.104}$$

$$R_{20}(r) = 2\left(\frac{Z}{2a_0}\right)^{3/2} \left(1-\frac{Zr}{2a_0}\right) \mathrm{e}^{-Zr/2a_0}, \tag{1.105}$$

$$R_{21}(r) = \frac{1}{\sqrt{3}}\left(\frac{Z}{2a_0}\right)^{3/2} \frac{Zr}{a_0} \mathrm{e}^{-Zr/2a_0}. \tag{1.106}$$

The spherical harmonics for $\ell = 0$ and 1 read

$$Y_0^0 = \sqrt{\frac{1}{4\pi}}, \tag{1.107}$$

$$Y_1^0(\theta) = \sqrt{\frac{3}{4\pi}}\cos\theta, \tag{1.108}$$

$$Y_1^{\pm 1}(\theta,\phi) = \mp\sqrt{\frac{3}{8\pi}}\sin\theta\, \mathrm{e}^{\pm \mathrm{i}\phi}. \tag{1.109}$$

With this we find for the matrix element $\boldsymbol{r}_{21m,100}$

$$\boldsymbol{r}_{21m,100} = \int_0^\infty R_{21}(r)R_{10}(r)r^3\,\mathrm{d}r \int [Y_1^m(\theta,\phi)]^* \boldsymbol{e}_r(\theta,\phi) Y_0^0\,\mathrm{d}\Omega. \tag{1.110}$$

The radial integral gives

$$\int_0^\infty R_{21}(r)R_{10}(r)r^3\,\mathrm{d}r = \left(\frac{Z}{a_0}\right)^4 \frac{1}{\sqrt{6}} \int_0^\infty r^4\,\mathrm{e}^{-3Zr/2a_0}\,\mathrm{d}r = \frac{a_0}{Z}\frac{24}{\sqrt{6}}\left(\frac{2}{3}\right)^5. \tag{1.111}$$

The angular integration can be performed using

$$\boldsymbol{e}_r \cdot \boldsymbol{e}_x = \cos\phi\sin\theta = \sqrt{\frac{2\pi}{3}}(-Y_1^1 + Y_1^{-1}), \tag{1.112}$$

$$\boldsymbol{e}_r \cdot \boldsymbol{e}_y = \sin\phi\sin\theta = \sqrt{\frac{2\pi}{3}}\mathrm{i}(Y_1^1 + Y_1^{-1}), \tag{1.113}$$

$$\boldsymbol{e}_r \cdot \boldsymbol{e}_z = \cos\theta = \sqrt{\frac{4\pi}{3}}Y_1^0 \tag{1.114}$$

(arguments of the Y_ℓ^ms suppressed) and the orthogonality of the spherical harmonics,

$$\int [Y_\ell^m(\theta,\phi)]^* Y_{\ell'}^{m'}(\theta,\phi)\,\mathrm{d}\Omega = \delta_{\ell\ell'}\delta_{mm'}. \tag{1.115}$$

For, e.g., the x-component we find

$$\begin{aligned}\int [Y_1^m(\theta,\phi)]^* \cos\phi \sin\theta \; Y_0^0 \, \mathrm{d}\Omega &= \int [Y_1^m]^* \sqrt{\frac{2\pi}{3}}(-Y_1^1 + Y_1^{-1}) \sqrt{\frac{1}{4\pi}} \, \mathrm{d}\Omega \\ &= \sqrt{\frac{1}{6}} \, (-\delta_{m,1} + \delta_{m,-1}) \end{aligned} \tag{1.116}$$

so that

$$\boldsymbol{r}_{21m,100} \cdot \boldsymbol{e}_x = x_{21m,100} = \frac{a_0}{Z} 4 \left(\frac{2}{3}\right)^5 (-\delta_{m,1} + \delta_{m,-1}) \tag{1.117}$$

and analogously

$$y_{21m,100} = \frac{a_0}{Z} 4 \left(\frac{2}{3}\right)^5 \mathrm{i}(\delta_{m,1} + \delta_{m,-1}), \tag{1.118}$$

$$z_{21m,100} = \frac{a_0}{Z} \frac{24}{\sqrt{18}} \left(\frac{2}{3}\right)^5 \delta_{m,0}. \tag{1.119}$$

Hence,

$$\begin{aligned}|\boldsymbol{r}_{21m,100}|^2 &= \left(\frac{a_0}{Z}\right)^2 \frac{24^2}{18} \left(\frac{2}{3}\right)^{10} \left(\delta_{m,0} + \frac{1}{2}(\delta_{m,1} + \delta_{m,-1}) + \frac{1}{2}(\delta_{m,1} + \delta_{m,-1})\right) \\ &= \left(\frac{a_0}{Z}\right)^2 \frac{2^{15}}{3^{10}} \, (\delta_{m,0} + \delta_{m,1} + \delta_{m,-1}) \qquad (1.120) \\ &= \frac{1}{Z^2} \left(\frac{\hbar}{mc\alpha}\right)^2 \frac{2^{15}}{3^{10}} \, (\delta_{m,0} + \delta_{m,1} + \delta_{m,-1}) \, , \qquad (1.121)\end{aligned}$$

and we see (using (1.85)) that all magnetic sublevels contribute with the same partial rate,

$$\begin{aligned}\tilde{W}^{\mathrm{sD}}_{21m,100} &= \frac{4\alpha}{3c^2} \underbrace{\left(\frac{3}{8}\frac{mc^2}{\hbar}(Z\alpha)^2\right)^3}_{\omega_{ba}^3} \underbrace{\frac{1}{Z^2}\left(\frac{\hbar}{mc\alpha}\right)^2 \frac{2^{15}}{3^{10}}}_{|\boldsymbol{r}_{21m,100}|^2 \text{ for any } m} \\ &= \left(\frac{2}{3}\right)^8 \frac{m\alpha^5 Z^4 c^2}{\hbar}. \end{aligned} \tag{1.122}$$

If all these levels are equally populated the average

$$\langle \tilde{W}^{\mathrm{sD}}_{21m,100} \rangle_m = \frac{1}{3} \sum_{m=-1}^{1} \tilde{W}^{\mathrm{sD}}_{21m,100} \tag{1.123}$$

yields the same result as (1.122),

$$\langle \tilde{W}^{\mathrm{sD}}_{21m,100} \rangle_m = \left(\frac{2}{3}\right)^8 \frac{m\alpha^5 Z^4 c^2}{\hbar} = 6.27 \times 10^8 \; Z^4 \; \mathrm{s}^{-1}. \tag{1.124}$$

Table 1.1: Lifetimes of hydrogenic levels.

level	2p	3s	3p	3d	4s	4p	4d	4f
$\tau/10^{-8}\,\mathrm{s}$	0.16	16	0.54	1.56	23	1.24	3.65	7.3

We see that there is a strong Z-dependence of the spontaneous decay rate. For light atoms and ions spontaneous decay is slow compared to, e.g., the pulse duration of picosecond ($10^{-12}\,\mathrm{s}$) or even femtosecond ($10^{-15}\,\mathrm{s}$) laser pulses. This is good news for several reasons. First, it allows the experimentalists to *prepare* atoms in desired states. They can, for instance, create a population inversion (laser), meaning that a higher state is more likely populated than a lower one. If spontaneous emission were faster, such a preparation would be quickly destroyed or simply not feasible to achieve in the first place. Second, the depopulation of excited states by spontaneous emission of photons need not be taken into account when the TDSE is solved numerically.[8]

1.3.9 Atomic lifetimes

The number of atoms $N(t)$ in an excited state b decreases according to the rate equation

$$\dot{N}(t) = -N(t) \sum_k \tilde{W}_{kb}^{\mathrm{sD}} \tag{1.125}$$

where k runs over all states to which the system can decay. Hence,

$$N(t) = N(0)\ \mathrm{e}^{-t/\tau_b} \tag{1.126}$$

where

$$\tau_b = \frac{1}{\sum_k \tilde{W}_{kb}^{\mathrm{sD}}} \tag{1.127}$$

is the *lifetime* of the level b. Lifetimes for hydrogenic levels are given in Table 1.1. Note that the transition rate for the 2s level vanishes in first order in dipole approximation. In fact, $\tau_{2\mathrm{s}} = 0.14\,\mathrm{s}$, which is very slow compared to the values in Table 1.1. The 2s-state is therefore called *metastable*. Two photons are emitted in the $2\mathrm{s} \to 1\mathrm{s}$ decay, which is less likely and requires second order perturbation theory for a description.

1.3.10 Selection rules

From (1.80) and (1.84) it is apparent that $\boldsymbol{\varepsilon} \cdot \boldsymbol{r}_{ba}$ determines whether a single-photon transition is dipole-allowed or not. This gives rise to so-called *selection rules*. We

[8] We shall come back to this later on when we study the quantum dynamics in strong and short laser pulses.

choose the quantization axis to be the z-axis[9] and express vectors in the *spherical basis*

$$\boldsymbol{e}_{\pm1} = \mp\frac{1}{\sqrt{2}}(\boldsymbol{e}_x \pm \mathrm{i}\boldsymbol{e}_y), \tag{1.128}$$

$$\boldsymbol{e}_0 = \boldsymbol{e}_z. \tag{1.129}$$

The spherical basis vectors have the property

$$\boldsymbol{e}_q \cdot \boldsymbol{e}^*_{q'} = \delta_{qq'}, \qquad q, q' = -1, 0, 1 \tag{1.130}$$

($\rightarrow$ exercise). The covariant spherical components of the position vector read

$$r_{\pm1} = \mp\frac{1}{\sqrt{2}}(x \pm \mathrm{i}y) = \mp\frac{1}{\sqrt{2}} r \sin\theta\, \mathrm{e}^{\pm\mathrm{i}\phi} = r\sqrt{\frac{4\pi}{3}} Y_1^{\pm1}(\theta, \phi), \tag{1.131}$$

$$r_0 = z = r\cos\theta = r\sqrt{\frac{4\pi}{3}} Y_1^0(\theta, \phi), \tag{1.132}$$

i.e.,

$$r_q = r\sqrt{\frac{4\pi}{3}} Y_1^q(\theta, \phi). \tag{1.133}$$

It is easy to verify that

$$\boldsymbol{r} = \sum_{q=-1}^{+1} r_q \boldsymbol{e}^*_q = \sum_{q=-1}^{+1} r^*_q \boldsymbol{e}_q. \tag{1.134}$$

The $r^*_q =: r^q$ are the contravariant spherical components of $\boldsymbol{r}$. We also expand the polarization vector

$$\boldsymbol{\varepsilon} = \sum_{q=-1}^{+1} \varepsilon_q \boldsymbol{e}^*_q = \sum_{q=-1}^{+1} \varepsilon^*_q \boldsymbol{e}_q \tag{1.135}$$

and obtain with (1.130)

$$\boldsymbol{\varepsilon} \cdot \boldsymbol{r} = \sum_{q=-1}^{+1} \sum_{q'=-1}^{+1} \varepsilon^*_q r_{q'}\ \boldsymbol{e}_q \cdot \boldsymbol{e}^*_{q'} = \sum_{q=-1}^{+1} \varepsilon^*_q r_q. \tag{1.136}$$

As a consequence,

$$\boldsymbol{\varepsilon} \cdot \boldsymbol{r}_{ba} = \sum_{q=-1}^{+1} \varepsilon^*_q \langle \Psi_b | r_q \, | \Psi_a \rangle \tag{1.137}$$

results for one-electron atoms, and, with (1.101),

$$\langle \Psi_{n'\ell'm'} | r_q \, | \Psi_{n\ell m} \rangle = \sqrt{\frac{4\pi}{3}} \int_0^\infty \mathrm{d}r\, r^3 R_{n'\ell'm'} R_{n\ell m} \int \mathrm{d}\Omega\, [Y^{m'}_{\ell'}]^* Y^q_1 Y^m_\ell. \tag{1.138}$$

[9] This defines the coordinate system for the spherical harmonics.

The integral $\langle\Psi_{n'\ell'm'}|r_q\,|\Psi_{n\ell m}\rangle = \int \mathrm{d}^3r\,\Psi^*_{n'\ell'm'}(\boldsymbol{r})r_q\Psi_{n\ell m}(\boldsymbol{r})$ can as well be performed using the substitution $\boldsymbol{r}\to-\boldsymbol{r}$ (reflection or space inversion) and must lead to the same result. Because under reflection $\boldsymbol{r}\to-\boldsymbol{r}$

$$R_{n\ell}(r)Y_\ell^m(\theta,\phi)\overset{\boldsymbol{r}\to-\boldsymbol{r}}{\longrightarrow}R_{n\ell}(r)Y_\ell^m(\pi-\theta,\phi+\pi)=R_{n\ell}(r)(-1)^\ell Y_\ell^m(\theta,\phi),\qquad(1.139)$$

that is, ℓ determines the parity of the wave function and r does not change, we find

$$\langle\Psi_{n'\ell'm'}|r_q\,|\Psi_{n\ell m}\rangle=(-1)^{\ell+\ell'+1}\langle\Psi_{n'\ell'm'}|r_q\,|\Psi_{n\ell m}\rangle\quad\Rightarrow\quad(\ell+\ell'+1)\text{ even}\qquad(1.140)$$

unless the matrix element vanishes. This means that the dipole operator only allows for transitions between states of opposite parity. We will now constrain the conditions for a transition being allowed further.

The radial integral in (1.138) never vanishes. Hence, it is the angular integral over the three spherical harmonics defining the selection rules. Because $Y_\ell^m\sim\mathrm{e}^{\mathrm{i}m\phi}$ the integral over the angle ϕ is of the form

$$J(m,m',q)=\int_0^{2\pi}\mathrm{e}^{\mathrm{i}(m+q-m')\phi}\,\mathrm{d}\phi,\qquad(1.141)$$

which is nonvanishing only if

$$m'=m+q.\qquad(1.142)$$

In case of $q=0$ the polarization vector is in z-direction (linear polarization) and $m'=m$, i.e., $\Delta m=m'-m=0$. In case of $q=\pm1$ the propagation vector $\boldsymbol{k}$ is in z-direction and $m'=m\pm1$, i.e., $\Delta m=\pm1$ (circular polarization, see next Subsection).

In order to extract the selection rule for the orbital angular momentum we need to consider the integral over the product of three spherical harmonics in (1.138),

$$\mathcal{A}(\ell,m,\ell',m',q)=\int\mathrm{d}\Omega\,[Y_{\ell'}^{m'}]^*Y_1^qY_\ell^m,\qquad(1.143)$$

which can be expressed in terms of *Clebsch-Gordan coefficients*,

$$\mathcal{A}(\ell,m,\ell',m',q)=\sqrt{\frac{3}{4\pi}\frac{(2\ell+1)}{(2\ell'+1)}}\langle\ell100|\ell'0\rangle\langle\ell1mq|\ell'm'\rangle.\qquad(1.144)$$

The Clebsch-Gordan coefficients are tabulated in books on the quantum theory of angular momentum.[10] It is found that $\langle\ell1mq|\ell'm'\rangle$ is only non-vanishing if $m'=m+q$, as observed previously, and

$$\ell'=\ell\pm1,\qquad(1.145)$$

i.e., $\Delta\ell=\ell'-\ell=\pm1$. This result can be also established without resorting to Clebsch-Gordan coefficients but just using the orthogonality of the spherical harmonics (1.115) and recurrence relations ($\rightarrow$ exercise).

[10] For instance, D.A. Varshalovich *et al.*, *Quantum Theory of Angular Momentum*, (World Scientific).

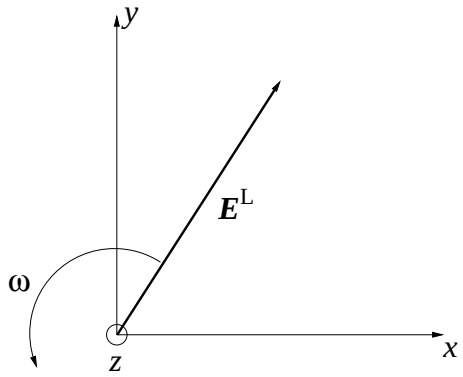

Figure 1.3: How the electric field vector rotates in an anti-clockwise (left-) polarized electromagnetic wave which propagates in z-direction (towards the reader).

Electron spin

The dipole operator does not couple to the electron spin, which is the reason why we have not considered the electron spin in the first place. The electron spin thus remains unaffected by the absorption or emission of dipole radiation.

1.3.11 Helicity of the photon

Let us consider the vector potential

$$\boldsymbol{A}^{\mathrm{L}}(z,t) = \frac{1}{\sqrt{2}}\hat{A}\left(\cos(kz-\omega t)\boldsymbol{e}_x - \sin(kz-\omega t)\boldsymbol{e}_y\right) \tag{1.146}$$

and the corresponding electric field $\boldsymbol{E}^{\mathrm{L}} = -\partial_t \boldsymbol{A}^{\mathrm{L}}$

$$\boldsymbol{E}^{\mathrm{L}}(z,t) = \frac{1}{\sqrt{2}}\hat{A}\omega\left(-\sin(kz-\omega t)\boldsymbol{e}_x - \cos(kz-\omega t)\boldsymbol{e}_y\right). \tag{1.147}$$

Figure 1.3 shows how the electric field vector rotates in the xy-plane, as seen from an observer looking towards the incoming wave.

By projecting onto the spherical basis vectors (1.128) we find

$$\boldsymbol{e}_{\pm1}\cdot\boldsymbol{A}^{\mathrm{L}} = \mp\frac{1}{2}\hat{A}(\cos\eta \mp \mathrm{i}\sin\eta) = \mp\frac{1}{2}\hat{A}\mathrm{e}^{\mp\mathrm{i}\eta} \tag{1.148}$$

with $\eta = kz - \omega t$. The vector potential can thus be expanded in the form

$$\boldsymbol{A}^{\mathrm{L}} = \frac{1}{2}\hat{A}(\mathrm{e}^{\mathrm{i}\eta}\boldsymbol{e}^*_{-1} - \mathrm{e}^{-\mathrm{i}\eta}\boldsymbol{e}^*_{+1}). \tag{1.149}$$

If we introduce

$$\boldsymbol{e}^*_{-1} = \frac{1}{\sqrt{2}}(\boldsymbol{e}_x + \mathrm{i}\boldsymbol{e}_y) =: \boldsymbol{e}^{\mathrm{L}}, \tag{1.150}$$

$$\boldsymbol{e}^*_{+1} = -\frac{1}{\sqrt{2}}(\boldsymbol{e}_x - \mathrm{i}\boldsymbol{e}_y) =: \boldsymbol{e}^{\mathrm{R}} \tag{1.151}$$

we can write for an anti-clockwise (left-) polarized vector potential

$$\boldsymbol{A}^{\mathrm{L}} = \frac{1}{2}\hat{A}(\boldsymbol{e}^{\mathrm{L}}\mathrm{e}^{\mathrm{i}(kz-\omega t)} + \mathrm{c.c.}) \tag{1.152}$$

and for a clockwise (right-) polarized wave

$$\boldsymbol{A}^{\mathrm{R}} = \frac{1}{2}\hat{A}(\boldsymbol{e}^{\mathrm{R}}\mathrm{e}^{\mathrm{i}(kz-\omega t)} + \mathrm{c.c.}). \tag{1.153}$$

From expression (1.43) we inferred that the term $\sim \mathrm{e}^{\mathrm{i}\boldsymbol{k}\cdot\boldsymbol{r}}$ gives rise to absorption and the term $\sim \mathrm{e}^{-\mathrm{i}\boldsymbol{k}\cdot\boldsymbol{r}}$ gives rise to emission of photons. Therefore the term $\sim \boldsymbol{e}^{\mathrm{L}}\cdot\boldsymbol{r}_{ba}$ describes the absorption of a left-hand circularly polarized photon, and the term $\sim \boldsymbol{e}^{\mathrm{R}}\cdot\boldsymbol{r}_{ba}$ that of a right-hand one. As we interchanged the labels a and b in the emission term in Sec. 1.3.3 we find that $\boldsymbol{e}^{\mathrm{L}^*}\cdot\boldsymbol{r}_{ab} = \boldsymbol{e}^{\mathrm{L}^*}\cdot\boldsymbol{r}^*_{ba}$ describes the emission of a left-hand circularly polarized photon, and $\boldsymbol{e}^{\mathrm{R}^*}\cdot\boldsymbol{r}_{ab} = \boldsymbol{e}^{\mathrm{R}^*}\cdot\boldsymbol{r}^*_{ba}$ that of a right-hand one.

Let us consider the emission of a left-hand circularly polarized photon,

$$\boldsymbol{e}^{\mathrm{L}^*}\cdot\boldsymbol{r}_{ab} = \frac{1}{\sqrt{2}}(\boldsymbol{e}_x - \mathrm{i}\boldsymbol{e}_y)\cdot\boldsymbol{r}_{ab} = \frac{1}{\sqrt{2}}(x_{ab} - \mathrm{i}y_{ab}) = \langle\Psi_a|r_{-1}\,|\Psi_b\rangle\,. \tag{1.154}$$

In the last step we used (1.131). Because of (1.142) and $q = -1$ in this case, obviously $m' = m - 1$, which means that in the final state the atom lost $1\,\hbar$ of angular momentum projected onto the z-axis (i.e., the quantization axis). With the same line of arguments one arrives at the conclusion that the emission of a right-hand circularly polarized photon increases the m-quantum number by one.

Because of angular momentum conservation of the total system atom + field, a photon has to carry an angular momentum $\pm\hbar$ *in propagation direction*. As there can never be an orbital angular momentum $\boldsymbol{L} = \boldsymbol{r}\times\boldsymbol{p}$ in propagation direction the angular momentum of the photon must be *intrinsic*. We call it the spin of the photon. Its projection onto the propagation direction is called *helicity*. It is $+\hbar$ for left-hand and $-\hbar$ for right-hand circularly polarized photons. There is none with $0\hbar$. This is different from a massive spin-1 particle, for which there would be three values (-1, 0, and $+1\hbar$) for m_s.

1.3.12 Spectrum of one-electron atoms

The non-relativistic expression for the eigenenergies reads

$$E_n = -\frac{e^2}{4\pi\varepsilon_0 a_0}\frac{Z^2}{2n^2} = -\frac{1}{2}mc^2\frac{(Z\alpha)^2}{n^2}, \qquad n = 1, 2, 3, \ldots \tag{1.155}$$

where

$$a_0 = \frac{4\pi\varepsilon_0\hbar^2}{me^2} \tag{1.156}$$

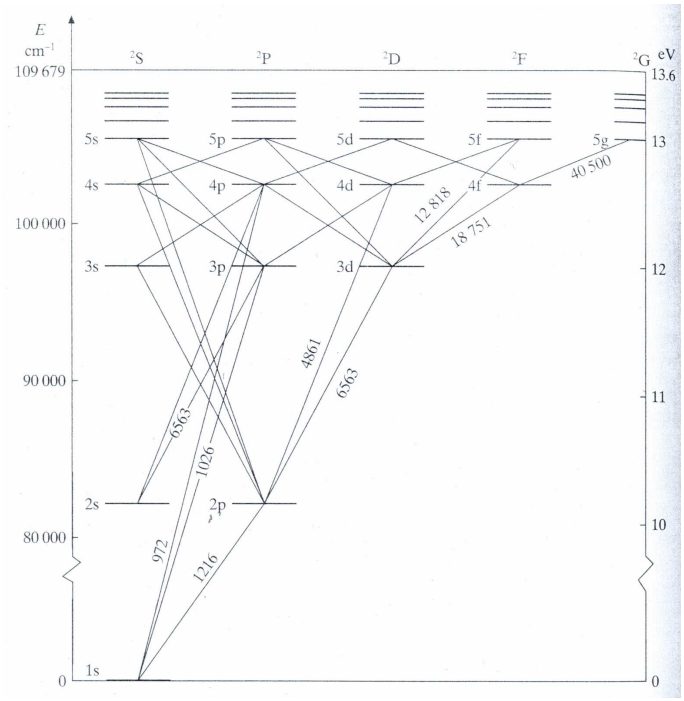

Figure 1.4: Grotrian diagram for atomic hydrogen (from Bransden & Joachain, *Physics of Atoms and Molecules*).

is the Bohr radius and n is the principal quantum number. As these energies only depend on the principal quantum number but the selection rules derived above involve only ℓ and m, the hydrogenic spectrum contains all frequencies

$$\nu_{ab} = \frac{E_{n_b} - E_{n_a}}{h} = \frac{1}{2} mc^2 \frac{\alpha^2}{h} Z^2 \left(\frac{1}{n_a^2} - \frac{1}{n_b^2} \right) \tag{1.157}$$

where $n_b > n_a$. The selection rule (1.145) restricts the possible transitions, as illustrated in the *Grotrian diagram* in Fig. 1.4.

1.3.13 Oscillator strengths

We define the *oscillator strength*

$$f_{ka} = \frac{2m\omega_{ka}}{3\hbar} |\boldsymbol{r}_{ka}|^2 \tag{1.158}$$

where $\omega_{ka} = (E_k - E_a)/\hbar$, $E_k > E_a$ so that $f_{ka} > 0$ for absorption and $f_{ka} < 0$ for emission. We will now show that

$$\sum_k f_{ka} = 1, \tag{1.159}$$

which is the *Thomas-Reiche-Kuhn* sum rule.

We start with

$$\frac{\hbar}{\mathrm{i}} = \langle\psi_a|[p_x, x]\,|\psi_a\rangle\,. \tag{1.160}$$

Inserting unity we obtain

$$\frac{\hbar}{\mathrm{i}} = \sum_k \langle\psi_a|p_x\,|\psi_k\rangle\,\langle\psi_k|x\,|\psi_a\rangle - \sum_k \langle\psi_a|x\,|\psi_k\rangle\,\langle\psi_k|p_x\,|\psi_a\rangle\,. \tag{1.161}$$

Making use of

$$\boldsymbol{p} = m\frac{\mathrm{i}}{\hbar}[H_0, \boldsymbol{r}], \tag{1.162}$$

where H_0 is the atomic Hamiltonian, (1.35) we have

$$\begin{aligned}
\frac{\hbar}{\mathrm{i}} &= m\frac{\mathrm{i}}{\hbar}\Big(\sum_k \langle\psi_a|[H_0, x]\,|\psi_k\rangle\,\langle\psi_k|x\,|\psi_a\rangle - \sum_k \langle\psi_a|x\,|\psi_k\rangle\,\langle\psi_k|[H_0, x]\,|\psi_a\rangle\Big) \\
&= m\frac{\mathrm{i}}{\hbar}\Big(\sum_k (E_a - E_k)\langle\psi_a|x\,|\psi_k\rangle\,\langle\psi_k|x\,|\psi_a\rangle - \sum_k (E_k - E_a)\langle\psi_a|x\,|\psi_k\rangle\,\langle\psi_k|x\,|\psi_a\rangle\Big) \\
&= \frac{2m}{\mathrm{i}\hbar}\sum_k \hbar\omega_{ka}|\langle\psi_k|x\,|\psi_a\rangle\,|^2.
\end{aligned} \tag{1.163}$$

Hence,

$$1 = \frac{2m}{\hbar}\sum_k \omega_{ka}|\langle\psi_k|x\,|\psi_a\rangle\,|^2. \tag{1.164}$$

The same is obtained for y and z so that

$$3 = \frac{2m}{\hbar}\sum_k \omega_{ka}|\boldsymbol{r}_{ka}|^2, \tag{1.165}$$

and with (1.158) follows (1.159).

If continuum states are involved the sum rule is easily extended to incorporate them as well. Defining

$$\frac{\mathrm{d}f_{Ea}}{\mathrm{d}E} = \frac{2m}{3\hbar}\omega_{Ea}|\boldsymbol{r}_{Ea}|^2 \tag{1.166}$$

where E labels the energy continuum eigenstates $|\psi_E\rangle$ which are supposed to be normalized according to

$$\langle\psi_E|\psi_{E'}\rangle = \delta(E - E') \tag{1.167}$$

and

$$\boldsymbol{r}_{Ea} = \langle\psi_E|\boldsymbol{r}\,|\psi_a\rangle \tag{1.168}$$

one finds

$$\sum_k f_{ka} + \int_0^\infty \frac{\mathrm{d}f_{Ea}}{\mathrm{d}E}\,\mathrm{d}E = 1. \tag{1.169}$$

We derived the Thomas-Reiche-Kuhn sum rule only for one-electron atoms here but it similarly holds for N-electron atoms,

$$\sum_k f_{ka}^{(N)} = N, \tag{1.170}$$

where

$$f_{ka}^{(N)} = \frac{2m\omega_{ka}}{3\hbar}|\boldsymbol{R}_{ka}|^2, \qquad \boldsymbol{R}_{ka} = \sum_{i=1}^{N} \boldsymbol{r}_{ka}^{(i)}, \qquad \boldsymbol{r}_{ka}^{(i)} = \langle\psi_k|\boldsymbol{r}_i\,|\psi_a\rangle \tag{1.171}$$

($\rightarrow$ exercise).

All transition rates in dipole approximation can be expressed in terms of oscillator strengths, e.g.,

$$\tilde{W}_{ab}^{\mathrm{sD}} = \frac{2\alpha\hbar}{mc^2}\omega_{ba}^2|f_{ba}|. \tag{1.172}$$

Sum rules are useful in numerical calculations where basis sets are necessarily restricted. One can then test in how far the sum rules are "exhausted", i.e., how close one is to 1 (or N) when summing up all the oscillator strengths in the numerical implementation.

1.3.14 Spectral lines

What is the energy of a photon being emitted in the process of spontaneous emission? The most likely energy will be $\hbar\omega_{ba}$ because it fits to the energy difference of the levels involved. However, if the lifetime of one of the states (or both) is finite, we expect an uncertainty in the photon energy because of the time-energy uncertainty relation. As a consequence, spectral lines broaden. This leads to a *natural line width* for a given transition, which we will discuss first.

Starting point is (1.39),

$$\dot{c}_b(t) = \frac{1}{\mathrm{i}\hbar}\sum_j \langle\psi_b|H_{\mathrm{int}}(t)\,|\psi_j\rangle\, c_j(t)\mathrm{e}^{\mathrm{i}\omega_{bj}t}. \tag{1.173}$$

We are interested in the spontaneous decay of an initial state b to the ground state a. The final state consists of the emitted photon (characterized by its polarization and the direction of emission) and the electron in the ground state. We characterize the corresponding amplitude by $c_a(\omega, \Omega, \lambda, t)$. Retaining only the two states involved we obtain two equations, namely one where $\dot{c}_b$ is coupled with c_a,

$$\dot{c}_b(t) = -\frac{e}{2m}\frac{V}{(2\pi)^3c^3}\sum_\lambda \int \mathrm{d}\omega\,\omega^2 \int \mathrm{d}\Omega\ \hat{A}(\omega)M_{ba}^{(\lambda)}(\omega)\mathrm{e}^{\mathrm{i}(\omega_{ba}-\omega)t}c_a(\omega,\Omega,\lambda,t), \tag{1.174}$$

and another one where $\dot{c}_a$ is coupled to c_b,

$$\dot{c}_a(\omega,\Omega,\lambda,t) = \frac{e}{2m}\hat{A}(\omega)M_{ba}^{(\lambda)*}(\omega)\ \mathrm{e}^{\mathrm{i}(\omega-\omega_{ba})t}c_b(t). \tag{1.175}$$

In (1.174), we sum on the right hand side over the polarization of the emitted photon and the direction of emission, and use the density of states (1.68). In (1.175) we made use of the fact that $M_{ab}^{(\lambda)} = -M_{ba}^{(\lambda)*}$. From (1.16) for $N = 1$ photon we infer the vector potential amplitude

$$\hat{A}(\omega) = \sqrt{\frac{2\hbar}{V\varepsilon_0\omega}}. \tag{1.176}$$

In the perturbative treatment of Sec. 1.3.1 we set $c_b = 1$. Now we allow for a decay from time $t = 0$ on:

$$c_b(t) = \Theta(t)\ \mathrm{e}^{-t/(2\tau_b)}. \tag{1.177}$$

The time-evolution of the initial state wavefunction then reads

$$\psi_b(\boldsymbol{r}, t) = c_b(t)\psi_b(\boldsymbol{r})\ \mathrm{e}^{-\mathrm{i}E_b t/\hbar} = \psi_b(\boldsymbol{r})\ \mathrm{e}^{-\mathrm{i}[E_b - \mathrm{i}\hbar/(2\tau_b)]t/\hbar} \tag{1.178}$$

for $t \geq 0$. This resembles the free evolution of a wavefunction with *complex* energy

$$\mathcal{E}_b = E_b - \mathrm{i}\frac{\hbar}{2\tau_b}. \tag{1.179}$$

Inserting (1.177) into (1.175) and integrating over t yields

$$\begin{aligned} c_a(\omega, \Omega, \lambda, t) &= \frac{e}{2m}\hat{A}(\omega)M_{ba}^{(\lambda)*}(\omega)\int_0^t \mathrm{e}^{\mathrm{i}(\omega-\omega_{ba})t' - t'/(2\tau_b)}\ \mathrm{d}t'. \\ &= \frac{e}{2m}\hat{A}(\omega)M_{ba}^{(\lambda)*}(\omega)\ \frac{\mathrm{e}^{\mathrm{i}(\omega-\omega_{ba})t - t/(2\tau_b)} - 1}{\mathrm{i}(\omega - \omega_{ba}) - 1/(2\tau_b)}. \end{aligned} \tag{1.180}$$

For $t \gg \tau_b$ it is seen that the probability $|c_a(\omega, \Omega, \lambda, t)|^2$ for a photon being emitted with polarization $\boldsymbol{\varepsilon}_\lambda$ into the direction Ω is proportional to

$$\left|\frac{1}{\mathrm{i}(\omega - \omega_{ba}) - 1/(2\tau_b)}\right|^2 = \frac{1}{(\omega - \omega_{ba})^2 + 1/(4\tau_b^2)}, \tag{1.181}$$

which is maximal for $\omega = \omega_{ba}$ and half of the maximum at $\omega = \omega_{ba} \pm 1/(2\tau_b)$. Hence, introducing the *natural line width*

$$\Gamma_b = \frac{\hbar}{\tau_b} \tag{1.182}$$

we see that the probability $|c_a(\omega, \Omega, \lambda, t)|^2$ is porportional to the *Lorentzian*

$$f(\omega - \omega_{ba}) = \frac{\Gamma_b^2/(4\hbar^2)}{(\omega - \omega_{ba})^2 + \Gamma_b^2/(4\hbar^2)}, \tag{1.183}$$

whose full width half maximum (FWHM) is $\Gamma_b/\hbar$ and which is shown in Fig. 1.5. The maximum of the function f is unity for all Γ_b so that $\lim_{\Gamma_b \to 0} f = 0$. Instead, with

$$\tilde{f}(\omega - \omega_{ba}) = \frac{1}{\pi}\frac{\Gamma_b/(2\hbar)}{(\omega - \omega_{ba})^2 + \Gamma_b^2/(4\hbar^2)} \tag{1.184}$$

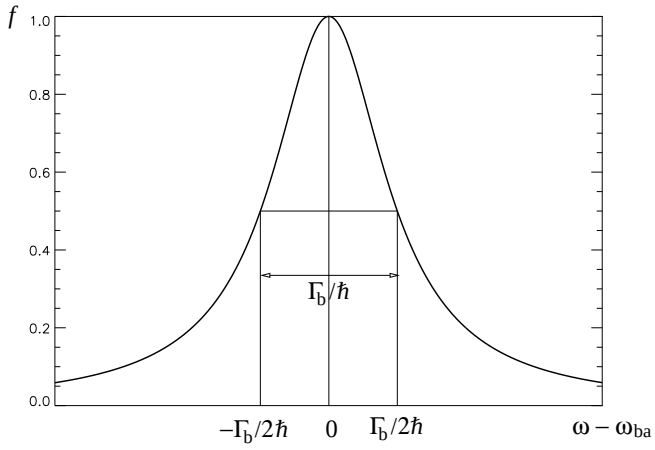

Figure 1.5: Lorentzian Eq. (1.183).

we have

$$\lim_{\Gamma_b \to 0} \tilde{f}(\omega - \omega_{ba}) = \delta(\omega - \omega_{ba}). \tag{1.185}$$

In order to determine the lifetime we insert c_a from (1.180) into the expression for $\dot{c}_b$ (1.174). This gives

$$\begin{aligned}
\dot{c}_b(t) &= -\frac{e^2}{4m^2}\frac{V}{(2\pi)^3 c^3}\sum_\lambda \int \mathrm{d}\omega\, \omega^2 \int \mathrm{d}\Omega\ \hat{A}^2(\omega)|M_{ba}^{(\lambda)}(\omega)|^2 \frac{\mathrm{e}^{-t/(2\tau_b)} - \mathrm{e}^{\mathrm{i}(\omega_{ba}-\omega)t}}{\mathrm{i}(\omega-\omega_{ba}) - 1/(2\tau_b)}. \\
&= -\frac{\hbar e^2}{2m^2}\frac{1}{\varepsilon_0(2\pi)^3 c^3}\sum_\lambda \int \mathrm{d}\omega\, \omega \int \mathrm{d}\Omega\ |M_{ba}^{(\lambda)}(\omega)|^2 \frac{\mathrm{e}^{-t/(2\tau_b)} - \mathrm{e}^{\mathrm{i}(\omega_{ba}-\omega)t}}{\mathrm{i}(\omega-\omega_{ba}) - 1/(2\tau_b)}. \\
&= -\frac{e^2}{4\pi\varepsilon_0}\frac{\hbar}{4\pi^2 m^2 c^3}\sum_\lambda \int \mathrm{d}\omega\, \omega \int \mathrm{d}\Omega\ |M_{ba}^{(\lambda)}(\omega)|^2 \left\{ \frac{\mathrm{e}^{-t/(2\tau_b)} - \mathrm{e}^{\mathrm{i}(\omega_{ba}-\omega)t}}{\mathrm{i}(\omega-\omega_{ba}) - 1/(2\tau_b)} \right\}.
\end{aligned}$$

The last term in brackets peaks sharply around $\omega = \omega_{ba}$ while $\omega|M_{ba}^{(\lambda)}(\omega)|^2$ is only slowly varying as a function of ω. Hence we can take $\omega|M_{ba}^{(\lambda)}(\omega)|^2 \simeq \omega_{ba}|M_{ba}^{(\lambda)}(\omega_{ba})|^2$ and the integral over ω can be performed using contour integration ($\rightarrow$ exercise). The result reads

$$\dot{c}_b(t) = -\frac{e^2}{4\pi\varepsilon_0}\frac{\hbar}{4\pi m^2 c^3}\sum_\lambda \int \mathrm{d}\Omega\ \omega_{ba}|M_{ba}^{(\lambda)}(\omega_{ba})|^2 \mathrm{e}^{-t/(2\tau_b)}. \tag{1.186}$$

On the other hand, from (1.177) follows

$$\dot{c}_b(t) = -\frac{1}{2\tau_b}\ \mathrm{e}^{-t/(2\tau_b)}, \qquad t > 0. \tag{1.187}$$

Equating this with (1.186) yields

$$\frac{1}{2\tau_b} = \frac{e^2}{4\pi\varepsilon_0}\frac{\hbar}{4\pi m^2 c^3}\sum_\lambda \int \mathrm{d}\Omega\ \omega_{ba}|M_{ba}^{(\lambda)}(\omega_{ba})|^2 \tag{1.188}$$

and because of

$$W_{ab}^{\mathrm{s}} = \frac{1}{\tau_b} \tag{1.189}$$

we see that

$$W_{ab}^{\mathrm{s}} = \frac{e^2}{4\pi\varepsilon_0}\frac{\hbar}{2\pi m^2 c^3}\sum_\lambda \int \mathrm{d}\Omega\ \omega_{ba}|M_{ba}^{(\lambda)}(\omega_{ba})|^2, \tag{1.190}$$

in accordance with the previously derived result (1.70).

One can show that if the state to which the transition takes place also decays the linewidth is given by

$$\Gamma = \hbar\left(\frac{1}{\tau_a} + \frac{1}{\tau_b}\right). \tag{1.191}$$

We saw in Table 1.1 that the lifetimes for hydrogenic levels with $Z = 1$ are on the order of $10^{-8}\,\mathrm{s}$. For instance, the energy of the 2p-level is $-3.4\,\mathrm{eV}$, the transition energy to the 1s ground state $13.6\,\mathrm{eV} - 3.4\ \mathrm{eV} = 10.2\,\mathrm{eV}$. The linewidth is $\Gamma = \hbar/\tau \simeq 4{\times}10^{-7}\,\mathrm{eV}$. In practice, the measured linewidths are usually much greater than the natural line widths, for reasons that will be discussed in the following.

As already suggested by (1.127) the rates of all channels via which a state b may decay should be added up so that

$$\bar{\tau}_b = \frac{1}{W_{\mathrm{tot}}}. \tag{1.192}$$

The same holds for level a and thus

$$\bar{\Gamma} = \hbar\left(\frac{1}{\bar{\tau}_a} + \frac{1}{\bar{\tau}_b}\right). \tag{1.193}$$

This increased linewidth enters (1.183).

Pressure broadening

One reason for an increased decay of levels are *collisions* between atoms. In such a collision the atoms may make transitions between state b and other states without emitting a photon (*radiationless* or *non-radiative transitions*). The collision rate is proportional to the *collision cross section* σ,

$$W_{\mathrm{c}} = nv\sigma \tag{1.194}$$

where nv is the flux, i.e., the density of atoms times their relative velocity. As the density depends (via an equation of state) on pressure, the broadening due

to collisions is also called *pressure broadening*. Both v and n depend also on the temperature. Hence, spectral lines contain information about the environment of the emitters. In fact, spectral methods are used in astrophysics to learn about stellar atmospheres and in the lab to charcterize plasmas.

Doppler broadening

Consider an atom that emits a photon of wavelength λ_0 but which moves with a velocity v towards you or away from you. In the nonrelativistic limit $v/c \ll 1$ the wavelength of the radiation will be shifted according

$$\lambda = \lambda_0 \left(1 \pm \frac{v}{c}\right) \tag{1.195}$$

(upper sign for atom moving away, lower sign for atom approaching). The corresponding angular frequency reads

$$\omega = \omega_0 \left(1 \mp \frac{v}{c}\right). \tag{1.196}$$

We assume that the atoms of mass M obey a Maxwell distribution. As a consequence, the spectral density of the emitted light will be of the form

$$u_{\rm em}(\omega) = u_{\rm em}(\omega_0)\ \exp\left[-\frac{Mv^2}{2kT}\right] = u_{\rm em}(\omega_0)\ \exp\left[-\frac{Mc^2}{2kT}\left(\frac{\omega-\omega_0}{\omega_0}\right)^2\right]. \tag{1.197}$$

The FWHM in this case reads ($\rightarrow$ exercise)

$$\Delta\omega = \frac{2\omega_0}{c}\left[\frac{2kT}{M}\ \ln 2\right]^{1/2}. \tag{1.198}$$

As expected, the Doppler linewidth increases with temperature and decreases with the atomic mass. However, note that it also depends on the central frequency ω_0 itself. Unlike the lines due to spontaneous decay and pressure broadening, Doppler broadening generates a *Gaussian* line shape, not a Lorentzian. Because the Gaussian decreases more rapidly as one moves away from the central frequency ω_0 than a Lorentzian, the wings of a spectral line are determined by the Lorentzian (see Fig. 1.6). Methods to eliminate the Doppler broadening are discussed in the experimental part of this lecture.

1.3.15 Photoelectric effect

Consider a hydrogenic atom whose electron is knocked out by a high-frequency photon of angular frequency ω and wave vector $\boldsymbol{k}$. The final state of the electron is a continuum state. The final (nonrelativistic) kinetic energy reads

$$E_f = \frac{\hbar^2 k_f^2}{2m} \ll mc^2. \tag{1.199}$$

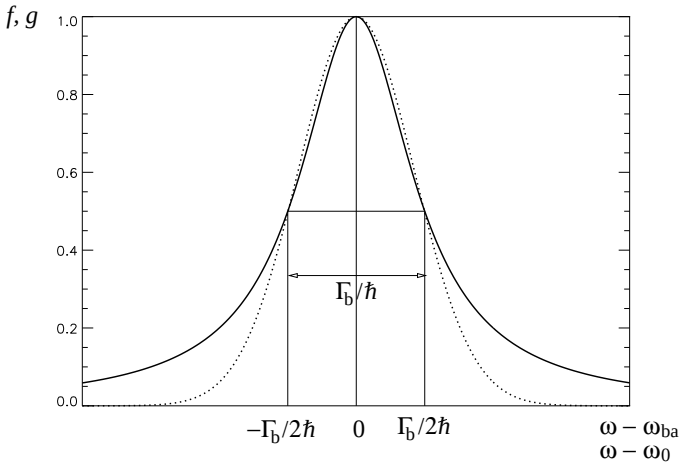

Figure 1.6: Lorentzian (solid) and Gaussian (dotted) with the same FWHM.

If we neglect the influence of the Coulomb potential on the knocked-out electron we can write its wavefunction as

$$\psi_b(\boldsymbol{k}_f, \boldsymbol{r}) = \frac{\mathrm{e}^{\mathrm{i}\boldsymbol{k}_f\cdot\boldsymbol{r}}}{(2\pi)^{3/2}}. \tag{1.200}$$

In Sec. 1.3.2, Eq. (1.55) we obtained for the absorption cross section

$$\sigma_{ba} = \frac{4\pi^2\alpha\hbar^2}{m^2\omega_{ba}}|M_{ba}(\omega_{ba})|^2\delta(\omega-\omega_{ba}). \tag{1.201}$$

The matrix element M_{ba} now governs a bound-free (b-f) transition,

$$M_{ba} \to M_{ba}^{(\mathrm{b-f})} = \frac{1}{(2\pi)^{3/2}}\int \underbrace{\mathrm{e}^{-\mathrm{i}\boldsymbol{k}_f\cdot\boldsymbol{r}}}_{\text{electron}}\ \underbrace{\mathrm{e}^{\mathrm{i}\boldsymbol{k}\cdot\boldsymbol{r}}}_{\text{photon}}\ \boldsymbol{\varepsilon}\cdot\boldsymbol{\nabla}\psi_{1s}(r)\,\mathrm{d}^3r. \tag{1.202}$$

Note that the dimension of this matrix element is not (length)$^{-1}$ anymore, as it was for a bound-bound transition, but (length)$^{1/2}$ because the plane waves (1.200) are dimensionless and normalized to the δ-function. However, by integrating (1.201) over the final wave vector the proper dimension (length)^2 is recovered for the cross section:

$$\sigma_{ba}^{(\mathrm{b-f})} = \frac{4\pi^2\alpha\hbar^2}{m^2}\int \mathrm{d}^3k_f\ \frac{1}{\omega_{ba}}|M_{ba}^{(\mathrm{b-f})}(\omega_{ba})|^2\ \delta(\omega-\omega_{ba}), \tag{1.203}$$

where now

$$\omega_{ba} = \frac{E_f - E_{1s}}{\hbar}, \tag{1.204}$$

and, because of the energy-conserving δ-function,

$$E_f = E_{1s} + \hbar\omega. \tag{1.205}$$

As

$$\mathrm{d}^3k_f = \frac{k_f m}{\hbar^2}\,\mathrm{d}E_f\,\mathrm{d}\Omega \tag{1.206}$$

we obtain

$$\begin{aligned}\sigma_{ba}^{(\mathrm{b-f})} &= \frac{4\pi^2\alpha\hbar^2}{m^2}\int \mathrm{d}E_f \int \mathrm{d}\Omega\ \frac{k_f m}{\hbar^2\omega_{ba}}|M_{ba}^{(\mathrm{b-f})}(\omega_{ba})|^2\ \delta\left(\omega - \frac{E_f - E_{1s}}{\hbar}\right)\\ &= \frac{4\pi^2\alpha\hbar^2}{m^2}\int \mathrm{d}E_f \int \mathrm{d}\Omega\ \frac{k_f m}{\hbar\omega_{ba}}|M_{ba}^{(\mathrm{b-f})}(\omega_{ba})|^2\ \delta\left(\hbar\omega - (E_f - E_{1s})\right)\\ &= \frac{4\pi^2\alpha\hbar k_f}{m\omega}\int \mathrm{d}\Omega\ |M_{ba}^{(\mathrm{b-f})}(\omega)|^2, \qquad k_f = \frac{1}{\hbar}\sqrt{2m(E_{1s}+\hbar\omega)},\end{aligned} \tag{1.207}$$

so that

$$\frac{\mathrm{d}\sigma_{ba}^{(\mathrm{b-f})}}{\mathrm{d}\Omega} = \frac{4\pi^2\alpha\hbar k_f}{m\omega}|M_{ba}^{(\mathrm{b-f})}(\omega)|^2. \tag{1.208}$$

The matrix element $M_{ba}^{(\mathrm{b-f})}$ can be integrated by parts, giving

$$M_{ba}^{(\mathrm{b-f})} = \frac{-\mathrm{i}\boldsymbol{\varepsilon}\cdot(\boldsymbol{k}-\boldsymbol{k}_f)}{(2\pi)^{3/2}}\int \mathrm{e}^{\mathrm{i}(\boldsymbol{k}-\boldsymbol{k}_f)\cdot\boldsymbol{r}}\,\psi_{1s}(r)\,\mathrm{d}^3r. \tag{1.209}$$

As the polarization direction is perpendicular to the propagation direction

$$\boldsymbol{k}\cdot\boldsymbol{\varepsilon} = 0 \tag{1.210}$$

and thus

$$\boldsymbol{\varepsilon}\cdot(\boldsymbol{k}-\boldsymbol{k}_f) = -\boldsymbol{\varepsilon}\cdot\boldsymbol{k}_f = -k_f\cos\gamma \tag{1.211}$$

with γ the angle between the direction of ejection and the polarization axis.

The integral in (1.209) is the Fourier-transform of the ground state wavefunction, i.e., with

$$\boldsymbol{K} = \boldsymbol{k} - \boldsymbol{k}_f \tag{1.212}$$

we find for a 1s hydrogenic wave function ($\rightarrow$ exercise)

$$\int \mathrm{e}^{\mathrm{i}\boldsymbol{K}\cdot\boldsymbol{r}}\,\psi_{1s}(r)\,\mathrm{d}^3r = 8\pi\left(\frac{Z^3}{\pi a_0^3}\right)^{1/2}\frac{Z/a_0}{[(Z/a_0)^2+K^2]^2}. \tag{1.213}$$

Putting everything together we obtain

$$M_{ba}^{(\mathrm{b-f})} = \frac{\mathrm{i}k_f\cos\gamma}{\pi}\left(\frac{8Z^5}{a_0^5}\right)^{1/2}\frac{1}{[(Z/a_0)^2+K^2]^2} \tag{1.214}$$

so that

$$\frac{\mathrm{d}\sigma_{ba}^{(\mathrm{b-f})}}{\mathrm{d}\Omega} = 32\alpha\frac{\hbar k_f^3}{m\omega}\frac{a_0^3Z^5\cos^2\gamma}{[Z^2+a_0^2K^2]^4}. \tag{1.215}$$

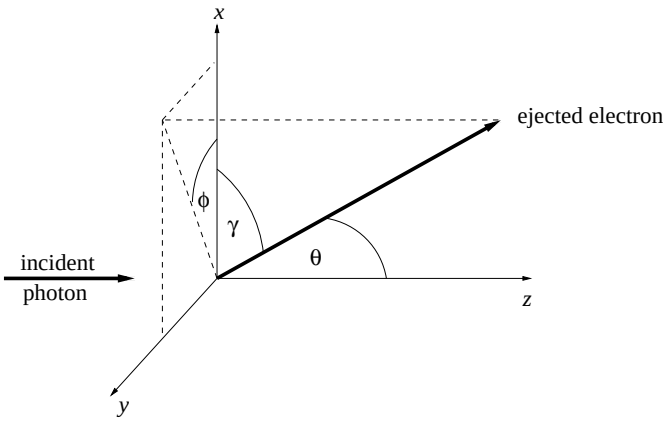

Figure 1.7: Geometry of the photoeffect.

We can choose as the propagation direction of the incident photon $\boldsymbol{e}_z$, and the polarization direction $\boldsymbol{\varepsilon} = \boldsymbol{e}_x$ (see Fig. 1.7). Then

$$\cos\gamma = \sin\theta\cos\phi. \tag{1.216}$$

Let us now study the case where the photon energy is significantly higher than the binding energy such that (see (1.205))

$$\hbar\omega = \hbar kc \simeq \frac{\hbar^2 k_f^2}{2m}, \tag{1.217}$$

i.e., (almost) the entire photon energy is converted to kinetic energy of the photo electron. Hence

$$\frac{k}{k_f} \simeq \frac{\hbar k_f}{2mc} = \frac{v_f}{2c} \ll 1. \tag{1.218}$$

In the last step we assume that the velocity of the ejected electron v_f is much smaller than the speed of light c. Then

$$K^2 = k^2 + k_f^2 - 2kk_f\cos\theta \simeq k_f^2\left(1 - 2\frac{k}{k_f}\cos\theta\right) = k_f^2\left(1 - \frac{v_f}{c}\cos\theta\right). \tag{1.219}$$

Because of

$$\hbar\omega = \frac{\hbar^2 k_f^2}{2m} \gg |E_{1s}| = \frac{Z^2}{2}\frac{e^2}{4\pi\varepsilon_0 a_0} \tag{1.220}$$

we have

$$a_0^2 k_f^2 \gg a_0^2\frac{2m}{\hbar^2}|E_{1s}| = Z^2\underbrace{\frac{m}{\hbar^2}\frac{e^2}{4\pi\varepsilon_0}}_{a_0}\ a_0 = Z^2 \tag{1.221}$$

or, with $k_f = 2\pi/\lambda_{\mathrm{dB}}$,

$$\left(\frac{a_0/Z}{\lambda_{\mathrm{dB}}}\right)^2 \gg \frac{1}{4\pi^2}, \tag{1.222}$$

which means that the de Broglie wavelength of the emitted electron (divided by the nuclear charge) should be much smaller than the Bohr radius in order to satisfy our assumption that the binding energy is much smaller than the photon energy. In the denominator of the differential cross section (1.215) appears

$$Z^2 + a_0^2 K^2 = Z^2 + a_0^2 k_f^2 \left(1 - \frac{v_f}{c}\cos\theta\right) \simeq a_0^2 k_f^2 \left(1 - \frac{v_f}{c}\cos\theta\right), \tag{1.223}$$

leading to

$$\frac{\mathrm{d}\sigma_{ba}^{(\mathrm{b-f})}}{\mathrm{d}\Omega} = 32\alpha \frac{\hbar}{m\omega}\left(\frac{Z}{a_0 k_f}\right)^5 \frac{\sin^2\theta\cos^2\phi}{\left(1 - \frac{v_f}{c}\cos\theta\right)^4}. \tag{1.224}$$

We see that the ejected photoelectrons are predominantly emitted along the polarization axis (see Fig. 1.8a). In fact, because $v_f/c \ll 1$ we have

$$\frac{\mathrm{d}\sigma_{ba}^{(\mathrm{b-f})}}{\mathrm{d}\Omega} \simeq 32\alpha \frac{\hbar}{m\omega}\left(\frac{Z}{a_0 k_f}\right)^5 \sin^2\theta\cos^2\phi\left(1 + 4\frac{v_f}{c}\cos\theta\right), \tag{1.225}$$

showing that the correction in v_f/c acts in favor of smaller θ (see Fig. 1.8c). For an unpolarized photon beam the differential cross section needs to be averaged over ϕ,

$$\frac{\mathrm{d}\sigma_{ba}^{(\mathrm{b-f})}}{\mathrm{d}\Omega} \simeq 16\alpha \frac{\hbar}{m\omega}\left(\frac{Z}{a_0 k_f}\right)^5 \sin^2\theta\left(1 + 4\frac{v_f}{c}\cos\theta\right). \tag{1.226}$$

The total cross section reads ($\rightarrow$ exercise)

$$\sigma_{\mathrm{tot}} = \frac{16\sqrt{2}\,\pi}{3}\alpha^8 Z^5 \left(\frac{mc^2}{\hbar\omega}\right)^{7/2} a_0^2. \tag{1.227}$$

It is proprtional $\sim \omega^{-7/2}$ and thus decreases with increasing photon energy, i.e., the atom becomes more transparent. The cross section increases with Z^5. One has to keep in mind that we restricted ourselves to high but nonrelativistic energies of the ejected electron, $|E_{1s}| \ll E_f \ll mc^2$. Moreover, $\alpha Z \ll 1$ for a nonrelativistic treatment of the atom being valid.

1.3.16 Scattering of radiation

The perturbative treatment of the scattering of radiation by atomic systems requires at least second-order perturbation theory because a photon is absorbed and (re-) emitted (or vice versa).

Let the initial (nondegenerate) state of the system be a, the excited state involved n, and the final state b. The absorbed photon is of energy $\hbar\omega$, the emitted one of energy $\hbar\omega'$.

In the simplest case $a = b$. Then, neglecting recoil effects ($\rightarrow$ exercise), we have elastic scattering $\omega' = \omega$, which is called *Rayleigh scattering*.

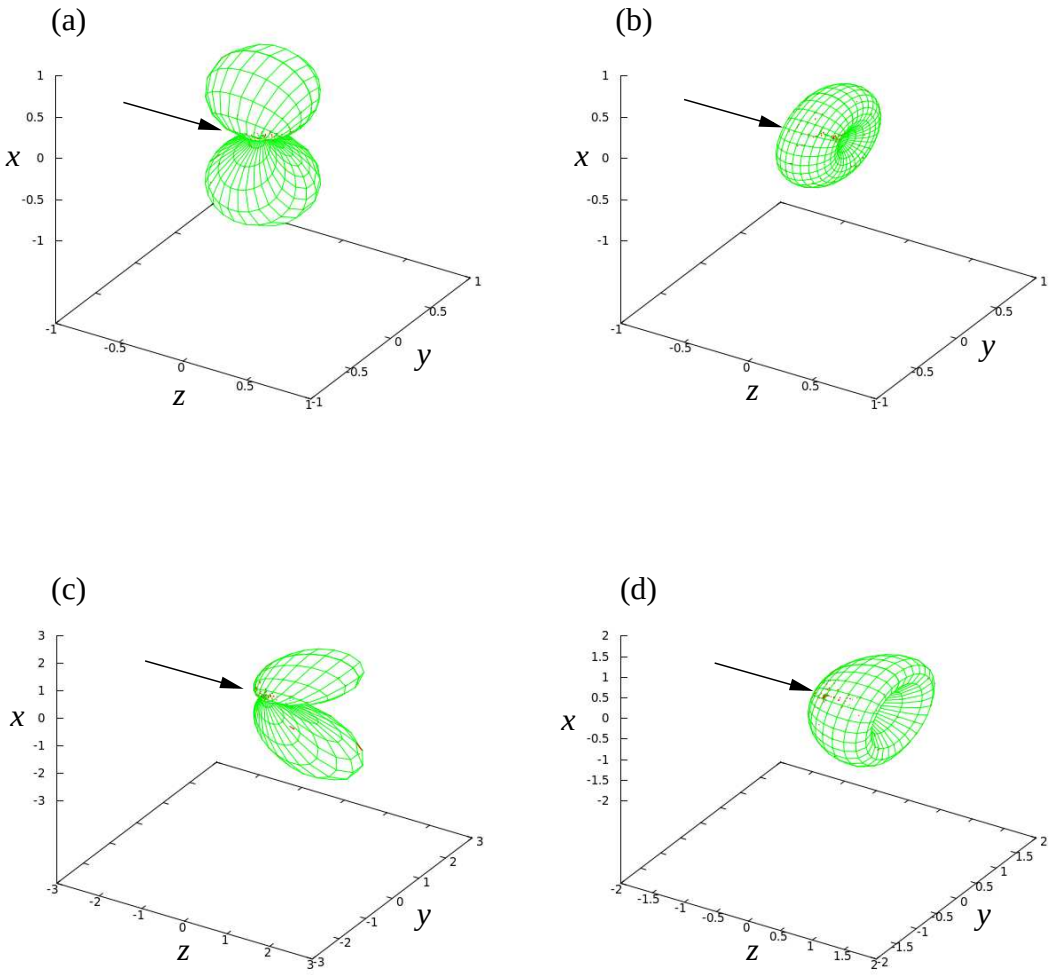

Figure 1.8: Angular distributions. 3D polar plots of the function $f(\theta,\phi) = \frac{\sin^2\theta\cos^2\phi}{\left(1-\frac{v_f}{c}\cos\theta\right)^4}$ are shown for $\frac{v_f}{c}=0$ in (a) and 0.5 in (c). The same for the ϕ-averaged function $\bar{f}(\theta) = \frac{\sin^2\theta}{2\left(1-\frac{v_f}{c}\cos\theta\right)^4}$ in (b) and (d), respectively. The arrow indicates the momentum $\hbar\boldsymbol{k}$ of the incident photon.

If initial and final state are different energy conservation requires (see Fig. 1.9)

$$\omega' = \omega - \omega_{ba}. \tag{1.228}$$

This inelastic scattering of radiation is called *Raman scattering.*

The coupled set of equations (1.39)

$$\dot{c}_b(t) = \frac{1}{\mathrm{i}\hbar} \sum_n \langle \psi_b | H_{\mathrm{int}}(t) \, | \psi_n \rangle \, c_n(t) \mathrm{e}^{\mathrm{i}\omega_{bn} t} \tag{1.229}$$

can be solved up to second order. To that end one formally integrates (1.229),

$$c_b(t) = c_b(0) + \frac{1}{\mathrm{i}\hbar} \int_0^t \mathrm{d}t' \; \sum_n \langle \psi_b | H_{\mathrm{int}}(t') \, | \psi_n \rangle \, c_n(t') \mathrm{e}^{\mathrm{i}\omega_{bn} t'}. \tag{1.230}$$

In first order one replaces $c_n(t')$ by the zeroth order $c_n(t') = c_n(0) = \delta_{na}$. Instead, we now iterate and obtain the (still formally exact) solution

$$c_b(t) = c_b(0) + \frac{1}{\mathrm{i}\hbar} \int_0^t \mathrm{d}t' \; \sum_n \langle \psi_b | H_{\mathrm{int}}(t') \, | \psi_n \rangle \, \mathrm{e}^{\mathrm{i}\omega_{bn} t'} \times \tag{1.231}$$

$$\times \left\{ c_n(0) + \frac{1}{\mathrm{i}\hbar} \int_0^{t'} \mathrm{d}t'' \; \sum_j \langle \psi_n | H_{\mathrm{int}}(t'') \, | \psi_j \rangle \, c_j(t'') \mathrm{e}^{\mathrm{i}\omega_{nj} t''} \right\}.$$

In order to obtain the result up to second order we make use of the fact that at time $t = 0$ only state a is populated and that $c_j(t'') \simeq c_j(0) = \delta_{ja}$, leading to

$$c_b(t) = \frac{1}{\mathrm{i}\hbar} \int_0^t \mathrm{d}t' \; \langle \psi_b | H_{\mathrm{int}}(t') \, | \psi_a \rangle \, \mathrm{e}^{\mathrm{i}\omega_{ba} t'} \tag{1.232}$$

$$+ \frac{1}{\mathrm{i}\hbar} \int_0^t \mathrm{d}t' \; \sum_n \langle \psi_b | H_{\mathrm{int}}(t') \, | \psi_n \rangle \, \mathrm{e}^{\mathrm{i}\omega_{bn} t'} \frac{1}{\mathrm{i}\hbar} \int_0^{t'} \mathrm{d}t'' \, \langle \psi_n | H_{\mathrm{int}}(t'') \, | \psi_a \rangle \, \mathrm{e}^{\mathrm{i}\omega_{na} t''}.$$

The first term is the "first order time-dependent perturbation theory"-result we know already. It describes absorption and emission of a photon but not the scattering processes we are interested in. Hence, in the following we consider only the second order term

$$c_b(t) = -\frac{1}{\hbar^2} \sum_n \int_0^t \mathrm{d}t' \int_0^{t'} \mathrm{d}t'' \;\; \langle \psi_b | H_{\mathrm{int}}(t') \, | \psi_n \rangle \, \langle \psi_n | H_{\mathrm{int}}(t'') \, | \psi_a \rangle \, \mathrm{e}^{\mathrm{i}(\omega_{na} t'' + \omega_{bn} t')}. \tag{1.233}$$

From the matrix element in this term one can infer immediately the process which is described: at time t'' the interaction with the radiation field $H_{\mathrm{int}}(t'')$ causes a transition from state a to some intermediate state n. Then, at time t', another interaction with the radiation field $H_{\mathrm{int}}(t')$ causes a transition from the intermediate

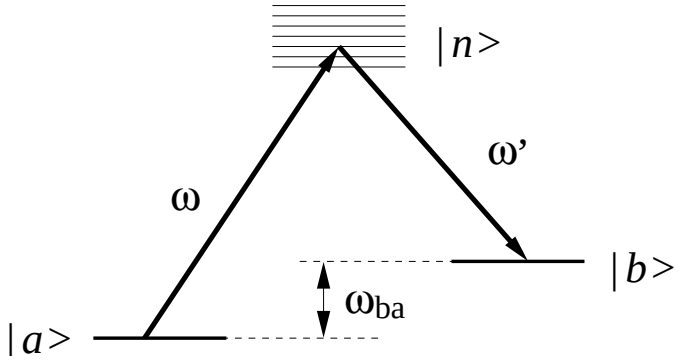

Figure 1.9: Scattering of an incoming photon of frequency ω, leading to an outgoing photon of frequency ω'. The relevant atomic states involved are the initial (ground) state a, the intermediate states n, and the final state b. The states b and a are separated by $\hbar\omega_{ba}$.

state n to the final state b. The scenario depicted in Fig. 1.9 is exactly of that kind. As the intermediate state n and the times $t'' \leq t'$ are not determined, they are summed and integrated over, respectively. If several states or times contribute, interference effects may occur. Note how the time-ordering $t'' \leq t'$ comes into play. There are also other two-photon processes described by the second-order term (1.233), not just scattering ($\rightarrow$ exercise).

One can show ($\rightarrow$ exercise) that in dipole approximation one obtains the differential cross section

$$\frac{\mathrm{d}\sigma}{\mathrm{d}\Omega} = r_0^2 \omega \omega'^3 \frac{m^2}{\hbar^2} \left| \sum_n \left[\frac{(\boldsymbol{\varepsilon}' \cdot \boldsymbol{r}_{bn})(\boldsymbol{\varepsilon} \cdot \boldsymbol{r}_{na})}{\omega_{na} - \omega} + \frac{(\boldsymbol{\varepsilon} \cdot \boldsymbol{r}_{bn})(\boldsymbol{\varepsilon}' \cdot \boldsymbol{r}_{na})}{\omega_{na} + \omega'} \right] \right|^2 . \tag{1.234}$$

Here, $\boldsymbol{\varepsilon}$, $\boldsymbol{\varepsilon}'$ are the polarization vectors of the photons ω, ω', and

$$r_0 = \frac{e^2}{4\pi\varepsilon_0 mc^2} = 2.82 \times 10^{-15}\,\mathrm{m} \tag{1.235}$$

is the *classical electron radius* (no $\hbar$ involved). The first term in (1.234) is called the *resonant term* because the incoming ω may be resonant with the transition from a to n. The second term is *off-resonant* as both ω_{na} and ω' are positive.

As one-photon transitions change the parity of the atomic system, the parity of the states a and b must be equal while the parity of the states n must be opposite to the one of a and b. For one-electron systems this implies $\Delta\ell = 0, \pm 2$.

Resonant scattering

The first denominator in (1.234) vanishes if $\omega_{na} = \omega$. This singularity is removed if we take the finite lifetimes of the states n into account. We saw in Sec. 1.3.14 that

in this case one has to replace

$$E_n \to E_n - \mathrm{i}\frac{\Gamma_n}{2}. \tag{1.236}$$

We assume that state a is the ground state and does not decay. Neglecting the off-resonant second term in (1.234) one obtains for the differential cross section in the *resonance region*

$$\frac{\mathrm{d}\sigma_{ba}}{\mathrm{d}\Omega} = r_0^2 \omega \omega'^3 \frac{m^2}{\hbar^2} \left| \frac{(\boldsymbol{\varepsilon}' \cdot \boldsymbol{r}_{bn})(\boldsymbol{\varepsilon} \cdot \boldsymbol{r}_{na})}{\omega_{na} - \mathrm{i}\Gamma_n/(2\hbar) - \omega} \right|^2 \tag{1.237}$$

and for the total cross section

$$\sigma_{ba}(\omega) = r_0^2 \omega \omega'^3 \frac{m^2}{\hbar^2} \frac{1}{(\omega - \omega_{na})^2 + \Gamma_n^2/(4\hbar^2)} \int \mathrm{d}\Omega \ \left| (\boldsymbol{\varepsilon}' \cdot \boldsymbol{r}_{bn})(\boldsymbol{\varepsilon} \cdot \boldsymbol{r}_{na}) \right|^2 . \tag{1.238}$$

If $\omega = \omega'$ ($E_a = E_b$) the scattered radiation is called *resonance radiation*, if $\omega > \omega'$ (ω' cannot be bigger than ω if a is the ground state) *resonance fluorescence* or resonant Raman scattering. Resonant scattering occurs naturally if the radiation emitted by one sort of atoms impinges on atoms of the same sort.

Non-resonant scattering

Let us consider again (1.234)

$$\frac{\mathrm{d}\sigma}{\mathrm{d}\Omega} = r_0^2 \omega \omega'^3 \frac{m^2}{\hbar^2} \left| \sum_n \left[\frac{(\boldsymbol{\varepsilon}' \cdot \boldsymbol{r}_{bn})(\boldsymbol{\varepsilon} \cdot \boldsymbol{r}_{na})}{\omega_{na} - \omega} + \frac{(\boldsymbol{\varepsilon} \cdot \boldsymbol{r}_{bn})(\boldsymbol{\varepsilon}' \cdot \boldsymbol{r}_{na})}{\omega_{na} + \omega'} \right] \right|^2$$

in the Rayleigh-case, i.e., $a = b$, $\omega = \omega'$, so that

$$\frac{\mathrm{d}\sigma}{\mathrm{d}\Omega} = r_0^2 \omega^4 \frac{m^2}{\hbar^2} \left| \sum_n (\boldsymbol{\varepsilon}' \cdot \boldsymbol{r}_{an})(\boldsymbol{\varepsilon} \cdot \boldsymbol{r}_{na}) \frac{2\omega_{na}}{\omega_{na}^2 - \omega^2} \right|^2 . \tag{1.239}$$

As the ground state a is an s-state ($\ell_a = 0$), the intermediate states n must be p-states $\ell_n = 1$. If we consider linear polarization with $\boldsymbol{\varepsilon}$ along the z-axis, $\boldsymbol{\varepsilon} = \boldsymbol{e}_z$, we have

$$\boldsymbol{\varepsilon} \cdot \boldsymbol{r}_{na} = z_{na}. \tag{1.240}$$

From (1.142) we know that

$$m_n = 0 \tag{1.241}$$

so that ($\to$ exercise)

$$\boldsymbol{r}_{an} = (0, 0, z_{an}) \tag{1.242}$$

and thus

$$\boldsymbol{\varepsilon}' \cdot \boldsymbol{r}_{an} = \varepsilon'_z z_{an} = (\boldsymbol{\varepsilon} \cdot \boldsymbol{\varepsilon}') z_{an}. \tag{1.243}$$

As a consequence

$$\begin{aligned}\frac{\mathrm{d}\sigma}{\mathrm{d}\Omega} &= r_0^2\omega^4\frac{m^2}{\hbar^2}\left|\sum_n(\boldsymbol{\varepsilon}'\cdot\boldsymbol{r}_{an})(\boldsymbol{\varepsilon}\cdot\boldsymbol{r}_{na})\frac{2\omega_{na}}{\omega_{na}^2-\omega^2}\right|^2 \\ &= r_0^2\omega^4\frac{m^2}{\hbar^2}(\boldsymbol{\varepsilon}\cdot\boldsymbol{\varepsilon}')^2\left|\sum_n|z_{an}|^2\,\frac{2\omega_{na}}{\omega_{na}^2-\omega^2}\right|^2. \qquad (1.244)\end{aligned}$$

Low-frequency limit. If $\omega^2 \ll \omega_{na}^2$ for all n then

$$\frac{\mathrm{d}\sigma}{\mathrm{d}\Omega} = r_0^2\omega^4\frac{m^2}{\hbar^2}(\boldsymbol{\varepsilon}\cdot\boldsymbol{\varepsilon}')^2\underbrace{\left|\sum_n|z_{an}|^2\,\frac{2}{\omega_{na}}\right|^2}_{(\hbar\bar{\alpha}_z/e^2)^2} \qquad (1.245)$$

with

$$\bar{\alpha}_z = 2e^2\sum_{n\neq a}\frac{|z_{an}|^2}{E_n-E_a} \qquad (1.246)$$

the *static dipole polarizability* of the atom in state a. It governs the electric dipole $\boldsymbol{p}_{\mathrm{el}}$ that is produced when a static electric field $\boldsymbol{E}$ is applied,

$$\boldsymbol{p}_{\mathrm{el}} = \bar{\alpha}\boldsymbol{E}, \qquad (1.247)$$

and in general is a tensor. We can write the differential cross section as

$$\frac{\mathrm{d}\sigma}{\mathrm{d}\Omega} = r_0^2\omega^4\left(\frac{m\bar{\alpha}_z}{e^2}\right)^2(\boldsymbol{\varepsilon}\cdot\boldsymbol{\varepsilon}')^2. \qquad (1.248)$$

The strong ω dependence shows that short-wavelength light is scattered more efficiently (explanation of why the sky is blue). Finally, the total cross section turns out to be

$$\sigma_{\mathrm{tot}} = \frac{8\pi}{3}\left(\frac{r_0 m\bar{\alpha}_z}{e^2}\right)^2\omega^4. \qquad (1.249)$$

High-frequency limit. In this case

$$\frac{\mathrm{d}\sigma}{\mathrm{d}\Omega} = 4r_0^2\frac{m^2}{\hbar^2}(\boldsymbol{\varepsilon}\cdot\boldsymbol{\varepsilon}')^2\left|\sum_n|z_{an}|^2\,\omega_{na}\right|^2. \qquad (1.250)$$

From the sum rule (1.164),

$$1 = \frac{2m}{\hbar}\sum_n\omega_{na}|z_{na}|^2, \qquad (1.251)$$

we infer

$$\begin{aligned}\frac{\mathrm{d}\sigma}{\mathrm{d}\Omega} &= \frac{\hbar^2}{4m^2}\,4r_0^2\frac{m^2}{\hbar^2}(\boldsymbol{\varepsilon}\cdot\boldsymbol{\varepsilon}')^2 \\ &= r_0^2(\boldsymbol{\varepsilon}\cdot\boldsymbol{\varepsilon}')^2. \qquad (1.252)\end{aligned}$$

This is the differential cross section for *Thomson scattering*. The total rate reads (→ exercise)

$$\sigma_{\text{tot}} = \frac{8\pi}{3} r_0^2. \tag{1.253}$$

There is no state-dependence left whatsoever, so it may be applied to the scattering on free electrons as well. Note that the two limits discussed do not involve $\hbar$. In fact, they can be derived also classically (→ Jackson). As our calculations are based on nonrelativistic theory $\hbar\omega \ll mc^2$ must be satisfied (unlike in Compton scattering).

1.4 Mechanical effects of light

James Clerk Maxwell derived in 1861 that a light beam of intensity I impinging on a surface of reflectivity R exerts a *light pressure*

$$P_{\text{L}} = (1+R)\frac{I}{c}. \tag{1.254}$$

This formula is most easily derived in terms of photons. Momentum conservation

$$p_{\text{before}} = N\hbar k = p_{\text{after}} = -RN\hbar k + p_{\text{body}} \tag{1.255}$$

yields

$$\Delta p = p_{\text{body}} = (1+R)\ N\hbar k \tag{1.256}$$

or, because of $\omega = kc$,

$$\Delta p\ c = (1+R)\ N\hbar\omega. \tag{1.257}$$

We consider N photons inside a volume $V = Ad$ in front of the surface so that

$$\frac{\Delta p}{A} \underbrace{\frac{c}{d}}_{1/\Delta t} = (1+R)\ \frac{N\hbar\omega}{V} \tag{1.258}$$

where Δt is the time intervall within which all the photons inside the volume hit the surface. With $\Delta p/\Delta t = F$ we have

$$\frac{F}{A} = P_{\text{L}} = (1+R)\ \frac{N\hbar\omega}{V} = (1+R)\ \frac{I}{c}. \tag{1.259}$$

The formula (1.254) suggests that a flake of matter coated such that it has a high reflectivity ($R \simeq 1$, silver) on one side and $R \simeq 0$ (black) on the other should set into motion if it is illuminated isotropically. The commercially available light mills seem to work in that way. However, their motion is not directly driven by radiation, as they move into the "wrong" direction. If light pressure is the driving force the vanes should move in the direction of the normal of the black surface because the light pressure is higher on the other (silver) side. In fact, the motion stops if the whole

setup is put into a high vacuum, indicating that the heating of the gas molecules plays the essential role (→ exercise). The direct measurement of light pressure in the lab requires more sophisticated setups. It has been first done in 1901 by Nichols and Hull[11] and by Lebedev.[12] At that time research on light pressure was mainly motivated by astrophysics. Only with the invention of the laser it became relevant also for lab experiments.

1.4.1 Ponderomotive force

The Lorentz-force on a particle of charge q is given by (SI units)

$$\boldsymbol{F} = q[\boldsymbol{E}(\boldsymbol{r},t) + \boldsymbol{v} \times \boldsymbol{B}(\boldsymbol{r},t)]. \tag{1.260}$$

This force $\boldsymbol{F} = \dot{\boldsymbol{p}}$ is also relativistically correct. In our case we have in mind $\boldsymbol{E}$ and $\boldsymbol{B}$ making up the electromagnetic field of a laser pulse, that is,

$$\boldsymbol{E}(\boldsymbol{r},t) = \hat{\boldsymbol{E}}(\boldsymbol{r},t)\ \mathrm{e}^{\mathrm{i}\omega t} \tag{1.261}$$

and, because of $\boldsymbol{\nabla} \times \boldsymbol{E} = -\partial_t \boldsymbol{B}$,

$$\boldsymbol{B}(\boldsymbol{r},t) = \frac{\mathrm{i}}{\omega}\boldsymbol{\nabla} \times \boldsymbol{E}(\boldsymbol{r},t), \tag{1.262}$$

but the derivation also holds for longitudinal waves as they occur in plasmas. The derivation of the ponderomotive force relies on the possibility to separate the relevant time scales: the "fast" motion on the time scale of the laser period $2\pi/\omega$ and a "secular" (slow) one due to the ponderomotive force. Hence we assume that $\hat{\boldsymbol{E}}(\boldsymbol{r},t)$, apart from containing $\mathrm{e}^{-\mathrm{i}\boldsymbol{k}\cdot\boldsymbol{r}}$, describes the laser field envelope, having only a "slow" time-dependence so that $\partial_t \boldsymbol{B} = \mathrm{i}\omega\boldsymbol{B}$ to high accuracy.

In lowest order the particle just oscillates around its current position $\boldsymbol{r}_0$ due to the electric field (the possible slow time-dependence in $\hat{\boldsymbol{E}}$ is suppressed for notational convenience):

$$m\ddot{\boldsymbol{r}}_1 = q\hat{\boldsymbol{E}}(\boldsymbol{r}_0)\mathrm{e}^{\mathrm{i}\omega t}. \tag{1.263}$$

The corresponding velocity and position are

$$\dot{\boldsymbol{r}}_1 = -\frac{\mathrm{i}q}{m\omega}\hat{\boldsymbol{E}}(\boldsymbol{r}_0)\mathrm{e}^{\mathrm{i}\omega t}, \qquad \boldsymbol{r}_1 = -\frac{q}{m\omega^2}\hat{\boldsymbol{E}}(\boldsymbol{r}_0)\mathrm{e}^{\mathrm{i}\omega t}. \tag{1.264}$$

In the next higher order one has

$$m\ddot{\boldsymbol{r}}_2 = q[(\boldsymbol{r}_1 \cdot \boldsymbol{\nabla})\boldsymbol{E}(\boldsymbol{r}_0,t) + \dot{\boldsymbol{r}}_1 \times \boldsymbol{B}(\boldsymbol{r}_0,t)] \tag{1.265}$$

[11] E.F. Nichols and G.F. Hull, *A preliminary communication on the pressure of heat and light radiation*, Phys. Rev. **13**, 307 (1901); *The pressure due to radiation*, Astrophys. J., **17**, 315 (1903).

[12] P. Lebedev, *Untersuchungen über die Druckkräfte des Lichtes*, Ann. Phys. **6**, 433 (1901).

where the electric field has been expanded around $\boldsymbol{r}_0$. So far we used complex fields and implicitly understood that the real part has to be taken. Now the calculation becomes nonlinear and this trick is not applicable anymore. Hence we write

$$\begin{aligned} m\ddot{\boldsymbol{r}}_2 &= q\Big(-\frac{q}{4m\omega^2}(\hat{\boldsymbol{E}}\mathrm{e}^{+}+\hat{\boldsymbol{E}}^{*}\mathrm{e}^{-})\cdot\boldsymbol{\nabla}(\hat{\boldsymbol{E}}\mathrm{e}^{+}+\hat{\boldsymbol{E}}^{*}\mathrm{e}^{-}) \\ &\qquad +\frac{q}{4m\omega^2}(-\mathrm{i}\hat{\boldsymbol{E}}\mathrm{e}^{+}+\mathrm{i}\hat{\boldsymbol{E}}^{*}\mathrm{e}^{-})\times\boldsymbol{\nabla}\times(\mathrm{i}\hat{\boldsymbol{E}}\mathrm{e}^{+}-\mathrm{i}\hat{\boldsymbol{E}}^{*}\mathrm{e}^{-})\Big) \qquad (1.266) \\ &= -\frac{q^2}{4m\omega^2}[\hat{\boldsymbol{E}}\cdot\boldsymbol{\nabla}\hat{\boldsymbol{E}}^{*}+\hat{\boldsymbol{E}}\times\boldsymbol{\nabla}\times\hat{\boldsymbol{E}}^{*}+\mathrm{c.c.}+\Omega_{2\omega}] \qquad (1.267) \end{aligned}$$

with $\mathrm{e}^{\pm}=\mathrm{e}^{\pm\mathrm{i}\omega t}$ and $\Omega_{2\omega}$ collecting all terms $\sim\mathrm{e}^{\pm\mathrm{i}2\omega t}$ which disappear upon averaging over a laser period (symbolized by an overline, i.e., for some time-dependent quantity $\langle f(t)\rangle_t=\overline{f(t)}=\overline{f}$ where $\overline{f}$ may still be time-dependent but only on a slower time scale),

$$m\overline{\ddot{\boldsymbol{r}}_2}=-\frac{q^2}{4m\omega^2}[\hat{\boldsymbol{E}}\cdot\boldsymbol{\nabla}\hat{\boldsymbol{E}}^{*}+\hat{\boldsymbol{E}}\times\boldsymbol{\nabla}\times\hat{\boldsymbol{E}}^{*}+\mathrm{c.c.}]. \qquad (1.268)$$

Using the identity

$$\boldsymbol{C}\times\boldsymbol{\nabla}\times\boldsymbol{D}+\boldsymbol{D}\times\boldsymbol{\nabla}\times\boldsymbol{C}+\boldsymbol{C}\cdot\boldsymbol{\nabla}\boldsymbol{D}+\boldsymbol{D}\cdot\boldsymbol{\nabla}\boldsymbol{C}=\boldsymbol{\nabla}\boldsymbol{C}\cdot\boldsymbol{D} \qquad (1.269)$$

we finally obtain the nonrelativistic ponderomotive force

$$\boldsymbol{F}_{\mathrm{p}}=m\overline{\ddot{\boldsymbol{r}}_2}=-\frac{q^2}{4m\omega^2}\boldsymbol{\nabla}|\hat{\boldsymbol{E}}(\boldsymbol{r},t)|^2. \qquad (1.270)$$

In $\hat{\boldsymbol{E}}(\boldsymbol{r},t)$ the position $\boldsymbol{r}$ now refers to the so-called *oscillation center*. We remind that the time dependence of the envelope must be "slow" as compared to the laser period because otherwise the separation of time-scales used in the derivation makes no sense. The ponderomotive force (1.270) can obviously be derived from the *ponderomotive potential*

$$\Phi_{\mathrm{p}}(\boldsymbol{r},t)=\frac{q^2}{4m\omega^2}|\hat{\boldsymbol{E}}(\boldsymbol{r},t)|^2 \qquad (1.271)$$

which is proportional to the laser intensity and independent of the sign of the particle's charge: it is always repulsive. Hence *all* charged particles are expelled from regions of high laser intensity (e.g., the laser focus). However, owing to the mass m in the denominator the immediate effect on electrons is much larger than on ions. The ponderomotive force is inverse proportional to the square of the laser frequency, meaning that its significance increases with increasing laser wavelength (despite the fact that the photons become less energetic).

In order for the derivation being valid, the particle must not oscillate "too much" around $\boldsymbol{r}_0$. More precisely, the conditions read

$$|\dot{\boldsymbol{r}}_1|\ll c, \qquad \boldsymbol{k}\cdot\boldsymbol{r}_1\ll 1 \qquad (1.272)$$

for an electromagnetic wave and a longitudinal wave, respectively. As a consequence, (1.271) is not applicable to relativistically intense laser pulses. The analytical expression for the relativistic ponderomotive force exerted by a plane-wave laser pulse can be also derived.[13]

The ponderomotive potential (at a certain position $\boldsymbol{r}$) equals the average quiver energy of the charged particle in the laser field (at that position). In fact, taking $\dot{\boldsymbol{r}}_1$ from (1.264) yields

$$U_\mathrm{p} = \frac{1}{2} m \overline{\dot{\boldsymbol{r}}_1^{\,2}} = \frac{q^2}{4m\omega^2} |\hat{\boldsymbol{E}}|^2. \tag{1.273}$$

Is there a connection between this mere number U_p and the potential Φ_p? Consider a spatially finite field structure which leads to Φ_p. Now, think of a particle injected into this structure with some kinetic energy W_0. While strolling through the field structure the particle will encounter regions of varying Φ_p. In regions of high Φ_p it will oscillate with larger amplitude (high U_p) than in regions of low Φ_p (low U_p). After averaging out the fast time scales, the whole system is conservative so that $W + U_\mathrm{p} = W_0$. This means that the *local* U_p indeed serves as a potential and is just the Φ_p derived above.

Ponderomotive force of a standing wave

The case of standing waves is of particular interest because standing waves provide the strongest field gradients possible for a given wavelength. Optical lattices can be constructed with crossed laser beams. On the lattice sites particles can be trapped. As the laser parameters allow to tune the features of such lattices, new solid state-like few and many-particle systems can be studied in a systematic and well-controllable way.

Let us consider the standing wave

$$\boldsymbol{E}(\boldsymbol{r}, t) = \hat{\boldsymbol{E}} \mathrm{e}^{\mathrm{i}\omega t} (\mathrm{e}^{-i\boldsymbol{k}\cdot\boldsymbol{r}} + \mathrm{e}^{i\boldsymbol{k}\cdot\boldsymbol{r}}) = 2\hat{\boldsymbol{E}} \mathrm{e}^{\mathrm{i}\omega t} \cos(\boldsymbol{k}\cdot\boldsymbol{r}). \tag{1.274}$$

Comparing this with (1.261) we identify

$$\hat{\boldsymbol{E}}(\boldsymbol{r}, t) = 2\hat{\boldsymbol{E}} \cos(\boldsymbol{k}\cdot\boldsymbol{r}) \tag{1.275}$$

and can immediately use expressions (1.270) and (1.271) to give

$$\Phi_\mathrm{p}(\boldsymbol{r}, t) = \frac{q^2 |\hat{\boldsymbol{E}}|^2}{m\omega^2} \cos^2(\boldsymbol{k}\cdot\boldsymbol{r}), \qquad \boldsymbol{F}_\mathrm{p}(\boldsymbol{r}, t) = \frac{q^2 |\hat{\boldsymbol{E}}|^2}{m\omega^2} \boldsymbol{k} \sin(2\boldsymbol{k}\cdot\boldsymbol{r}). \tag{1.276}$$

The ponderomotive force will push the particle towards the nodes of the standing wave where the field vanishes. Depending on its initial velocity, the particles may be trapped inside the "valleys" of the standing wave. If we assume that the propagation

[13] See, e.g., P. Mulser and D. Bauer, *High-Power Laser-Matter Interaction*, (Springer, Berlin Heidelberg, 2010).

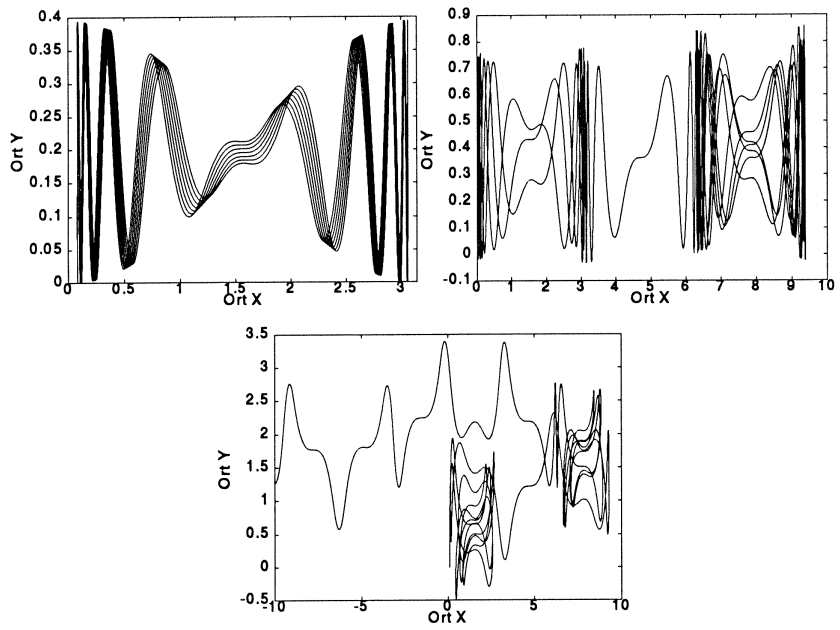

Figure 1.10: Trajectories of an electron in a standing laser wave (1.274) (polarized along $\boldsymbol{e}_y$, propagation directions along $\boldsymbol{e}_x$) that starts at $t = 0$ from $y = 0$ and $kx = \pi/40$. The amplitudes were $e\hat{A}/mc = -e\hat{E}/m\omega c = -0.1$ (upper left), -0.2 (upper right), and -0.5 (lower). With increasing laser intensity, the electron is able to escape from the "valley" in which it is released. It can then be trapped temporarily in other valleys (upper right and lower plot), and the dynamics can be shown to become chaotic.

direction is $\boldsymbol{e}_x$ and expand the force around the position of a node, we obtain a ponderomotive force of the form

$$F_{\rm p}^{\text{"valley"}} \simeq -\Omega^2 x, \qquad \Omega^2 = \frac{2q^2|\hat{E}|^2}{mc^2}. \tag{1.277}$$

The trapped particle will thus undergo harmonic secular motion with a frequency Ω that is proportional to the electric field (which reminds of the Rabi-frequency in resonant laser-atom interaction, to be discussed later on). However, since the frequency increases with the field strength, the whole idea of separation of time scales breaks down at some point. In fact, the numerical solution of the (relativistic) equations of motion shows that for sufficiently high field strengths the particle may leave the valley in which it was trapped. The motion can be shown to be chaotic then. The particle may be temporarily trapped in other valleys, leaving them again, and strolling around erratically (cf. Fig. 1.10).

It is clear from the ponderomotive force (1.276) that a standing wave pattern may be used as a grating with a separation of "slits" that is half a laser wavelength

(*Kapitza-Dirac effect*). Particles injected perpendicular to the propagation direction of the two laser beams will be deflected. If the de Broglie wavelength is chosen properly, a detector on the opposite side will measure an interference pattern.

*Ponderomotive force on a classical dipole in a standing wave

This part has not been discussed in the lecture. It is included here for the sake of completeness and for the interested students.

Consider two particles both of mass m but with opposite charge $\pm e$ in a standing laser wave (1.274),

$$\boldsymbol{E}(\boldsymbol{r},t) = \Re\hat{\boldsymbol{E}}\mathrm{e}^{\mathrm{i}\omega t}(\mathrm{e}^{-i\boldsymbol{k}\cdot\boldsymbol{r}} + \mathrm{e}^{i\boldsymbol{k}\cdot\boldsymbol{r}}) = 2\hat{\boldsymbol{E}}\cos(\omega t)\cos(\boldsymbol{k}\cdot\boldsymbol{r}). \tag{1.278}$$

The two particles are coupled by a spring of constant D and oriented along the polarization axis of the laser, $\boldsymbol{e}_y$. The propagation direction of the standing laser field is along x. The vector potential reads

$$\boldsymbol{A}(x,t) = \hat{A}(x)\boldsymbol{e}_y\sin(\omega t), \tag{1.279}$$

where $\hat{A}(x) = -2(\hat{E}/\omega)\cos kx$ is a slowly varying spatial pulse envelope.

This is probably the simplest nontrivial model for a *neutral* system with an *internal* degree of freedom. We are now interested in the secular motion of the center of mass. The particle dynamics takes place in the xy-plane with the particle positions (x_+, y_+), (x_-, y_-). We can choose initial conditions such that (i) the particles behave identically in x-direction ($\rightarrow$ exercise) and, (ii),

$$y_+ = -y_- \tag{1.280}$$

at all times. Then only the distance $y_+ - y_-$ is relevant (the y-component of the center of mass remains at rest) and the new coordinates

$$\ell = \frac{y_+ - y_-}{2}, \qquad X = x_+ = x_- \tag{1.281}$$

are sufficient to describe the dynamics.

Instead of separating the equations of motion according timescales we will now average the Lagrangian[14]

$$L(X,\dot{X},\ell,\dot{\ell},t) = \frac{1}{2}M\dot{X}^2 + \frac{1}{2}M\dot{\ell}^2 - 2eA(X,t)\dot{\ell} - 2D\ell^2 \tag{1.282}$$

where

$$M = 2m \tag{1.283}$$

[14]Note that $S = \int L\,\mathrm{d}t$ is the action. Hence, the time-average of the Lagrangian over one oscillation period is proportional to the corresponding difference in action ($\rightarrow$ *adiabatic invariants*).

is the total mass. The full equations of motion follow from

$$\frac{\partial L}{\partial \dot{X}} = M\dot{X}, \qquad \frac{\partial L}{\partial \dot{\ell}} = M\dot{\ell} - 2eA(X,t), \tag{1.284}$$

$$\frac{\partial L}{\partial X} = -2eA'(X,t)\dot{\ell}, \qquad \frac{\partial L}{\partial \ell} = -4D\ell \tag{1.285}$$

as

$$m\ddot{X} = -eA'(X,t)\dot{\ell} = e\dot{\ell}[k\hat{A}(x)\cos\omega t - \hat{A}'(x)\sin\omega t], \tag{1.286}$$

$$m\ddot{\ell} - e\dot{A}(X,t) = -2D\ell \tag{1.287}$$

so that

$$\ddot{\ell} + \underbrace{\frac{2D}{m}}_{\Omega^2}\ell = \frac{e}{m}[\hat{A}'(X)\dot{X}\sin\omega t + \hat{A}(X)\omega\cos\omega t]. \tag{1.288}$$

In lowest order the two charges oscillate at a constant position X, i.e., $\dot{X} = 0$ and the driven harmonic oscillator results:

$$\ddot{\ell} + \Omega^2\ell = \frac{e}{m}\hat{A}(X)\omega\cos\omega t. \tag{1.289}$$

The solution for the initial conditions $\ell(0) = \dot{\ell}(0) = 0$ is

$$\ell(t) = \underbrace{\frac{e}{m}\hat{A}(X)\frac{\omega}{\Omega^2 - \omega^2}}_{=:\xi(X)}[\cos\omega t - \cos\Omega t]\,. \tag{1.290}$$

The Lagrangian for the secular motion in X is now obtained by averaging:

$$\overline{L(X,\dot{X},\ell,\dot{\ell})} = \overline{\frac{1}{2}M\dot{X}^2 + \frac{1}{2}M\dot{\ell}^2 - 2eA(X,t)\dot{\ell} - 2D\ell^2}. \tag{1.291}$$

While $\ell(t)$ has a fast time-dependence, $X(t)$ has only a slow time-dependence so that $X = \overline{X}$,

$$\overline{\frac{1}{2}M\dot{X}^2} = \frac{1}{2}M\dot{\overline{X}}^2 = \frac{1}{2}M\dot{X}^2 \tag{1.292}$$

and thus

$$\overline{L}(X,\dot{X}) = \frac{1}{2}M\dot{X}^2 + \frac{1}{2}M\overline{\dot{\ell}^2} - 2e\overline{A(X,t)\dot{\ell}} - 2D\overline{\ell^2}, \tag{1.293}$$

i.e., ℓ and $\dot{\ell}$ will disappear due to cycle-averaging.

We assume the oscillator frequency Ω and the driver frequency ω to be commensurate:

$$\Omega = n\omega, \qquad n \neq 1, \qquad n = 2,3,\ldots \qquad \text{or} \qquad n = \frac{1}{2},\frac{1}{3},\frac{1}{4},\ldots \tag{1.294}$$

(depending on whether ω or Ω is greater) so that no beating frequencies appear. Then, using

$$\overline{\ell^2} = \xi^2(X), \tag{1.295}$$

$$\overline{\dot{\ell}^2} = \frac{1}{2}\xi^2(X)\left[\Omega^2 + \omega^2\right], \tag{1.296}$$

$$\overline{A(X,t)\dot{\ell}} = -\frac{1}{2}\xi(X)\hat{A}(X)\omega, \tag{1.297}$$

the secular Lagrange function $\overline{L}' = \overline{L}/2$,

$$\overline{L}'(X,\dot{X}) = \frac{1}{2}m\dot{X}^2 - \frac{\omega^2}{\omega^2-\Omega^2}\frac{e^2\hat{A}^2(X)}{4m} \tag{1.298}$$

is obtained, and the ponderomotive potential

$$\Phi_{\rm p}(\boldsymbol{r},t) = \frac{\omega^2}{\omega^2-\Omega^2}\frac{e^2\hat{A}^2(X)}{4m} \tag{1.299}$$

can be inferred.

We observe the following: (i) for $\Omega = 0$ (i.e., no spring) the standard ponderomotive potential for the charged particle (1.270) is recovered ($\hat{E} = -\omega\hat{A}$); (ii) for nonvanishing Ω the ponderomotive force is enhanced as long as $\Omega < \omega$; (iii) the sign of the ponderomotive force changes when $\Omega > \omega$, which means that the dipole is accelerated towards regions of higher radiation intensity (so-called *high-field seekers*); (iv) for $\omega \simeq \Omega$ the ponderomotive force is large (we ignored damping); (v) for $\Omega \gg \omega$ the ponderomotive force tends to zero because the particles are so tightly bound together that they cannot oscillate in y-direction—and without any fast dynamics in first order no secular motion results.

The motion of a charged particle in an electromagnetic wave plus a static, homogeneous magnetic field yields a very similar result in which the cyclotron frequency plays the role of the harmonic oscillator frequency above ($\rightarrow$ exercise).

Some remarks

In the physics of laser-matter interaction, the importance of the ponderomotive potential is hard to overestimate. In many effects it sets the relevant energy scale, as we shall see later on. In laser-atom interaction, for instance, $U_{\rm p}$ determines not only the cut-offs of photoelectron and harmonics spectra but also equals the AC Stark-shift of the continuum. In laser-plasma physics, instabilities can be understood in terms of the ponderomotive force.

As a historical side remark it should be mentioned that the ponderomotive force has been re-invented several times in the literature although it is derived already in Landau & Lifshitz's *Mechanics* volume.

What we did in this Section in order to obtain a potential for the *oscillation center* is done in the physics of magnetized plasmas for the so-called *guiding center*.

In the same way we got rid of the fast but uninteresting oscillations on the time scale of a laser period (and twice the laser period), the fast cyclotron motion around the field lines of a strong magnetic field is eliminated, and what remains is the equation of motion of the "guiding center".

The method of separation of time scales was originally invented for the study of celestial mechanics. This is also where the term *secular motion* comes from. The effect of Jupiter on the earth's motion around the sun, for instance, is negligible on the time scale of a few years but may have to be taken into account on longer time scales. One practical advantage of the separation of time scales is for numerical simulations. Imagine you want to simulate one second of the laser plasma dynamics using a fluid code. All effects you are interested in happen on the time scale of, say, microseconds or longer. However, there is this oscillatory motion in the laser field on a ten order of magnitude shorter time scale. Resolving this with the fluid code would lead to run-times of years. However, all you need are the secular effects generated by the laser pulse. The ponderomotive potential comes to your rescue: there only the laser pulse *envelope* enters while the time scales of the laser period (and faster) are adiabatically eliminated.

1.4.2 *Relativistic dynamics of a charged particle in an electromagnetic wave

This Section (including Subsections) has not been discussed in the lecture. It is included here for the sake of completeness and for the interested students.

Let us consider the motion of a particle of charge q and mass m in an electromagnetic field of the form

$$\boldsymbol{A}(\boldsymbol{r},t) = \hat{A}\boldsymbol{\sigma}(\eta)\mathcal{P}(\eta), \qquad \eta = \omega t - \boldsymbol{k}\cdot\boldsymbol{r} = k^\mu x_\mu, \qquad \boldsymbol{A}\cdot\boldsymbol{k} = 0. \tag{1.300}$$

Here, $\boldsymbol{A}(\boldsymbol{r},t)$ is the vector potential of amplitude $\hat{A}$, $\boldsymbol{\sigma}(\eta)$ carries the fast time-dependence, and $\mathcal{P}(\eta)$ is the slowly varying envelope. The phase η is a relativistic invariant, as it is evident from $\eta = k^\mu x_\mu$ where we use common relativistic notation ($\mu = 0,1,2,3$), $x^\mu = (ct, \boldsymbol{r})$, $k^\mu = (\omega/c, \boldsymbol{k})$, the sum convention, and the metric $g = \mathrm{diag}(1,-1,-1,-1)$. The fields are

$$\boldsymbol{E} = -\partial_t \boldsymbol{A}, \qquad \boldsymbol{B} = \boldsymbol{\nabla}\times\boldsymbol{A}. \tag{1.301}$$

There are various ways to solve the equations of motion for a charged particle in the field (1.300). A particularly elegant method is used in Landau & Lifshitz's *Classical Theory of Fields*, based on the relativistic Hamilton-Jacobi equation.

The relativistic Hamiltonian governing the motion of a charged particle in an electromagnetic field given by the scalar potential ϕ and the vector potential $\boldsymbol{A}$ reads

$$H = c^2\sqrt{m^2c^2 + (\boldsymbol{P} - q\boldsymbol{A})^2} + q\phi. \tag{1.302}$$

Here, $\boldsymbol{P}$ is the canonical momentum (while $\boldsymbol{p} = \boldsymbol{P} - q\boldsymbol{A}$ is the kinetic momentum). As in the derivation of the Klein-Gordon equation we square (1.302) and obtain

$$\frac{1}{c^2}(H - q\phi)^2 = m^2c^2 + (\boldsymbol{P} - q\boldsymbol{A})^2. \tag{1.303}$$

The goal of the Hamilton-Jacobi method is to find a generating function S, called *action*, for a canonical transformation to new, *constant* variables. These constant variables are then used to fulfill the initial conditions. The action S, depending on the "old" positions (+ time) and the new canonical momenta (+ energy) has to be chosen such that

$$\mathcal{E} = H = -\partial_t S, \qquad \boldsymbol{P} = \boldsymbol{\nabla} S. \tag{1.304}$$

Plugging this into (1.303) yields

$$(\partial_{ct} S + q\phi/c)^2 = m^2c^2 + (\boldsymbol{\nabla} S - q\boldsymbol{A})^2. \tag{1.305}$$

This expression can be written in a covariant manner. Introducing the four vectors

$$\partial^\mu S = (\partial_{ct} S, -\boldsymbol{\nabla} S) = (-\mathcal{E}/c, -\boldsymbol{P}) =: -P^\mu \tag{1.306}$$

and

$$A^\mu = (\phi/c, \boldsymbol{A}), \tag{1.307}$$

eq. (1.305) can be written as

$$g_{\mu\nu}(\partial^\mu S + qA^\mu)(\partial^\nu S + qA^\nu) = m^2c^2. \tag{1.308}$$

We are interested in the dynamics of a charged particle in an electromagnetic wave and therefore have

$$A^\mu = (0, \boldsymbol{A}), \qquad A^\mu k_\mu = 0. \tag{1.309}$$

With the Ansatz

$$S = S_{\text{free}} + S_{\text{field}}(\eta) = \beta_\mu x^\mu + S_{\text{field}}(\eta) \tag{1.310}$$

where the β_μ play the role of the new, constant momenta (+ energy), we obtain

$$\partial_\mu S = \beta_\mu + \partial_\mu S_{\text{field}} = \beta_\mu + \partial_\mu \eta \frac{\partial S_{\text{field}}}{\partial \eta} = \beta_\mu + k_\mu S'_{\text{field}} \tag{1.311}$$

where $S'_{\text{field}} = \partial_\eta S_{\text{field}}$. The Ansatz with S_{field} depending only on the invariant phase η but not on space and time separately is crucial. The fact that it works makes the problem soluble at all.

Plugging (1.311) into (1.308) leads to

$$(\beta_\mu + k_\mu S'_{\text{field}} + qA_\mu)(\beta^\mu + k^\mu S'_{\text{field}} + qA^\mu) = m^2c^2. \tag{1.312}$$

Making use of $k_\mu k^\mu = 0$ and $A_\mu k^\mu = 0$, this equation can be solved for $S_{\rm field}$:

$$S_{\rm field}(\eta) = \frac{1}{2\beta_\mu k^\mu} \int_{\eta_0}^{\eta} {\rm d}\eta' \, \left(m^2c^2 - [\beta_\mu + qA_\mu(\eta')][\beta^\mu + qA^\mu(\eta')] \right) \tag{1.313}$$

and the total action thus is

$$\begin{aligned} S &= \beta_\mu x^\mu + \frac{1}{2\beta_\mu k^\mu} \int_{\eta_0}^{\eta} {\rm d}\eta' \, \left(m^2c^2 - [\beta_\mu + qA_\mu(\eta')][\beta^\mu + qA^\mu(\eta')] \right) \qquad (1.314) \\ &= \beta_\mu x^\mu + \frac{1}{2\beta_\mu k^\mu} \int_{\eta_0}^{\eta} {\rm d}\eta' \, \left(m^2c^2 - \beta_\mu\beta^\mu - 2q\beta_\mu A^\mu(\eta') - q^2 A_\mu(\eta')A^\mu(\eta') \right) . \end{aligned}$$

The new, constant four-momentum fulfills

$$\beta_\mu \beta^\mu = m^2c^2 \tag{1.315}$$

and is given through the initial conditions. The canonical four-momentum is given by [making use also of (1.315)]

$$P^\mu = -\partial^\mu S = -\beta^\mu + \frac{2q\beta\cdot A(\eta) + q^2 A(\eta)\cdot A(\eta)}{2\beta\cdot k}\, k^\mu \tag{1.316}$$

with $a \cdot b = a_\mu b^\mu$. The derivatives of the action (1.314) with respect to the βs are constant and give us the trajectory:

$$\begin{aligned} \frac{\partial S}{\partial \beta^\mu} = x_{{\rm ini}\mu} &= x_\mu - \frac{k_\mu}{2(\beta\cdot k)^2} \int_{\eta_0}^{\eta} {\rm d}\eta' \, \left(m^2c^2 - \beta\cdot\beta - 2q\beta\cdot A(\eta') - q^2 A(\eta')\cdot A(\eta') \right) \\ &\quad - \frac{1}{\beta\cdot k} \int_{\eta_0}^{\eta} {\rm d}\eta' \, (\beta_\mu + qA_\mu(\eta')) \qquad (1.317) \\ \Rightarrow \quad x_\mu &= x_{{\rm ini}\mu} + \frac{1}{\beta\cdot k} \int_{\eta_0}^{\eta} {\rm d}\eta' \, (\beta_\mu + qA_\mu(\eta')) \qquad (1.318) \\ &\quad - \frac{k_\mu}{2(\beta\cdot k)^2} \int_{\eta_0}^{\eta} {\rm d}\eta' \, \left(2q\beta\cdot A(\eta') + q^2 A(\eta')\cdot A(\eta') \right) . \end{aligned}$$

In the last line we used (1.315) again.

We shall now specialize on an electromagnetic wave

$$\boldsymbol{A}(\eta) = \hat{A}\boldsymbol{e}_y \sin\eta, \qquad \boldsymbol{k} = k\boldsymbol{e}_x, \tag{1.319}$$

i.e.,

$$A^\mu = (0, 0, \hat{A}\sin\eta, 0), \qquad k^\mu = (\omega/c, k, 0, 0) = (k, k, 0, 0). \tag{1.320}$$

In this case we have

$$\beta\cdot A = -\beta^2 \hat{A}\sin\eta, \qquad A\cdot A = -\hat{A}^2\sin^2\eta, \qquad \beta\cdot k = k(\beta^0 - \beta^1), \tag{1.321}$$

(the reader should be careful not to mix up upper indices with powers!) and (1.316) becomes explicitly

$$P^0 = \frac{\mathcal{E}}{c} = -\beta^0 - \frac{2q\beta^2\hat{A}\sin\eta + q^2\hat{A}^2\sin^2\eta}{2(\beta^0-\beta^1)}, \tag{1.322}$$

$$P^1 = p_x = -\beta^1 - \frac{2q\beta^2\hat{A}\sin\eta + q^2\hat{A}^2\sin^2\eta}{2(\beta^0-\beta^1)}, \tag{1.323}$$

$$P^2 = p_y + q\hat{A}\sin\eta = -\beta^2, \tag{1.324}$$

$$P^3 = p_z = -\beta^3. \tag{1.325}$$

Clearly, the canonical momenta in y- and z-direction are conserved, and the relation between canonical and kinetic momentum is included in (1.324).

*Oscillation center frame

We are still free to choose the initial conditions β^μ. This is equivalent to choose a certain reference frame in which we want to study the dynamics. The only restriction is $\beta\cdot\beta = m^2c^2$. Let us choose the βs in such a way that the *oscillation center* of the particle is at rest:

$$\overline{p_x} = \overline{p_y} = \overline{p_z} \stackrel{!}{=} 0. \tag{1.326}$$

From eqs. (1.324) and (1.325) follows

$$\beta^2 = \beta^3 = 0 \tag{1.327}$$

so that with

$$\beta\cdot\beta = m^2c^2 \qquad \Rightarrow \qquad \beta^0 = -\sqrt{m^2c^2 + (\beta^1)^2} \tag{1.328}$$

(minus sign because $\mathcal{E}$ in (1.322) must be positive in the free particle case where $\hat{A} = 0$). From $\overline{p_x} = 0$ and (1.323) we have

$$2\beta^1\left(\beta^1 + \sqrt{m^2c^2 + (\beta^1)^2}\right) = \overline{2q\beta^2\hat{A}\sin\eta + q^2\hat{A}^2\sin^2\eta}. \tag{1.329}$$

The cycle average of $\sin\eta$ vanishes while $\overline{\sin^2\eta} = 1/2$. Equation (1.329) can then be solved for β^1,

$$|\beta^1| = \frac{1}{4}\frac{q^2\hat{A}^2}{\sqrt{m^2c^2 + q^2\hat{A}^2/2}}. \tag{1.330}$$

The sign will be chosen later. The trajectory in the oscillation center frame can be calculated from (1.318) and reads

$$ct = ct_{\rm ini} + \frac{\beta^0}{k(\beta^0-\beta^1)}(\eta-\eta_0) + \frac{q^2\hat{A}^2}{2k(\beta^0-\beta^1)^2}\int_{\eta_0}^{\eta} {\rm d}\eta'\,\sin^2\eta', \tag{1.331}$$

$$x^1 = {x_{\rm ini}}^1 + \frac{\beta^1}{k(\beta^0-\beta^1)}(\eta-\eta_0) + \frac{q^2\hat{A}^2}{2k(\beta^0-\beta^1)^2}\int_{\eta_0}^{\eta} {\rm d}\eta'\,\sin^2\eta', \quad (1.332)$$

$$x^2 = {x_{\rm ini}}^2 + \frac{q\hat{A}}{k(\beta^0-\beta^1)}\int_{\eta_0}^{\eta} {\rm d}\eta'\,\sin\eta', \quad (1.333)$$

$$x^3 = {x_{\rm ini}}^3. \quad (1.334)$$

The difference of (1.331) and (1.332) yields

$$ct - x^1 = ct_{\rm ini} - {x_{\rm ini}}^1 + \frac{\eta-\eta_0}{k} \quad (1.335)$$

so that

$$\eta = \omega t - kx, \qquad \eta_0 = \omega t_{\rm ini} - kx_{\rm ini}, \quad (1.336)$$

as it should. Since in the oscillation center x^1 should only oscillate but not drift, the term $\sim(\eta-\eta_0)$ has to be canceled by the first term of the integral

$$\int {\rm d}\eta\,\sin^2\eta = \frac{1}{2}\eta - \frac{1}{4}\sin 2\eta. \quad (1.337)$$

This is the case if we choose the positive sign in (1.330),

$$\beta^1 = \frac{1}{4}\frac{q^2\hat{A}^2}{\sqrt{m^2c^2+q^2\hat{A}^2/2}}. \quad (1.338)$$

Explicitly, we have

$$\beta^0 = -\frac{m^2c^2+q^2\hat{A}^2/4}{\sqrt{m^2c^2+q^2\hat{A}^2/2}}, \qquad \beta^0-\beta^1 = -\sqrt{m^2c^2+q^2\hat{A}^2/2}, \quad (1.339)$$

and the trajectory is given by [setting $\boldsymbol{r}_{\rm ini}$ appropriately and $x^\mu=(ct,x,y,z)$]

$$x = -\frac{q^2\hat{A}^2}{8k(m^2c^2+q^2\hat{A}^2/2)}\sin 2\eta, \quad (1.340)$$

$$y = \frac{q\hat{A}}{k\sqrt{m^2c^2+q^2\hat{A}^2/2}}\cos\eta, \quad (1.341)$$

$$z = 0. \quad (1.342)$$

This describes a figure-eight motion in the plane defined by the polarization vector ($\boldsymbol{e}_y$ in our case) and the propagation direction $\boldsymbol{k}/k$ ($\boldsymbol{e}_x$ in our case), as shown in Fig. 1.11. If we define the dimensionless vector potential amplitude as

$$a = \frac{q\hat{A}}{mc} \quad (1.343)$$

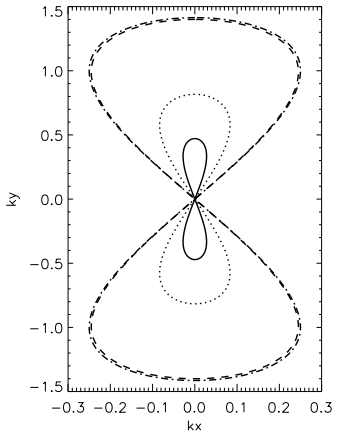

Figure 1.11: Figure-eight dynamics of a charged particle in an electromagnetic wave, as seen in the oscillation center frame. The trajectory in the xy-plane, where x is the propagation direction of the laser pulse, and y is the polarization direction, is shown for $a = 0.5$ (solid), $a = 1$ (dotted), $a = 10$ (dashed), and $a = 100$ (dashed-dotted). As a increases, the amplitudes $k\hat{x}$ and $k\hat{y}$ approach the calculated values $1/4$ and $\sqrt{2}$, respectively.

we have

$$kx = -\underbrace{\frac{a^2}{8(1+a^2/2)}}_{k\hat{x}} \sin 2\eta, \qquad ky = \underbrace{\frac{a}{\sqrt{1+a^2/2}}}_{k\hat{y}} \cos\eta, \qquad kz = 0. \tag{1.344}$$

The size of the figure-eight does not increase infinitely as the laser intensity goes to infinity:

$$\lim_{a\to\infty} k\hat{x} = \frac{1}{4}, \qquad \lim_{a\to\infty} k\hat{y} = \sqrt{2}, \qquad \lim_{a\to\infty} \frac{\hat{x}}{\hat{y}} = \frac{1}{4\sqrt{2}} \simeq 0.177. \tag{1.345}$$

Note that we only have the orbit parameterized with the invariant phase η (which is proportional to the proper time). We do not know the explicit expressions for x and y as functions of t. Parameterized with η, the trajectory looks extremely simple. In fact, only η and 2η shows up. If η were just ωt we could talk about the fundamental and the second harmonic and nothing else. However, since $\eta = \omega t - kx$ and x itself depends on t (or η), *all* frequencies, that is, *all* multiples of the laser frequency enter. This has consequences for the radiation emitted by such a particle.

*The adiabatically ramped pulse in the lab frame

We shall now investigate the same situation in the lab frame. We assume that the laser pulse has been ramped up adiabatically from $\mathcal{P} = 0$ at $\eta \to -\infty$ to $\mathcal{P} = 1$, and

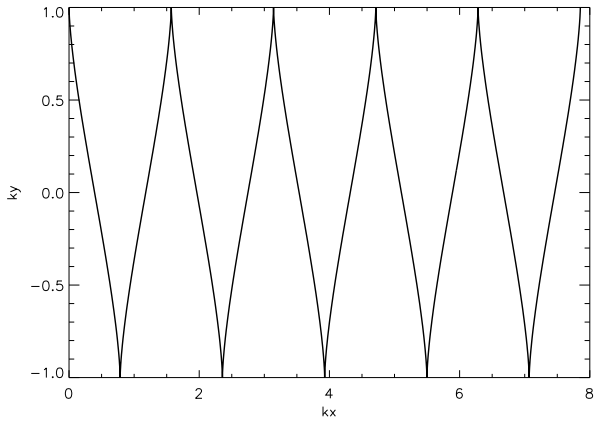

Figure 1.12: Particle motion in the lab frame for $a = 1$. While oscillating in polarization direction, the particle is drifting in propagation direction. The laser pulse is adiabatically ramped up and of constant amplitude afterwards. The particle was initially at rest. Note that there is no backward motion in x-direction (no loops but spikes).

that the particle starts from rest. Equations (1.322)–(1.325) hold in the lab frame as well. However, note that four-vectors such as k^μ change if we switch from one frame to the other (relativistic Doppler effect). Since it should be clear from the context in which frame we are working, we suppress explicit indices indicating the frame.

The initial condition $\boldsymbol{p} = 0$ for $\eta \to -\infty$ implies that $\beta^1 = \beta^2 = \beta^3 = 0$ and $\beta_0 = -mc$. For the trajectory one finds

$$x = \frac{a^2}{4k}\left(\eta - \frac{1}{2}\sin 2\eta\right), \tag{1.346}$$

$$y = \frac{a}{k}\cos\eta, \tag{1.347}$$

$$z = 0, \tag{1.348}$$

where we used the previously introduced dimensionless vector potential amplitude a [cf. (1.343)]. One sees that in polarization direction the particle just oscillates as before while in laser propagation direction it is drifting. An example of such an orbit is shown in Fig. 1.12.

There seems to be a contradiction as far as the excursion of the particle in polarization direction is concerned: in the lab frame this excursion is just proportional to a and thus is, in principle, unlimited. In the oscillation center frame the excursion was limited to $\sqrt{2}k$, despite the fact that a is the same in both frames. The resolution, of course, lies in k. With respect to the lab, the laser pulse is red-shifted in the oscillation center frame.

Finally, we shall calculate the velocity of the oscillation center frame with respect

to the lab frame. In the latter, eqs. (1.322)–(1.325) can be written as

$$\frac{P^0}{mc} = \frac{\mathcal{E}}{mc^2} = 1 + \frac{a^2}{2}\sin^2\eta, \quad \frac{P^1}{mc} = \frac{p_x}{mc} = \frac{a^2}{2}\sin^2\eta, \quad P^2 = P^3 = p_z = 0. \tag{1.349}$$

It is obvious that for our choice of the vector potential, the Lorentz transformation has to be performed parallel to $\boldsymbol{e}_x$ so that

$$\Lambda^\mu_\nu = \begin{pmatrix} \gamma_{\rm oc} & -v_{\rm oc}\gamma_{\rm oc}/c & 0 & 0 \\ -v_{\rm oc}\gamma_{\rm oc}/c & \gamma_{\rm oc} & 0 & 0 \\ 0 & 0 & 1 & 0 \\ 0 & 0 & 0 & 1 \end{pmatrix} \tag{1.350}$$

with $v_{\rm oc}$ the oscillation center velocity we are looking for and $\gamma_{\rm oc} = (1 - {v_{\rm oc}}^2/c^2)^{-1/2}$. Applying this transformation to (1.349), i.e., $P'^\mu = \Lambda^\mu_\nu P^\nu$ gives us

$$\frac{P'^1}{\gamma_{\rm oc} mc} = -\frac{v_{\rm oc}}{c}\left(1 + \frac{a^2}{2}\sin^2\eta\right) + \frac{a^2}{2}\sin^2\eta. \tag{1.351}$$

The condition $\overline{P'^1} = \overline{p'_x} = 0$ yields

$$v_{\rm oc} = \frac{a^2}{4 + a^2}\, c. \tag{1.352}$$

This is the velocity of the oscillation center of the particle in the lab frame if it was at rest before the pulse arrived.

1.4.3 *Relativistic ponderomotive force

This Section (including Subsections) has not been discussed in the lecture. It is included here for the sake of completeness and for the interested students.

We shall now derive the relativistic orbit of the oscillation center for a vector potential of the form (1.300). It is desirable to consider the oscillation center as a relativistic *pseudo particle*. However, it is *a priori* not given for granted that the oscillation center coordinates and momenta automatically "behave" in a relativistic, proper way. The correct averaging over a laser period is crucial here. The situation is somewhat similar to the relativistic center of mass, which is ill-defined if one naively extends the nonrelativistic expression and writes $\boldsymbol{R} = \left(\sum_i \boldsymbol{r}_i \gamma_i m_i\right) / \left(\sum_i \gamma_i m_i\right)$, where $\gamma_i = (1 - v_i^2/c^2)^{-1/2}$, without specifying in which system this expression should be evaluated. This is easily illustrated by the following example: Imagine two particles of equal rest mass moving with velocities $\pm v\boldsymbol{e}_x$ in the lab frame, and v very close to c. The observer in the lab frame will come to the conclusion that the center of mass (as defined above) is half way between both particles and stationary. Let us now transform to the reference frame in which one of the two particles is at rest. In this

frame the other particle will have a so much higher "effective mass" $\gamma m \gg m$ that the center of mass will be effectively at the position of this second particle. The two centers of mass measured by the two observers will not transform properly into each other by a Lorentz transformation. The ambiguity can be circumvented by *defining* the center of mass in the system in which it is at rest. Once determined it can then be transformed to any other system by a Lorentz transformation.

In the case of the relativistic oscillation center of a charged particle in a laser field such as (1.300) we are in the fortunate situation to have an invariant phase $\eta = k \cdot k$ over which we can average in an invariant manner. Already in a standing wave there is not such a single invariant η anymore. In the lab frame, for instance, the two phases $\eta_1 = \omega t - \boldsymbol{k} \cdot \boldsymbol{r}$ and $\eta_2 = \omega t + \boldsymbol{k} \cdot \boldsymbol{r}$ show up. In a reference frame moving along $\boldsymbol{k}$ one of the two waves will be red-shifted while the other will be blue-shifted, i.e., in this frame there will be no standing wave at all. As in the center of mass-problem, in such a situation the oscillation center — if existing — has to be defined in the system where it is at rest, and averaging has to be done over the proper time.

In this lecture we will restrict ourselves to the relativistic ponderomotive force in the travelling laser pulse where averaging over the invariant phase η can be done in any frame.

Averaging of (1.316) and (1.318) yields [with $\beta^\mu = (\beta^0, \boldsymbol{\beta})$]

$$\boldsymbol{r}_{\rm oc} = \overline{\boldsymbol{r}}(\overline{\eta}) = \boldsymbol{r}_{\rm ini} + \boldsymbol{\beta}\frac{\overline{\eta} - \eta_0}{\beta \cdot k} - \boldsymbol{k}\frac{q^2}{2(\beta \cdot k)^2}\int_{\eta_0}^{\overline{\eta}} {\rm d}\eta' \, \overline{A \cdot A}, \tag{1.353}$$

$$\boldsymbol{p}_{\rm oc} = \overline{\boldsymbol{P}}(\overline{\eta}) = -\boldsymbol{\beta} + \boldsymbol{k}\frac{q^2\overline{A \cdot A}}{2\beta \cdot k}, \tag{1.354}$$

$$\frac{\mathcal{E}_{\rm oc}}{c} = \frac{\overline{\mathcal{E}}}{c} = -\beta^0 + k\frac{q^2\overline{A \cdot A}}{2\beta \cdot k}. \tag{1.355}$$

Here, the averaged phase $\overline{\eta}$ is given by

$$\overline{\eta} = \omega t - \boldsymbol{k} \cdot \boldsymbol{r}_{\rm oc}. \tag{1.356}$$

The *rest* mass of the new pseudoparticle called oscillation center is given through

$$p_{\rm oc}{}^\mu p_{{\rm oc}_\mu} = M^2c^2, \qquad p_{\rm oc}{}^\mu = (\mathcal{E}_{\rm oc}/c, \boldsymbol{p}_{\rm oc}). \tag{1.357}$$

For consistency, this mass has also to fulfill

$$\boldsymbol{p}_{\rm oc} = \gamma_{\rm oc} M \boldsymbol{v}_{\rm oc}, \qquad \boldsymbol{v}_{\rm oc} = \dot{\boldsymbol{r}}_{\rm oc}, \qquad \gamma_{\rm oc} = \left(1 - \frac{{v_{\rm oc}}^2}{c^2}\right)^{-1/2}. \tag{1.358}$$

For the velocity one finds

$$\boldsymbol{v}_{\rm oc} = (\omega - \boldsymbol{k} \cdot \boldsymbol{v}_{\rm oc})\frac{{\rm d}\boldsymbol{r}_{\rm oc}}{{\rm d}\overline{\eta}} = (\omega - \boldsymbol{k} \cdot \boldsymbol{v}_{\rm oc})\frac{\boldsymbol{\beta} - \boldsymbol{k}\Gamma}{\beta \cdot k} \tag{1.359}$$

where the abbreviation

$$\Gamma = \frac{q^2\overline{A\cdot A}}{2\beta\cdot k} \tag{1.360}$$

has been introduced. In order to solve (1.359) for $\boldsymbol{v}_{\rm oc}$ we decompose the oscillation center velocity and $\boldsymbol{\beta}$ in components parallel and perpendicular to $\boldsymbol{k}$,

$$\boldsymbol{v}_{\rm oc} = v_{{\rm oc}\parallel}\frac{\boldsymbol{k}}{k} + \boldsymbol{v}_{{\rm oc}\perp}, \qquad \boldsymbol{\beta} = \beta_\parallel\frac{\boldsymbol{k}}{k} + \boldsymbol{\beta}_\perp. \tag{1.361}$$

This yields

$$v_{{\rm oc}\parallel} = \omega\frac{\beta_\parallel - k\Gamma}{\beta^0 k - k^2\Gamma}, \qquad \boldsymbol{v}_{{\rm oc}\perp} = \omega\frac{\boldsymbol{\beta}_\perp}{\beta^0 k - k^2\Gamma}, \tag{1.362}$$

and

$$\gamma_{\rm oc} = -\frac{\beta^0 - k\Gamma}{\sqrt{m^2c^2 - 2k\Gamma(\beta^0 - \beta_\parallel)}}. \tag{1.363}$$

In the same way we decompose $\boldsymbol{p}_{\rm oc}$,

$$\boldsymbol{p}_{\rm oc} = p_{{\rm oc}\parallel}\frac{\boldsymbol{k}}{k} + \boldsymbol{p}_{{\rm oc}\perp} \tag{1.364}$$

with (1.354) leading to

$$p_{{\rm oc}\parallel} = -\beta_\parallel + k\Gamma, \qquad \boldsymbol{p}_{{\rm oc}\perp} = -\boldsymbol{\beta}_\perp. \tag{1.365}$$

We then obtain

$$p_{\rm oc}{}^\mu p_{{\rm oc}\mu} = \beta\cdot\beta - q^2\overline{A\cdot A} \stackrel{!}{=} M^2c^2 \tag{1.366}$$

so that, using $\beta\cdot\beta = m^2c^2$, the mass of the oscillation center is given by

$$M = \frac{1}{c}\sqrt{m^2c^2 - q^2\overline{A\cdot A}}. \tag{1.367}$$

It is left as an exercise to the interested reader to check that this mass is indeed consistent with $\boldsymbol{p}_{\rm oc} = \gamma_{\rm oc}M\boldsymbol{v}_{\rm oc}$.

Another check is the following: if we transform to the system moving with $\boldsymbol{v}_{\rm oc}$, the energy $\mathcal{E}'_{\rm oc}$ in this system should be simply Mc^2. The transformation reads

$$\frac{\mathcal{E}'_{\rm oc}}{c} = \gamma_{\rm oc}\left(\frac{\mathcal{E}_{\rm oc}}{c} - \frac{\boldsymbol{v}_{\rm oc}\cdot\boldsymbol{p}_{\rm oc}}{c}\right). \tag{1.368}$$

Using (1.355), (1.363), and the decompositions for $\boldsymbol{v}_{\rm oc}$ and $\boldsymbol{p}_{\rm oc}$ above, one readily checks that indeed

$$\mathcal{E}'_{\rm oc} = Mc^2. \tag{1.369}$$

The relativistic oscillation center pseudo particle possesses a rest mass which is not a constant but depends on the phase $\overline{\eta}$ and thereby on space and time, that is, a mass *field*.

What remains to be calculated is the ponderomotive force

$$\boldsymbol{F}_{\rm p} = \dot{\boldsymbol{p}}_{\rm oc} = (\omega - k v_{{\rm oc}\parallel}) \frac{\rm d}{{\rm d}\overline{\eta}} \boldsymbol{p}_{\rm oc}. \tag{1.370}$$

Using (1.354) and (1.360) one obtains

$$\boldsymbol{F}_{\rm p} = \frac{\boldsymbol{k}}{k} \frac{\omega q^2}{2(\beta^0 - k\Gamma)} \frac{\rm d}{{\rm d}\overline{\eta}} \overline{A \cdot A}. \tag{1.371}$$

The Minkowski force

$$\boldsymbol{F}_{\rm p}^{\rm M} = \frac{\rm d}{{\rm d}\tau} \boldsymbol{p}_{\rm oc} = \gamma_{\rm oc} \boldsymbol{F}_{\rm p} \tag{1.372}$$

(where τ is the proper time) assumes a particularly simple form. Using (1.363) (note that the denominator of $\gamma_{\rm oc}$ is proportional to M) and

$$\frac{\rm d}{{\rm d}\overline{\eta}} = -\frac{1}{k} \boldsymbol{\nabla} \tag{1.373}$$

one obtains

$$\boldsymbol{F}_{\rm p}^{\rm M} = -\boldsymbol{\nabla} \mathcal{E}'_{\rm oc} = -c^2 \boldsymbol{\nabla} M. \tag{1.374}$$

The phase-dependent rest mass is the origin of the oscillation center motion. In the nonrelativistic case we saw already that the local quiver motion gives rise to the ponderomotive potential. Relativistically, this quiver motion is included in the rest mass of the oscillation center.

*Example: $\sin^2$-pulse

Let us consider a pulse envelope of the form

$$\mathcal{P}(\eta) = \sin^2(\epsilon\eta), \qquad 0 < \epsilon \ll 1 \tag{1.375}$$

which may describe a pulsed laser beam in which one pulse lasts from $\eta = n\pi/\epsilon$ to $\eta = (n+1)\pi/\epsilon$ with $n = 0, 1, 2, \ldots$. At time $t = 0$ the particle is assumed to be at rest at $\boldsymbol{r} = 0$ so that

$$\boldsymbol{\beta} = 0, \qquad \beta^0 = -mc. \tag{1.376}$$

Equations (1.353) and (1.354) become in this case

$$\boldsymbol{r}_{\rm oc} = \frac{q^2 \hat{A}^2}{4m^2c^2k} \left(\frac{3}{8}\overline{\eta} - \frac{1}{4\epsilon} \sin(2\epsilon\overline{\eta}) + \frac{1}{32\epsilon} \sin(4\epsilon\overline{\eta}) \right) \frac{\boldsymbol{k}}{k}, \tag{1.377}$$

$$\boldsymbol{p}_{\rm oc} = \frac{q^2 \hat{A}^2}{4mc} \sin^4(\epsilon\overline{\eta}) \frac{\boldsymbol{k}}{k}. \tag{1.378}$$

The relativistic ponderomotive force (1.371) is

$$\boldsymbol{F}_{\rm p}^{\sin^2} = \left(\frac{\omega mc\, a^2}{a^2 \sin^4(\epsilon\overline{\eta}) + 4} \right) \frac{\rm d}{{\rm d}\overline{\eta}} \sin^4(\epsilon\overline{\eta}) \tag{1.379}$$

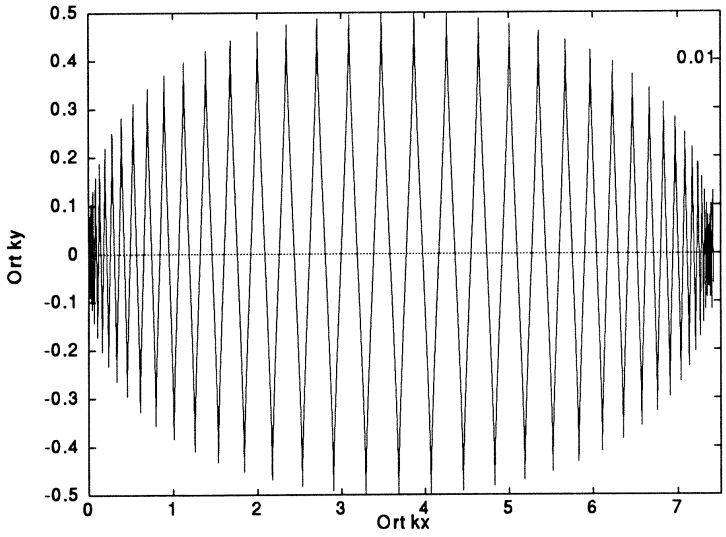

Figure 1.13: Electron trajectory for $a = -0.5$ and $\epsilon = 0.01$. Polarization and propagation directions are $\boldsymbol{e}_y$ and $\boldsymbol{e}_x$, respectively. The displacement after the first pulse agrees with formula (1.380) (which yields $\boldsymbol{k} \cdot \boldsymbol{r}_{\mathrm{oc}1} = 7.36$ in this case).

where $a = q\hat{A}/mc$ has been used again. In the nonrelativistic limit $|a| \ll 1$ the nonrelativistic ponderomotive force (1.270) is recovered (using (1.373) and $\hat{A}^2 = \hat{E}^2/\omega^2$). From (1.377) we can immediately infer the displacement of the particle after the first pulse:

$$\boldsymbol{r}_{\mathrm{oc}1} = \frac{a^2}{4k}\frac{3}{8}\overline{\eta}_1\frac{\boldsymbol{k}}{k}, \qquad \overline{\eta}_1 = \frac{\pi}{\epsilon}. \tag{1.380}$$

Figure 1.13 shows the trajectory of an electron for $a = -0.5$ and $\epsilon = 0.01$ during the first pulse, confirming formula (1.380).

1.4.4 Optical Bloch equations

We now turn to a quantum treatment of radiation forces on neutral atoms. To that end we need a non-perturbative approach in the external field because weak fields have not much of a mechanical effect. In fact, we need to saturate atomic transitions. It is also essential to allow for photon emission in previously unoccupied modes. On the other hand, the external driving field can well be described classically.

To simplify as much as possible we consider a single atom at position $\boldsymbol{R} = \boldsymbol{0}$ with a ground state a and a discrete state b with energy $\hbar\omega_0$ above a and natural width Γ. The Hamiltonian

$$H = H_{\mathrm{A}} + H_{\mathrm{R}} - \boldsymbol{d} \cdot [\boldsymbol{E}(\boldsymbol{0}, t) + \boldsymbol{E}_\perp(\boldsymbol{0})] \tag{1.381}$$

consists of the atomic part $H_{\rm A}$, the radiation part $H_{\rm R}$, and the coupling to the classical external field $\boldsymbol{E}(\boldsymbol{0},t)$ and the quantum radiation field $\boldsymbol{E}_\perp(\boldsymbol{0})$. The dipole operator is $\boldsymbol{d}=-e\boldsymbol{r}$. The external field is supposed to be monochromatic,

$$\boldsymbol{E}(\boldsymbol{0},t)=\hat{\boldsymbol{E}}\cos\omega_{\rm L}t \tag{1.382}$$

with a laser frequency $\omega_{\rm L}\simeq\omega_0$ close to resonance.

In general, the von Neumann equation for a density matrix ρ reads

$$\mathrm{i}\hbar\dot{\rho}=[H,\rho]. \tag{1.383}$$

We are dealing here with the density matrix of the atom $\sigma=\mathrm{Tr}_{\rm rad}\,\rho$ (radiation field degrees of freedom traced-out). If there was only the classical external field this density matrix would evolve according

$$\mathrm{i}\hbar\dot{\sigma}=[H_{\rm A}-\boldsymbol{d}\cdot\hat{\boldsymbol{E}}\cos\omega_{\rm L}t,\sigma]\qquad\text{if}\quad\boldsymbol{E}_\perp(\boldsymbol{0})=\boldsymbol{0} \tag{1.384}$$

(and the dynamics could also be described without resorting to the density matrix formalism). With

$$H_A=E_a\left|a\right\rangle\left\langle a\right|+E_b\left|b\right\rangle\left\langle b\right| \tag{1.385}$$

and

$$\hbar\Omega_1=-\boldsymbol{d}_{ab}\cdot\hat{\boldsymbol{E}},\qquad\boldsymbol{d}_{ab}=\left\langle a\right|\boldsymbol{d}\left|b\right\rangle=\left\langle b\right|\boldsymbol{d}\left|a\right\rangle \tag{1.386}$$

(we assume $\boldsymbol{d}_{ab}=\langle a|\boldsymbol{d}\,|b\rangle$ to be real) we find for

$$\sigma_{aa}=\left\langle a\right|\sigma\left|a\right\rangle,\quad\sigma_{bb}=\left\langle b\right|\sigma\left|b\right\rangle,\quad\sigma_{ab}=\left\langle a\right|\sigma\left|b\right\rangle,\quad\sigma_{ba}=\left\langle b\right|\sigma\left|a\right\rangle \tag{1.387}$$

the differential equations

$$\begin{aligned}
\dot{\sigma}_{bb} &= \mathrm{i}\Omega_1\cos\omega_{\rm L}t\,(\sigma_{ba}-\sigma_{ab}), &(1.388)\\
\dot{\sigma}_{aa} &= -\mathrm{i}\Omega_1\cos\omega_{\rm L}t\,(\sigma_{ba}-\sigma_{ab}), &(1.389)\\
\dot{\sigma}_{ab} &= \mathrm{i}\omega_0\sigma_{ab}-\mathrm{i}\Omega_1\cos\omega_{\rm L}t\,(\sigma_{bb}-\sigma_{aa}), &(1.390)\\
\dot{\sigma}_{ba} &= -\mathrm{i}\omega_0\sigma_{ba}+\mathrm{i}\Omega_1\cos\omega_{\rm L}t\,(\sigma_{bb}-\sigma_{aa}). &(1.391)
\end{aligned}$$

Here,

$$\omega_0=\omega_{ba}+\Delta_{ba} \tag{1.392}$$

where Δ_{ba} are possible level shifts due to the presence of radiation. Ω_1 is the *Rabi frequency*.

On the other hand, the evolution of the density matrix σ' for a two-level atom interacting with an initially empty radiation field can be solved.[15] This is spontaneous emission discussed previously, but now expressed in terms of the density matrix. We denote the rate (1.70) in what follows by Γ,

$$\Gamma=W^{\rm s}_{ab}. \tag{1.393}$$

[15] See any quantum optics textbook.

The diagonal elements of σ' fulfill the rate equations

$$\dot{\sigma'}_{bb} = -\Gamma \sigma'_{bb}, \tag{1.394}$$

$$\dot{\sigma'}_{aa} = \Gamma \sigma'_{bb}, \tag{1.395}$$

describing the exponential decay of the population of state b down to state a. The nondiagonal elements (so-called *coherences*) evolve according

$$\dot{\sigma'}_{ba} = -\mathrm{i}\omega_0 \sigma'_{ba} - \frac{\Gamma}{2}\sigma'_{ba}, \tag{1.396}$$

$$\dot{\sigma'}_{ab} = \mathrm{i}\omega_0 \sigma'_{ab} - \frac{\Gamma}{2}\sigma'_{ab}. \tag{1.397}$$

As the degrees of freedom of the quantized electromagnetic field (which allows for spontaneous emission) are traced-out a density matrix description is required.[16] It is not possible to find an atomic Hamiltonian alone (even if we allow for complex eigenenergies so that the Hamiltonian becomes non-Hermitian) which reproduces the Bloch equations we discuss in the following.

We now combine Eqs. (1.388)–(1.397), assuming that the modification of spontaneous emission due to the presence of the external field is low. This is true as long as

$$\Omega_1 \ll \omega_0. \tag{1.398}$$

We obtain[17]

$$\begin{aligned}
\dot{\sigma}_{bb} &= \mathrm{i}\Omega_1 \cos\omega_{\mathrm{L}} t\ (\sigma_{ba} - \sigma_{ab}) - \Gamma\sigma_{bb}, && (1.399)\\
\dot{\sigma}_{aa} &= -\mathrm{i}\Omega_1 \cos\omega_{\mathrm{L}} t\ (\sigma_{ba} - \sigma_{ab}) + \Gamma\sigma_{bb}, && (1.400)\\
\dot{\sigma}_{ab} &= \mathrm{i}\omega_0\sigma_{ab} - \mathrm{i}\Omega_1 \cos\omega_{\mathrm{L}} t\ (\sigma_{bb} - \sigma_{aa}) - \frac{\Gamma}{2}\sigma_{ab}, && (1.401)\\
\dot{\sigma}_{ba} &= -\mathrm{i}\omega_0\sigma_{ba} + \mathrm{i}\Omega_1 \cos\omega_{\mathrm{L}} t\ (\sigma_{bb} - \sigma_{aa}) - \frac{\Gamma}{2}\sigma_{ba}. && (1.402)
\end{aligned}$$

Note that $\mathrm{d}(\sigma_{bb} + \sigma_{aa})/\mathrm{d}t = 0$.

For the two-level approximation to be valid at all we also must have

$$|\omega_{\mathrm{L}} - \omega_0| \ll \omega_0, \tag{1.403}$$

i.e., the incident radiation has to be close to resonance.

[16] The atomic system alone is an *open system*.

[17] Contributions $\sim \omega_0$ due to H_A have to be taken into account only once!

Rotating-wave approximation

Equations (1.399)–(1.402) are still quite complicated because of the explicit time-dependence. In the following we will simplify this set of equations.

As $\boldsymbol{d}$ has only nondiagonal terms we may write

$$\boldsymbol{d} = \boldsymbol{d}_{ab}(|b\rangle\langle a| + |a\rangle\langle b|) =: \boldsymbol{d}_+ + \boldsymbol{d}_-, \tag{1.404}$$

$$\boldsymbol{d}_\pm = \boldsymbol{d}_{ab}\mathcal{S}_\pm, \qquad \mathcal{S}_+ = |b\rangle\langle a|, \qquad \mathcal{S}_- = |a\rangle\langle b|. \tag{1.405}$$

$\mathcal{S}_\pm$ are the raising and lowering operators from state a to b and *vice versa*. The interaction with the external field can be expressed as

$$-\boldsymbol{d}\cdot\hat{\boldsymbol{E}}\cos\omega_{\rm L}t = \frac{1}{2}\hbar\Omega_1(\mathcal{S}_+\mathrm{e}^{-\mathrm{i}\omega_{\rm L}t} + \mathcal{S}_-\mathrm{e}^{\mathrm{i}\omega_{\rm L}t} + \mathcal{S}_-\mathrm{e}^{-\mathrm{i}\omega_{\rm L}t} + \mathcal{S}_+\mathrm{e}^{\mathrm{i}\omega_{\rm L}t}). \tag{1.406}$$

The first two terms describe the *resonant* processes where the atom makes a transition from the lower state a to the higher state b upon absorption of a photon and a transition from the upper state b to the lower state a upon emission of a photon, respectively. The last two *anti-resonant* terms will be neglected. This is called the *rotating wave approximation*.

Instead of (1.399)–(1.402) we then have

$$\dot\sigma_{bb} = \mathrm{i}\frac{\Omega_1}{2}(\sigma_{ba}\,\mathrm{e}^{\mathrm{i}\omega_{\rm L}t} - \sigma_{ab}\,\mathrm{e}^{-\mathrm{i}\omega_{\rm L}t}) - \Gamma\sigma_{bb}, \tag{1.407}$$

$$\dot\sigma_{aa} = -\mathrm{i}\frac{\Omega_1}{2}(\sigma_{ba}\,\mathrm{e}^{\mathrm{i}\omega_{\rm L}t} - \sigma_{ab}\,\mathrm{e}^{-\mathrm{i}\omega_{\rm L}t}) + \Gamma\sigma_{bb}, \tag{1.408}$$

$$\dot\sigma_{ab} = \mathrm{i}\omega_0\sigma_{ab} - \mathrm{i}\frac{\Omega_1}{2}\,\mathrm{e}^{\mathrm{i}\omega_{\rm L}t}\,(\sigma_{bb} - \sigma_{aa}) - \frac{\Gamma}{2}\sigma_{ab}, \tag{1.409}$$

$$\dot\sigma_{ba} = -\mathrm{i}\omega_0\sigma_{ba} + \mathrm{i}\frac{\Omega_1}{2}\,\mathrm{e}^{-\mathrm{i}\omega_{\rm L}t}\,(\sigma_{bb} - \sigma_{aa}) - \frac{\Gamma}{2}\sigma_{ba}. \tag{1.410}$$

Introducing

$$\hat\sigma_{ba} = \sigma_{ba}\,\mathrm{e}^{\mathrm{i}\omega_{\rm L}t}, \qquad \hat\sigma_{ab} = \sigma_{ab}\,\mathrm{e}^{-\mathrm{i}\omega_{\rm L}t}, \qquad \hat\sigma_{aa} = \sigma_{aa}, \qquad \hat\sigma_{bb} = \sigma_{bb} \tag{1.411}$$

we obtain the explicitly time-independent Bloch equations

$$\dot{\hat\sigma}_{bb} = \mathrm{i}\frac{\Omega_1}{2}(\hat\sigma_{ba} - \hat\sigma_{ab}) - \Gamma\hat\sigma_{bb}, \tag{1.412}$$

$$\dot{\hat\sigma}_{aa} = -\mathrm{i}\frac{\Omega_1}{2}(\hat\sigma_{ba} - \hat\sigma_{ab}) + \Gamma\hat\sigma_{bb}, \tag{1.413}$$

$$\dot{\hat\sigma}_{ab} = -\mathrm{i}\delta_{\rm L}\hat\sigma_{ab} - \mathrm{i}\frac{\Omega_1}{2}(\hat\sigma_{bb} - \hat\sigma_{aa}) - \frac{\Gamma}{2}\hat\sigma_{ab}, \tag{1.414}$$

$$\dot{\hat\sigma}_{ba} = \mathrm{i}\delta_{\rm L}\hat\sigma_{ba} + \mathrm{i}\frac{\Omega_1}{2}(\hat\sigma_{bb} - \hat\sigma_{aa}) - \frac{\Gamma}{2}\hat\sigma_{ba} \tag{1.415}$$

where

$$\delta_{\rm L} = \omega_{\rm L} - \omega_0 \tag{1.416}$$

is the *detuning* between the photon energy of the incident radiation and the atomic transition.

We observe that it is Ω_1 that couples the coherences $\hat{\sigma}_{ab}$, $\hat{\sigma}_{ba}$ to the populations $\hat{\sigma}_{aa}$, $\hat{\sigma}_{bb}$. This is because of the coherent nature of the driving field. The relative phase between the atomic dipole expectation value $\langle \boldsymbol{d} \rangle$ and the external driver determines whether photons are absorbed or emitted. This will become clearer below.

Bloch vector

Defining the three components of the Bloch vector

$$u = \frac{1}{2}(\hat{\sigma}_{ab} + \hat{\sigma}_{ba}), \qquad v = \frac{1}{2\mathrm{i}}(\hat{\sigma}_{ab} - \hat{\sigma}_{ba}), \qquad w = \frac{1}{2}(\hat{\sigma}_{bb} - \hat{\sigma}_{aa}) \tag{1.417}$$

Eqs. (1.412)–(1.415) can be rewritten as

$$\dot{u} = \delta_{\mathrm{L}} v - \frac{\Gamma}{2} u, \tag{1.418}$$

$$\dot{v} = -\delta_{\mathrm{L}} u - \Omega_1 w - \frac{\Gamma}{2} v, \tag{1.419}$$

$$\dot{w} = \Omega_1 v - \Gamma w - \frac{\Gamma}{2}. \tag{1.420}$$

Three components are sufficient because of $\mathrm{d}(\hat{\sigma}_{bb} + \hat{\sigma}_{aa})/\mathrm{d}t = 0$. Obviously, $w = 1/2$ if the system is in state b and $w = -1/2$ if the system is in state a. For values in between it is in a superposition. But how can u and v be interpreted? To that end we consider the dipole expectation value,

$$\langle \boldsymbol{d} \rangle = \mathrm{Tr}(\sigma \boldsymbol{d}) = \langle a|\sigma \boldsymbol{d}\,|a\rangle + \langle b|\sigma \boldsymbol{d}\,|b\rangle = \langle a|\sigma(\underbrace{|a\rangle\langle a| + |b\rangle\langle b|}_{1})\boldsymbol{d}\,|a\rangle + \langle b|\sigma(|a\rangle\langle a| + |b\rangle\langle b|)\boldsymbol{d}\,|b\rangle$$

$$= \boldsymbol{d}_{ab}(\sigma_{ab} + \sigma_{ba}) = \boldsymbol{d}_{ab}(\hat{\sigma}_{ab}\,\mathrm{e}^{\mathrm{i}\omega_{\mathrm{L}}t} + \hat{\sigma}_{ba}\,\mathrm{e}^{-\mathrm{i}\omega_{\mathrm{L}}t}) = 2\boldsymbol{d}_{ab}(u\cos\omega_{\mathrm{L}}t - v\sin\omega_{\mathrm{L}}t). \tag{1.421}$$

Hence, u and v are the components in phase with the driving laser $\sim \cos\omega_{\mathrm{L}}t$ and $\pi/2$ out of phase $\sim -\sin\omega_{\mathrm{L}}t = \cos(\omega_{\mathrm{L}}t + \pi/2)$ ("quadrature phase"), respectively.

Every two-level system can formally be mapped to a fictitious spin 1/2-system. In fact, one can show that the system under study, i.e., a two-level atom in the presence of a classical driving field plus the quantum vacuum behaves like a spin-1/2 in crossed magnetic fields $B_0\boldsymbol{e}_z$ and $2B_1\boldsymbol{e}_x\cos\omega_{\mathrm{L}}t$ where the role of the Bloch vector components is played by the expectation values of the spin components ($\rightarrow$ exercise).

Evolution of average atomic values

We are now ready to calculate observables such as populations or the mean dipole. Moreover, we can evaluate mean forces on the atom, which is our main goal, as we are interested in mechanical effects of light in this Section.

The Bloch equations (1.418)–(1.420) are a set of linear differential equations with constant coefficients. The general solutions are superpositions of exponentials $\mathrm{e}^{-r_\lambda t}$. Let us investigate some limiting cases

1. For weak ($\Omega_1 \to 0$) but exactly resonant ($\delta_\mathrm{L} = 0$) driving one has

$$\dot{u} = -\frac{\Gamma}{2}u, \tag{1.422}$$

$$\dot{v} = -\frac{\Gamma}{2}v, \tag{1.423}$$

$$\dot{w} = -\Gamma w - \frac{\Gamma}{2}, \tag{1.424}$$

describing a purely damped system without any oscillation ($\to$ exercise). Thus at very low intensities[18] spontaneous decay dominates, the components u and v of the Bloch vector shrink to zero, and $w \to -1/2$, i.e., the atom ultimately will be in the ground state.

2. For strong resonant driving $\Omega_1 \gg \Gamma$, $\delta_\mathrm{L} = 0$ we have pure Rabi-oscillations. In fact, (1.418)–(1.420) read in lowest order

$$\dot{u} = -\frac{\Gamma}{2}u, \tag{1.425}$$

$$\dot{v} = -\Omega_1 w, \tag{1.426}$$

$$\dot{w} = \Omega_1 v, \tag{1.427}$$

or

$$\ddot{w} + \Omega_1^2 w = 0, \tag{1.428}$$

and the difference in the populations of levels a and b indeed oscillates with the Rabi-frequency.

3. The steady state solutions $\bar{u}$, $\bar{v}$, $\bar{w}$ follow from

$$0 = \delta_\mathrm{L}\bar{v} - \frac{\Gamma}{2}\bar{u}, \tag{1.429}$$

$$0 = -\delta_\mathrm{L}\bar{u} - \Omega_1\bar{w} - \frac{\Gamma}{2}\bar{v}, \tag{1.430}$$

$$0 = \Omega_1\bar{v} - \Gamma\bar{w} - \frac{\Gamma}{2}. \tag{1.431}$$

One finds

$$\bar{u} = \frac{\Omega_1}{2}\frac{\delta_\mathrm{L}}{\delta_\mathrm{L}^2 + (\Gamma^2/4) + (\Omega_1^2/2)}, \tag{1.432}$$

$$\bar{v} = \frac{\Omega_1}{2}\frac{\Gamma/2}{\delta_\mathrm{L}^2 + (\Gamma^2/4) + (\Omega_1^2/2)}, \tag{1.433}$$

$$\bar{w} + \frac{1}{2} = \bar{\sigma}_{bb} = \frac{\Omega_1^2}{4}\frac{1}{\delta_\mathrm{L}^2 + (\Gamma^2/4) + (\Omega_1^2/2)}. \tag{1.434}$$

[18] Remember that Ω_1 is proportional to the field amplitude.

Here we observe the following:

(a) For δ_{L} and Γ fixed, $\bar{u}$ and $\bar{v}$ increase linearly in Ω_1 for small Ω_1 and approach zero for large Ω_1. Hence, because of (1.421) the mean dipole goes to zero for strong driving.

(b) The population $\bar{\sigma}_{bb}$ starts to increase quadratically with Ω_1 and approaches $1/2$ for large Ω_1. This means that strong driving equilibrates the populations equally over the two levels.

Energy balance

The work done by an electromagnetic field (with electric field $\boldsymbol{E}$) per unit time on a charged particle (charge q) is

$$\frac{\mathrm{d}W}{\mathrm{d}t} = q\boldsymbol{E}\cdot\boldsymbol{v}. \tag{1.435}$$

The energy W is absorbed by the charged particle, which in our case is the electron bound inside an atom. We plug-in the corresponding quantum mechanical expectation values, i.e., with $q\langle\boldsymbol{r}\rangle = \langle\boldsymbol{d}\rangle$,

$$\left\langle\frac{\mathrm{d}W}{\mathrm{d}t}\right\rangle = \hat{\boldsymbol{E}}\cos\omega_{\mathrm{L}}t\cdot\langle\dot{\boldsymbol{d}}\rangle. \tag{1.436}$$

Using (1.421) we have

$$\left\langle\frac{\mathrm{d}W}{\mathrm{d}t}\right\rangle = \hat{\boldsymbol{E}}\cos\omega_{\mathrm{L}}t\cdot 2\boldsymbol{d}_{ab}\omega_{\mathrm{L}}(-u\sin\omega_{\mathrm{L}}t - v\cos\omega_{\mathrm{L}}t). \tag{1.437}$$

Averaging over a laser cycle yields

$$\overline{\left\langle\frac{\mathrm{d}W}{\mathrm{d}t}\right\rangle} = -\hat{\boldsymbol{E}}\cdot\boldsymbol{d}_{ab}\omega_{\mathrm{L}}v = \hbar\Omega_1\omega_{\mathrm{L}}v, \tag{1.438}$$

showing that the absorption of energy is governed by the out-of-phase component v of the Bloch vector. In fact, the velocity of a free electron is $\pi/2$ out of phase with respect to the driving electric field so that $\overline{\boldsymbol{E}\cdot\boldsymbol{v}} = 0$, i.e., no laser energy is absorbed by free electrons.

Dividing (1.438) by $\hbar\omega_{\mathrm{L}}$ we obtain the mean number of photons absorbed

$$\left\langle\frac{\mathrm{d}N}{\mathrm{d}t}\right\rangle = \Omega_1 v. \tag{1.439}$$

The third Bloch equation (1.420) can thus be written

$$\dot{w} = \left\langle\frac{\mathrm{d}N}{\mathrm{d}t}\right\rangle - \Gamma w - \frac{\Gamma}{2}. \tag{1.440}$$

With $w + 1/2 = \sigma_{bb}$ this turns into

$$\dot{\sigma}_{bb} = \left\langle \frac{\mathrm{d}N}{\mathrm{d}t} \right\rangle - \Gamma\sigma_{bb}, \tag{1.441}$$

which is the expected rate equation: the population of the excited state b occurs via absorption of photons from the external field while the decay is due to spontaneous emission with rate Γ and proportional to the population in the excited state. In the stationary situation

$$\left\langle \frac{\mathrm{d}\bar{N}}{\mathrm{d}t} \right\rangle = \Gamma\bar{\sigma}_{bb}. \tag{1.442}$$

The right hand side tells us how many photons are emitted spontaneously per unit time. We know already that in saturation $\bar{\sigma}_{bb} = 1/2$ so that

$$\left\langle \frac{\mathrm{d}\bar{N}}{\mathrm{d}t} \right\rangle_{\mathrm{sat}} = \frac{\Gamma}{2} \tag{1.443}$$

($\rightarrow$ this has been already used in one of the exercises).

Radiation forces on the atom

We now allow the atom to move. The Hamiltonian (1.381) needs to be modified by incorporating the center of mass (total mass M) at the position $\boldsymbol{R}$ and the corresponding momentum $\boldsymbol{P}$,

$$H = \frac{\boldsymbol{P}^2}{2M} + H_{\mathrm{A}} + H_{\mathrm{R}} - \boldsymbol{d} \cdot [\boldsymbol{E}(\boldsymbol{R}, t) + \boldsymbol{E}_{\perp}(\boldsymbol{R})]. \tag{1.444}$$

The Heisenberg equations of motion for the center of mass read

$$\dot{\boldsymbol{R}} = \frac{\partial H}{\partial \boldsymbol{P}} = \frac{\boldsymbol{P}}{M}, \qquad \dot{\boldsymbol{P}} = M\ddot{\boldsymbol{R}} = -\frac{\partial H}{\partial \boldsymbol{R}} = \sum_{j=x,y,z} d_j \boldsymbol{\nabla}_{\boldsymbol{R}}[E_j(\boldsymbol{R}, t) + E_{\perp j}(\boldsymbol{R})] \tag{1.445}$$

so that with Ehrenfest and $\langle \boldsymbol{R} \rangle = \boldsymbol{r}_{\mathrm{c}}$

$$M\ddot{\boldsymbol{r}}_{\mathrm{c}} = \sum_j \langle d_j \boldsymbol{\nabla}_{\boldsymbol{R}}[E_j(\boldsymbol{R}, t) + E_{\perp j}(\boldsymbol{R})] \rangle \,. \tag{1.446}$$

In order to evaluate the right hand side we need to make additional approximations.

1. We assume that the de Broglie wavelength of the atom is much smaller than the wavelength of the external field,

$$\lambda_{\mathrm{dB}} = \frac{h}{M v_{\mathrm{c}}} \ll \lambda, \tag{1.447}$$

where $v_{\mathrm{c}} = |\dot{\boldsymbol{r}}_{\mathrm{c}}|$, so that we can write $\boldsymbol{r}_{\mathrm{c}}$ for the argument in the external field on the right hand side.

2. It can be shown that the electromagnetic field generated by spontaneous emission cannot exert a force on the atom itself (self-force). Hence, the second term in (1.446) is zero so that

$$M\ddot{\boldsymbol{r}}_{\rm c} = \sum_j \langle d_j\rangle \boldsymbol{\nabla}_{\boldsymbol{r}_{\rm c}} E_j(\boldsymbol{r}_{\rm c}, t). \tag{1.448}$$

3. An upper limit for the internal time scales of the atom is determined by $T_{\rm int} = \max\{\Omega_1^{-1}, \Gamma^{-1}\}$. We will only consider atoms with velocity $\boldsymbol{v}_{\rm c}$ slow enough so that $|\boldsymbol{v}_{\rm c}|T_{\rm int} \ll \lambda$. This is the "usual" case, for we will see later on that the external time scale over which the velocity changes is given by $T_{\rm ext} = \hbar/E_{\rm rec}$ with $E_{\rm rec}$ the recoil energy $E_{\rm rec} = \hbar^2 k_{\rm L}^2/2M$. In the classical treatment of the ponderomotive force in Sec. 1.4.1 we made the same assumption: the oscillation center does only move small distances $\ll \lambda$ during one period of the rapidly varying external field.

   As we are able to separate the time scales $T_{\rm int}$ and $T_{\rm ext}$ we can safely assume that the mean dipole $\langle \boldsymbol{d}\rangle$ has always time to reach its steady-state value so that we can use the above derived expression for $\langle \boldsymbol{d}\rangle$. If an atom has an initial velocity $\boldsymbol{v}_{\rm c}$ we can transform to its rest frame in which the external field will be Doppler-shifted.

We now analyze the force (1.448) on an atom located at $\boldsymbol{r}_{\rm c} = \boldsymbol{0}$ and allow the field amplitude and phase to vary in space,

$$\boldsymbol{E}(\boldsymbol{r}_{\rm c}, t) = \boldsymbol{\varepsilon}\hat{E}(\boldsymbol{r}_{\rm c})\cos[\omega_{\rm L}t + \phi(\boldsymbol{r}_{\rm c})]. \tag{1.449}$$

Here, for simplicity we keep the polarization vector constant and set

$$\phi(\boldsymbol{0}) = 0. \tag{1.450}$$

For (1.448) we need

$$\boldsymbol{\nabla} E_j = \varepsilon_j[\cos\omega_{\rm L}t\ \boldsymbol{\nabla}\hat{E} - \sin\omega_{\rm L}t\ \hat{E}\boldsymbol{\nabla}\phi] \tag{1.451}$$

where all $\boldsymbol{\nabla}$ are with respect to $\boldsymbol{r}_{\rm c}$ and all terms are evaluated at $\boldsymbol{r}_{\rm c} = \boldsymbol{0}$. For $\langle d_j\rangle$ we employ (1.421) evaluated with the steady-state Bloch vector components $\bar{u}$ and $\bar{v}$,

$$\langle d_j\rangle = 2(\boldsymbol{d}_{ab})_j[\bar{u}\cos\omega_{\rm L}t - \bar{v}\sin\omega_{\rm L}t]. \tag{1.452}$$

Plugging this into (1.448) and averaging over a laser period yields the force

$$\boldsymbol{F} = \sum_j \overline{\langle d_j\rangle \boldsymbol{\nabla} E_j} = \sum_j \overline{2(\boldsymbol{d}_{ab})_j[\bar{u}\cos\omega_{\rm L}t - \bar{v}\sin\omega_{\rm L}t]\varepsilon_j[\cos\omega_{\rm L}t\ \boldsymbol{\nabla}\hat{E} - \sin\omega_{\rm L}t\ \hat{E}\boldsymbol{\nabla}\phi]}$$

$$= \boldsymbol{d}_{ab}\cdot\boldsymbol{\varepsilon}\ [\bar{u}\boldsymbol{\nabla}\hat{E} + \bar{v}\hat{E}\boldsymbol{\nabla}\phi]. \tag{1.453}$$

The first force term we call the *reactive force*,

$$\boldsymbol{F}_{\text{react}} = \boldsymbol{d}_{ab} \cdot \boldsymbol{\varepsilon}\ \bar{u} \boldsymbol{\nabla} \hat{E}. \tag{1.454}$$

It is proportional to the component $\bar{u}$ in phase with the driving radiation field. The second force term we call *dissipative*, as it is proportional to the out-of-phase Bloch vector component $\bar{v}$,

$$\boldsymbol{F}_{\text{diss}} = \boldsymbol{d}_{ab} \cdot \boldsymbol{\varepsilon}\ \bar{v} \hat{E} \boldsymbol{\nabla} \phi. \tag{1.455}$$

Using the Rabi frequency

$$\Omega_1 = -\boldsymbol{d}_{ab} \cdot \boldsymbol{\varepsilon}\ \hat{E}/\hbar \tag{1.456}$$

we can write

$$\boldsymbol{F}_{\text{react}} = -\hbar \Omega_1 \bar{u}\ \boldsymbol{\alpha}, \qquad \boldsymbol{F}_{\text{diss}} = -\hbar \Omega_1 \bar{v}\ \boldsymbol{\beta} \tag{1.457}$$

where

$$\boldsymbol{\alpha} = \frac{\boldsymbol{\nabla} \Omega_1}{\Omega_1}, \qquad \boldsymbol{\beta} = \boldsymbol{\nabla} \phi. \tag{1.458}$$

Dissipative force: radiation pressure

For a plane wave $\phi(\boldsymbol{r}_{\text{c}}) = -\boldsymbol{k}_{\text{L}} \cdot \boldsymbol{r}_{\text{c}}$ so that

$$\boldsymbol{E}(\boldsymbol{r}_{\text{c}}, t) = \boldsymbol{\varepsilon} \hat{E} \cos(\omega_{\text{L}} t - \boldsymbol{k}_{\text{L}} \cdot \boldsymbol{r}_{\text{c}}). \tag{1.459}$$

Because $\boldsymbol{\nabla} \hat{E} = \boldsymbol{0}$ we find

$$\boldsymbol{\alpha} = \boldsymbol{0}, \qquad \boldsymbol{\beta} = \boldsymbol{\nabla} \phi = -\boldsymbol{k}_{\text{L}} \tag{1.460}$$

and thus

$$\boldsymbol{F}_{\text{react}} = \boldsymbol{0}, \qquad \boldsymbol{F}_{\text{diss}} = \hbar \Omega_1 \bar{v} \boldsymbol{k}_{\text{L}}. \tag{1.461}$$

From (1.439) we know $\langle \mathrm{d}N/\mathrm{d}t \rangle = \Omega_1 v$ so that in saturation

$$\boldsymbol{F}_{\text{diss}} = \left\langle \frac{\mathrm{d}\bar{N}}{\mathrm{d}t} \right\rangle_{\text{sat}} \hbar \boldsymbol{k}_{\text{L}} \tag{1.462}$$

which can be interpreted in a very straightforward way: the momentum carried by the absorbed photon is $\hbar \boldsymbol{k}_{\text{L}}$. If it is re-emitted by stimulated emission the atom does not gain any net momentum and the photon is added to the external field again. Instead, if it is re-emitted by spontaneous emission the net momentum gain is—on average—$\hbar \boldsymbol{k}_{\text{L}}$ because spontaneous emission is equally likely in two opposite directions. In this case the photon is taken away from the incident radiation and added to the quantized field $\boldsymbol{E}_{\perp}$. This loss of photons in the incident beam is precisely what is described by $\left\langle \frac{\mathrm{d}\bar{N}}{\mathrm{d}t} \right\rangle_{\text{sat}}$ in the steady-state regime. The force exerted by photons being absorbed (or without preferred direction re-emitted) is called *radiation pressure force* or *resonant scattering force*.

Using (1.442) we can also write

$$\boldsymbol{F}_{\rm diss} = \Gamma \bar{\sigma}_{bb} \hbar \boldsymbol{k}_{\rm L}, \tag{1.463}$$

and with (1.434)

$$\boldsymbol{F}_{\rm diss} = \hbar \boldsymbol{k}_{\rm L} \Gamma \, \frac{\Omega_1^2}{4} \frac{1}{\delta_{\rm L}^2 + (\Gamma^2/4) + (\Omega_1^2/2)} = \hbar \boldsymbol{k}_{\rm L} \frac{\Gamma}{2} \frac{\Omega_1^2/2}{\delta_{\rm L}^2 + (\Gamma^2/4) + (\Omega_1^2/2)}. \tag{1.464}$$

The dissipative force $\boldsymbol{F}_{\rm diss}$ as a function of the laser frequency $\omega_{\rm L} = \delta_{\rm L} + \omega_0$ is a Lorentzian centered at $\omega_{\rm L} = \omega_0$ with a FWHM of $\sqrt{\Gamma^2 + 2\Omega_1^2}$. At low intensity it is proportional to Ω_1^2 (and thus to the intensity itself). For strong driving it saturates at

$$\boldsymbol{F}_{\rm diss,sat} = \hbar \boldsymbol{k}_{\rm L} \, \frac{\Gamma}{2}, \tag{1.465}$$

and does not increase further with increasing laser field strength.

For the sodium atom Na and its yellow line we obtain an acceleration

$$a = |F_{\rm diss,sat}|/M \tag{1.466}$$

of $10^6\,{\rm m/s^2} \simeq 10^5 g$.

We can now also show why the external time scale is given by $T_{\rm ext} = \hbar/E_{\rm rec}$. Once the atom moves with a velocity v_m such that the Doppler-shifted frequency is out of resonance,

$$k_{\rm L} v_m \simeq \Gamma \tag{1.467}$$

it will not be further accelerated. We take $T_{\rm ext}$ as the time during which the atom is accelerated up to this velocity:

$$a T_{\rm ext} \simeq \frac{\hbar k_{\rm L}}{M} \frac{\Gamma}{2} T_{\rm ext} = v_m = \frac{\Gamma}{k_{\rm L}} \tag{1.468}$$

where in the last step (1.467) was used. Hence

$$T_{\rm ext} \simeq \frac{2M}{\hbar k_{\rm L}^2} = \frac{\hbar}{E_{\rm rec}}, \tag{1.469}$$

confirming the estimate made above.

Reactive force: dipole force

We need $\boldsymbol{\nabla} \hat{E} \neq \boldsymbol{0}$ in order $\boldsymbol{F}_{\rm react}$ not to vanish. It is thus necessary to superimpose different $\boldsymbol{k}_{\rm L}$. The simplest situation is that of a standing wave studied already in Sec. 1.4.1. We assume $\boldsymbol{k}_{\rm L} = k_{\rm L} \boldsymbol{e}_z$ and add another wave with wave vector $-\boldsymbol{k}_{\rm L}$. Both waves are assumed to be polarized in x-direction so that

$$\boldsymbol{E}(\boldsymbol{r}_{\rm c}, t) = \boldsymbol{e}_x \hat{E} \cos k_{\rm L} z \, \cos \omega_{\rm L} t. \tag{1.470}$$

According (1.457),

$$\boldsymbol{F}_{\text{react}} = -\hbar\Omega_1 \bar{u}\ \boldsymbol{\alpha}, \tag{1.471}$$

$\boldsymbol{F}_{\text{react}}$ is proportional to the in-phase component $\bar{u}$ of the Bloch vector. On the other hand, the number of absorbed photons is $\sim \bar{v}$, showing that the reactive force does not involve the net absorption of photons. How is it then possible that there is an effect on the atom at all?

The key to the understanding why an atom can be moved without a net absorption of energy by the atom is to realize that as soon as we have a superposition of modes describing the incident external field, the atom may *redistribute* photons. In the standing wave case the atom may absorb one photon from one beam and emit it into the other beam. Energy is conserved in such a process while the momentum of the atom changes by $\pm 2\hbar\boldsymbol{k}_{\text{L}}$.

Substituting (1.432) into (1.471) we obtain

$$\boldsymbol{F}_{\text{react}} = -\hbar\Omega_1 \underbrace{\frac{\Omega_1}{2}\frac{\delta_{\text{L}}}{\delta_{\text{L}}^2 + (\Gamma^2/4) + (\Omega_1^2/2)}}_{\bar{u}} \underbrace{\frac{\boldsymbol{\nabla}\Omega_1}{\Omega_1}}_{\boldsymbol{\alpha}} = -\frac{\hbar\delta_{\text{L}}}{4}\frac{\boldsymbol{\nabla}\Omega_1^2}{\delta_{\text{L}}^2 + (\Gamma^2/4) + (\Omega_1^2/2)}. \tag{1.472}$$

We discuss this expression in the following:

1. We see that for a red detuning $\delta_{\text{L}} = \omega_{\text{L}} - \omega_0 < 0$ the force (1.472) attracts atoms to regions of higher intensity.

2. For a blue detuning $\delta_{\text{L}} = \omega_{\text{L}} - \omega_0 > 0$ the force (1.472) repels atoms from regions of higher intensity.

3. This is the same behavior we observed for our model of a classical dipole in Sec. 1.4.1 if we identify the oscillator frequency Ω there with the atomic transition ω_0 and the driver ω with ω_{L}. However, note that the functional dependence is different.

4. Both for the limit $\Omega \to 0$ in the classical case and $\omega_0 \to 0$ here the dipole/atom is repelled from high-intensity regions (blue detuning).

5. For which detuning δ_{L} is the force $|\boldsymbol{F}_{\text{react}}|$ maximum? One easily checks that the optimal detuning is on the order of $|\Omega_1|$ so that

$$|\boldsymbol{F}_{\text{react}}| \sim \left|\frac{\hbar\boldsymbol{\nabla}\Omega_1^2}{\Omega_1}\right| \sim \hbar|\boldsymbol{\nabla}\Omega_1|. \tag{1.473}$$

   Contrary to the dissipative force (1.465) the reactive force does not saturate but increases further with increasing driver. As the maximal gradient is on the order of the wave number one obtains

$$|\boldsymbol{F}_{\text{react}}| \sim \hbar k_{\text{L}}\ \Omega_1, \tag{1.474}$$

which describes the absorption and stimulated emission of photons at a rate Ω_1. This may be compared to the expression (1.465) for the dissipative force where photons are absorbed and spontaneously emitted with a rate on the order of Γ.

6. The force (1.472) has a potential U,

$$\boldsymbol{F}_{\text{react}} = -\boldsymbol{\nabla} U \tag{1.475}$$

given by ($\rightarrow$ exercise).

$$U = \frac{\hbar \delta_{\text{L}}}{2} \ln \left[1 + \frac{\Omega_1^2/2}{\delta_{\text{L}}^2 + (\Gamma^2/4)} \right]. \tag{1.476}$$

7. The reaction force (1.472) is also called *dipole force*.

Chapter 2

Condensates, superfluids, and clusters

In this Chapter we study ensembles of atoms. It depends on the atomic properties and the thermodynamic variables such as pressure, temperature, and the particle number whether an ensemble of atoms aggregates to molecules, clusters, crystals etc. or to more exotic types of matter like a Bose-Einstein condensate (BEC) or a superfluid. The two latter ones are particularly fascinating, as they display macroscopic quantum phenomena. BECs are produced using the traps and cooling techniques discussed in the experimental part of this lecture.

2.1 Bose-Einstein condensation

The BEC is the simplest macroscopic quantum state. In 1924 S.N. Bose wrote to Einstein, describing his idea to treat the black-body radiation as a gas of identical particles, namely photons. Einstein realized that this idea should also be applicable to massive particles.

In this Section we follow the book by J.F. Annett.[1]

2.1.1 Reminder: Bose-Einstein statistics

N_s identical Bose particles can be distributed among M_s available quantum states in

$$W_s = \frac{(N_s + M_s - 1)!}{N_s!\,(M_s - 1)!} \tag{2.1}$$

ways. This is easy to understand if one counts the possibilities to arrange N_s particles in M_s boxes (see Fig. 2.1). As there are $M_s - 1$ walls we have $(N_s + M_s - 1)!$

[1] James F. Annett, *Superconductivity, Superfluids and Condensates* (Oxford University Press, Oxford, 2010).

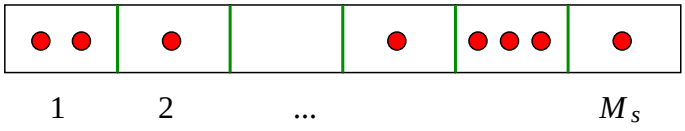

Figure 2.1: Bosons in quantum states $1, 2, \ldots M_s$.

ways to order the particles and the walls. Because both particles and walls are indistinguishable we have to divide by $N_s!$ and $(M_s - 1)!$.

Consider a box of volume $V = L_x L_y L_z$ and periodic boundary conditions. The wavefunctions of the particles are of the form

$$\psi(\boldsymbol{r}) = \frac{1}{\sqrt{V}} \, \mathrm{e}^{\mathrm{i}\boldsymbol{k}\cdot\boldsymbol{r}} \tag{2.2}$$

with

$$\boldsymbol{k} = \left(\frac{2\pi n_x}{L_x}, \frac{2\pi n_y}{L_y}, \frac{2\pi n_z}{L_z} \right), \qquad n_{x,y,z} = 0, 1, 2, \ldots . \tag{2.3}$$

The number of quantum states within an infinitesimal volume d^3k is

$$\frac{V}{(2\pi)^3} \, \mathrm{d}^3k, \tag{2.4}$$

and their energy reads

$$\epsilon_{\boldsymbol{k}} = \frac{\hbar^2 k^2}{2m}. \tag{2.5}$$

The number of states in a thin shell of thickness δk_s is

$$M_s = 4\pi k_s^2 \, \delta k_s \, \frac{V}{(2\pi)^3}. \tag{2.6}$$

Expressing k_s^2 and δk_s by $\epsilon_s = \epsilon_{\boldsymbol{k}_s}$ leads to

$$M_s = V g(\epsilon_s) \, \delta\epsilon_s \tag{2.7}$$

with the density of states

$$g(\epsilon) = \frac{m^{3/2}}{\sqrt{2}\,\pi^2\hbar^3} \, \sqrt{\epsilon}. \tag{2.8}$$

In order to derive the Bose-Einstein distribution function we want to maximize the entropy

$$S = k_\mathrm{B} \ln W \tag{2.9}$$

with W the number of available microstates for a given total energy E. If we know that N_s Bose particles are in shell s, the number of available microstates is the product of the number of states available in the shells,

$$W = \prod_s W_s = \prod_s \frac{(N_s + M_s - 1)!}{N_s! \; (M_s - 1)!}. \tag{2.10}$$

With Stirling's formula $\ln N! \simeq N \ln N - N$ follows for N_s and $M_s \gg 1$

$$S = k_\mathrm{B} \ln W = k_\mathrm{B} \sum_s \{(N_s + M_s) \ln(N_s + M_s) - N_s \ln N_s - M_s \ln M_s\}. \tag{2.11}$$

The entropy has to be maximized in a way keeping the total number of particles

$$N = \sum_s N_s \tag{2.12}$$

and the given total energy

$$U = \sum_s \epsilon_s N_s \tag{2.13}$$

constant. Introducing Lagrange multipliers $-k_\mathrm{B}\beta$ and $k_\mathrm{B}\beta\mu$ we have

$$\frac{\partial S}{\partial N_s} - k_\mathrm{B}\beta \frac{\partial U}{\partial N_s} + k_\mathrm{B}\beta\mu \frac{\partial N}{\partial N_s} = 0 \tag{2.14}$$

which gives

$$\ln(N_s + M_s) - \ln N_s - \beta\epsilon_s + \beta\mu = 0 \tag{2.15}$$

and

$$\frac{N_s}{M_s} = \frac{1}{\mathrm{e}^{\beta(\epsilon_s - \mu)} - 1}. \tag{2.16}$$

This is the average number of Bose particles occupying any single quantum state of energy $\epsilon = \epsilon_s$ and follows the *Bose-Einstein distribution* (BED)

$$f_\mathrm{BE}(\epsilon) = \frac{1}{\mathrm{e}^{\beta(\epsilon - \mu)} - 1}. \tag{2.17}$$

Using the first law $\mathrm{d}U = T\,\mathrm{d}S - P\,\mathrm{d}V + \mu\,\mathrm{d}N$ one can show ($\rightarrow$ exercise) that $\beta = 1/k_\mathrm{B}T$ and μ is the chemical potential.

2.1.2 Phase transition

Despite the fact that the Bose-Einstein ideal gas is non-interacting, it displays a phase transition! This is remarkable, as it does neither occur for the classical ideal gas nor for a Fermi-Dirac gas. The BEC phase transition is one of the examples where the *particle statistics* has astonishing observable effects [another one being, e.g., magnetism ($\rightarrow$ Heisenberg exchange operator)].

Phase transition means that thermodynamic variables make an abrupt change at a certain critical temperature T_c. In a gas-liquid phase transition, for instance, "condensed" particles (in droplets) coexist with gas particles. Liquid and gas are separated in position space. In BEC it turns out that particles separate in momentum space. The condensed particles occupy the zero-momentum state, the other, "normal" Bose-Einstein gas particles have finite momentum.

The number of Bose particles in the box is

$$N = \sum_{\boldsymbol{k}} \frac{1}{\mathrm{e}^{\beta(\epsilon_{\boldsymbol{k}}-\mu)}-1} \to \frac{V}{(2\pi)^3}\int \frac{1}{\mathrm{e}^{\beta(\epsilon_{\boldsymbol{k}}-\mu)}-1}\,\mathrm{d}^3k \tag{2.18}$$

so that the particle density as a function of temperature and chemical potential reads

$$n(T,\mu) = \frac{1}{(2\pi)^3}\int \frac{1}{\mathrm{e}^{\beta(\epsilon_{\boldsymbol{k}}-\mu)}-1}\,\mathrm{d}^3k = \int_0^\infty \frac{1}{\mathrm{e}^{\beta(\epsilon-\mu)}-1}\,g(\epsilon)\,\mathrm{d}\epsilon \tag{2.19}$$

with $g(\epsilon)$ given in (2.8).

What we need is $\mu(T,n)$. Introducing the fugacity

$$z = \mathrm{e}^{\beta\mu} \tag{2.20}$$

and

$$x = \beta\epsilon \tag{2.21}$$

one can write

$$n = \frac{(mk_{\mathrm{B}}T)^{3/2}}{\sqrt{2}\,\pi^2\hbar^3}\int_0^\infty \frac{z\mathrm{e}^{-x}}{1-z\mathrm{e}^{-x}}\sqrt{x}\,\mathrm{d}x = \left(\frac{mk_{\mathrm{B}}T}{2\pi\hbar^2}\right)^{3/2} g_{3/2}(z) \tag{2.22}$$

where

$$g_q(z) = \sum_{p=1}^{\infty}\frac{z^p}{p^q}. \tag{2.23}$$

It can be shown that the series converges for $|z| \le 1$ and diverges for $|z| > 1$. Especially,

$$g_{3/2}(1) = \zeta(3/2) = 2.612 \tag{2.24}$$

with $\zeta(s) = \sum_{p=1}^{\infty} 1/p^s$ the Riemann zeta function.

$$\frac{\mathrm{d}g_{3/2}(z)}{\mathrm{d}z} = \frac{1}{z}\sum_{p=1}^{\infty}\frac{z^p}{p^{1/2}} \tag{2.25}$$

diverges at $z = 1$. It thus looks as depicted in Fig. 2.2

From (2.22) we see that

$$g_{3/2}\left(\mathrm{e}^{\beta\mu}\right) = \left(\frac{2\pi\hbar^2}{mk_{\mathrm{B}}T}\right)^{3/2} n. \tag{2.26}$$

For low densities or high temperatures the right hand side is small so that on the left hand side we can expand $g_{3/2}(z) \simeq z + \cdots$ and obtain

$$\mu \simeq -\frac{3}{2}k_{\mathrm{B}}T\,\ln\left(\frac{mk_{\mathrm{B}}T}{2\pi\hbar^2 n^{2/3}}\right), \tag{2.27}$$

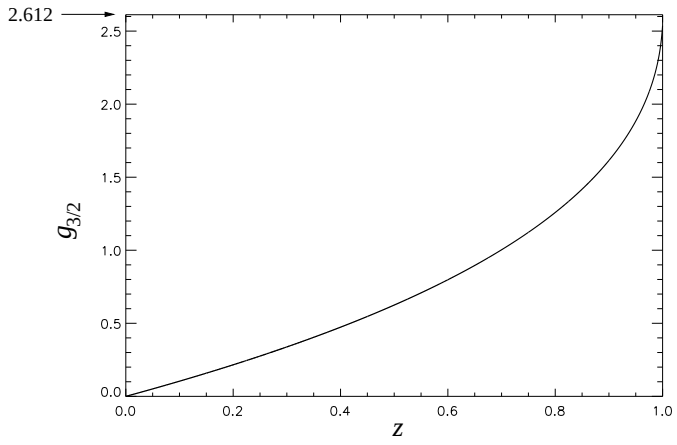

Figure 2.2: Function $g_{3/2}(z)$. The first derivative diverges at $z = 1$.

which is the well-known chemical potential for the ideal gas.

Because the expression in the brackets is > 1 at high temperatures or low densities the chemical potential is negative in this regime. Upon cooling, the chemical potential increases and becomes zero at the *critical BEC temperature*

$$T_c = \frac{2\pi\hbar^2}{k_{\mathrm{B}} m} \left(\frac{n}{2.612}\right)^{2/3}. \tag{2.28}$$

Now the big question is what happens when we go below T_c. Einstein realized that in the limit $T \to 0$ all Bose particles occupy the $\epsilon_{\boldsymbol{k}} = 0$-state. In the thermodynamic limit where $N, V \to \infty$ but N/V =const this means that infinitely many particles end up in the $\epsilon_{\boldsymbol{k}} = 0$-state. The number of particles in this state is

$$N_0 = \frac{1}{\mathrm{e}^{-\beta\mu} - 1} \tag{2.29}$$

which, for large N_0 means that

$$\mu = -k_{\mathrm{B}} T \ln\left(1 + \frac{1}{N_0}\right) \simeq -k_{\mathrm{B}} T \frac{1}{N_0} \overset{N_0 \to \infty}{\longrightarrow} 0. \tag{2.30}$$

If a finite fraction of the total number of particles is in the ground state then $\mu \to 0$ as $V, N_0 \to \infty$. Therefore, below T_c the chemical potential remains zero.

We now treat the density of the particles in the ground state separately because the continuum approximation for the sum over $\boldsymbol{k}$ actually does not apply for $\boldsymbol{k} = 0$ ($\to$ exercise). We then have with $\mu = 0$ (i.e., $z = 1$)

$$N = N_0 + \sum_{\boldsymbol{k} \neq 0} \frac{1}{\mathrm{e}^{\beta\epsilon_{\boldsymbol{k}}} - 1} \tag{2.31}$$

and

$$n = n_0 + \frac{(mk_{\rm B}T)^{3/2}}{\sqrt{2}\pi^2\hbar^3}\int_0^\infty \frac{{\rm e}^{-x}}{1-{\rm e}^{-x}}\sqrt{x}\,{\rm d}x. \tag{2.32}$$

For $T < T_c$ one finds

$$n = n_0 + 2.612\left(\frac{mk_{\rm B}T}{2\pi\hbar^2}\right)^{3/2} = n_0 + n_n \tag{2.33}$$

where n_0 is the condensate density and n_n is the density of the "normal" Bose gas. The fraction n_0/n can be written as

$$\frac{n_0}{n} = 1 - \left(\frac{T}{T_c}\right)^{3/2}. \tag{2.34}$$

The total internal energy density u is

$$u = \int_0^\infty \frac{\epsilon}{{\rm e}^{\beta(\epsilon-\mu)}-1}\,g(\epsilon)\,{\rm d}\epsilon = (k_{\rm B}T)^{5/2}\frac{m^{3/2}}{\sqrt{2}\pi^2\hbar^3}\int_0^\infty \frac{z{\rm e}^{-x}}{1-z{\rm e}^{-x}}\,x^{3/2}\,{\rm d}x. \tag{2.35}$$

For $T > T_c$ one obtains

$$u = \frac{3}{2}k_{\rm B}T\frac{g_{5/2}(z)}{g_{3/2}(z)} \tag{2.36}$$

which, in the high-temperature limit goes to $(3/2)k_{\rm B}T$ because both $g_{3/2}(z)$ and $g_{5/2}(z) \to z$ for $z \to 0$. Thus we recover the ideal gas behavior in the high-temperature limit where the statistics of the particles involved is not important anymore.

For $T < T_c$ one obtains

$$u = \frac{3}{2}k_{\rm B}\frac{T^{5/2}}{T_c^{3/2}}\frac{g_{5/2}(1)}{g_{3/2}(1)} \tag{2.37}$$

with $g_{5/2}(1) = \zeta(5/2) = 1.342$.

2.1.3 BEC in ultra-cold atomic gases

^{4}He becomes a superfluid but is not a BEC because the interactions between the ^{4}He atoms cannot be neglected. It took till 1995 for a BEC to be realized. In order for the non-interacting gas assumption to be valid one needs a dilute sample of atoms. However, (2.28)

$$T_c = \frac{2\pi\hbar^2}{k_{\rm B}m}\left(\frac{n}{2.612}\right)^{2/3} \tag{2.38}$$

indicates that a low density will decrease T_c, which makes it harder for the experimentalist. In fact, we have

$$n_{\text{liqu. He}} \simeq 2\times 10^{22}{\rm cm}^{-3} \gg n_{\text{Rb atoms}} \simeq 10^{11} - 10^{15}\ {\rm cm}^{-3} \tag{2.39}$$

where $n_{\text{Rb atoms}}$ is a typical density of alkali metal atoms in the trap in actual experiments. The first atomic BEC was achieved for the heavy ^{87}Rb alkali metal atoms. Unfortunately, T_c drops with increasing mass as well so that a dilute ensemble of rather heavy atoms seems a hopeless candidate for BEC. In fact, (2.38) shows that T_c for ^{87}Rb should be about $10^{-6} - 10^{-8}$ times smaller than the $T_c = 3.1\,\text{K}$ for ^{4}He (if it was non-interacting). Hence, one expects T_c in the range of $10\,\text{nK} - 1\,\mu\text{K}$ for dilute atomic alkali gases in traps. Employing cooling and trapping techniques based on lasers and magnetic fields it is nowadays possible to achieve such low temperatures, as discussed in the experimental part of this lecture.

An atom consists of electrons, protons, and neutrons. So how can such an object made of fermions be a Boson? Alkali metal atoms have a single valence electron. Hence, the electronic spin is $S_e = 1/2$. As a consequence, the nuclear spin must be also half-integer in order for the total spin being integer and the whole system bosonic. We thus need an odd number of protons plus neutrons. ^{7}Li, ^{23}Na, and ^{87}Rb have nuclear spin $S_n = 3/2$. The total spin is

$$S = \frac{3}{2} - \frac{1}{2} = 1 \qquad \text{or} \qquad S = \frac{3}{2} + \frac{1}{2} = 2. \tag{2.40}$$

If both total spins are present in the Bose gas it is a mixture in which $S = 1$ atoms are distinguishable from the $S = 2$ ones.

How can such atoms be trapped and cooled? We employ the Zeeman splitting of the energy levels with different magnetic quantum number M_S. For the $S = 2$ atoms there are the five states with

$$M_S = 2, 1, 0, -1, -2. \tag{2.41}$$

In order to construct them we start from the state

$$|S = 2, M_S = 2\rangle = \left|\frac{3}{2}, \frac{1}{2}\right\rangle \tag{2.42}$$

where on the right hand side we used the uncoupled spin states $|M_{S_n}, M_{S_e}\rangle$. Using the ladder operator

$$\hat{S}_- \, |M\rangle = \sqrt{S(S+1) - M(M-1)} \, |M-1\rangle \tag{2.43}$$

and $\hat{S}_- = \hat{S}_{n-} + \hat{S}_{e-}$ we find

$$\begin{aligned} \hat{S}_- \, |S = 2, M_S = 2\rangle &= (\hat{S}_n + \hat{S}_e) \left|\frac{3}{2}, \frac{1}{2}\right\rangle \\ \Rightarrow \sqrt{2 \cdot 3 - 2 \cdot 1} \, |S = 2, M_S = 1\rangle &= \sqrt{\frac{3}{2} \cdot \frac{5}{2} - \frac{3}{2} \cdot \frac{1}{2}} \left|\frac{3}{2} - 1, \frac{1}{2}\right\rangle \\ &\quad + \sqrt{\frac{1}{2} \cdot \frac{3}{2} - \frac{1}{2} \cdot \left(-\frac{1}{2}\right)} \left|\frac{3}{2}, \frac{1}{2} - 1\right\rangle \end{aligned}$$

$$\Rightarrow 2\,|S=2,M_S=1\rangle = \sqrt{3}\left|\frac{1}{2},\frac{1}{2}\right\rangle + \left|\frac{3}{2},-\frac{1}{2}\right\rangle$$
$$\Rightarrow |S=2,M_S=1\rangle = \frac{1}{2}\left(\sqrt{3}\left|\frac{1}{2},\frac{1}{2}\right\rangle + \left|\frac{3}{2},-\frac{1}{2}\right\rangle\right). \quad (2.44)$$

Applying the ladder operator three more times we obtain

$$|S=2,M_S=0\rangle = \frac{1}{\sqrt{2}}\left(\left|\frac{1}{2},-\frac{1}{2}\right\rangle + \left|-\frac{1}{2},\frac{1}{2}\right\rangle\right), \quad (2.45)$$
$$|S=2,M_S=-1\rangle = \frac{1}{2}\left(\sqrt{3}\left|-\frac{1}{2},-\frac{1}{2}\right\rangle + \left|-\frac{3}{2},\frac{1}{2}\right\rangle\right), \quad (2.46)$$
$$|S=2,M_S=-2\rangle = \left|-\frac{3}{2},-\frac{1}{2}\right\rangle. \quad (2.47)$$

For the $S=1$ states one finds

$$|S=1,M_S=1\rangle = \frac{1}{2}\left(\left|\frac{1}{2},\frac{1}{2}\right\rangle - \sqrt{3}\left|\frac{3}{2},-\frac{1}{2}\right\rangle\right), \quad (2.48)$$
$$|S=1,M_S=0\rangle = \frac{1}{\sqrt{2}}\left(\left|\frac{1}{2},-\frac{1}{2}\right\rangle - \left|-\frac{1}{2},\frac{1}{2}\right\rangle\right), \quad (2.49)$$
$$|S=1,M_S=-1\rangle = \frac{1}{2}\left(\left|-\frac{1}{2},-\frac{1}{2}\right\rangle - \sqrt{3}\left|-\frac{3}{2},\frac{1}{2}\right\rangle\right). \quad (2.50)$$

The degeneracy of $S=1$ and $S=2$ states is removed by the hyperfine interaction J between the electron and the nucleus. In the presence of a magnetic field $\boldsymbol{B}=B_z\boldsymbol{e}_z$ the degeneracy with respect to M_S is also removed,

$$\hat{H} = J\hat{\boldsymbol{S}}_e\cdot\hat{\boldsymbol{S}}_n + 2\mu_{\rm B}\hat{S}_{ez}B_z. \quad (2.51)$$

Here $\mu_{\rm B}=e\hbar/2m_e$ is the Bohr magneton and $2\mu_{\rm B}$ is the magnetic moment of the valence electron. For $B_z=0$ we find using

$$\hat{\boldsymbol{S}}_e\cdot\hat{\boldsymbol{S}}_n = \frac{1}{2}\left(\hat{\boldsymbol{S}}^2-\hat{\boldsymbol{S}}_e^2-\hat{\boldsymbol{S}}_n^2\right) \quad (2.52)$$

the eigenenergies

$$E_{S=2} = \frac{1}{2}J\hbar^2\left\{2(2+1)-\frac{1}{2}\left(\frac{1}{2}+1\right)-\frac{3}{2}\left(\frac{3}{2}+1\right)\right\} = \frac{3}{4}J\hbar^2. \quad (2.53)$$

and

$$E_{S=1} = \frac{1}{2}J\hbar^2\left\{1(1+1)-\frac{1}{2}\left(\frac{1}{2}+1\right)-\frac{3}{2}\left(\frac{3}{2}+1\right)\right\} = -\frac{5}{4}J\hbar^2. \quad (2.54)$$

We can apply perturbation theory and calculate the energy shifts $\Delta E=\langle\hat{H}'\rangle$ with $\hat{H}=2\mu_{\rm B}\hat{S}_{ez}B_z$ using the spin states above. The resulting Zeeman splitting is sketched in Fig. 2.3.

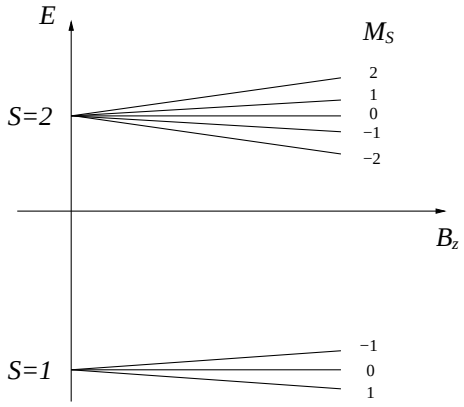

Figure 2.3: Energy levels for an alkali metal atom with a nuclear spin $S_n = 3/2$ in a magnetic field B_z.

Imagine now a space-dependent magnetic field $\boldsymbol{B}(\boldsymbol{r})$ with a local minimum in $|\boldsymbol{B}(\boldsymbol{r})|$. Atoms in the states $|S = 2, M_S = 2, 1\rangle$ and $|S = 1, M_S = -1\rangle$ minimize their energy by moving towards the minimum of $|\boldsymbol{B}(\boldsymbol{r})|$. Instead, atoms in the states $|S = 2, M_S = -2, -1\rangle$ and $|S = 1, M_S = 1\rangle$ are expelled by the field minimum. Too hot atoms will not be trapped, which leads to an automatic cooling of the atomic ensemble inside the trap (*evaporative cooling*). The lower the barrier around the minimum of $|\boldsymbol{B}(\boldsymbol{r})|$ the higher is the cooling rate. Temperatures below μK can be reached in this way.

2.1.4 Macroscopic wave function

The neglect of any interaction between the atoms is only an approximation. At very short distances they repel each other while at large distances there is a van der Waals attraction. In fact, two-body collisions are necessary to establish a thermal equilibrium. At high densities alkali metal atoms are known to form clusters. This does not occur in the BEC experiments because the gas of atoms is dilute and thus the probability of three-body collisions, necessary for binding (why?), is small. If we assume an atom density of $\simeq 10^{11} - 10^{15}\,\mathrm{cm}^{-3}$ in the trap, the typical distance between two atoms r_s, defined via

$$n = \frac{N}{V} = \frac{1}{\frac{4}{3}\pi r_s^3} \tag{2.55}$$

is about $r_s \simeq 50 - 600\,\mathrm{nm}$ whereas the length scale for the interatomic interaction is $< 1\,\mathrm{nm}$. While being crucial for establishing a thermal equilibrium, two-body collisions do not cause transitions between the hyperfine levels $S = 1$ and $S = 2$ so that atoms cannot switch from low-field seeking states to high-field-seeking states, which would lead to an additional loss of atoms inside the trap.

The many-body Hamiltonian for the atoms in one of the above spin states in second quantization reads

$$\hat{H}_a = \int \mathrm{d}^3 r\ \hat{\psi}^\dagger(\boldsymbol{r}) \left(-\frac{\hbar^2}{2m}\boldsymbol{\nabla}^2 + V_{\mathrm{trap}}(\boldsymbol{r}) \right) \hat{\psi}(\boldsymbol{r}) \tag{2.56}$$
$$+ \int \mathrm{d}^3 r \int \mathrm{d}^3 r'\ \hat{\psi}^\dagger(\boldsymbol{r}) \hat{\psi}^\dagger(\boldsymbol{r}') W(|\boldsymbol{r}-\boldsymbol{r}'|) \hat{\psi}(\boldsymbol{r}') \hat{\psi}(\boldsymbol{r}).$$

Here, $\hat{\psi}^{(\dagger)}(\boldsymbol{r})$ are bosonic field operators, V_{trap} is the potential of the magnetic trap, and $W(|\boldsymbol{r}-\boldsymbol{r}'|)$ is the interaction between the bosonic atoms. Because the interaction $W(|\boldsymbol{r}-\boldsymbol{r}'|)$ is repulsive and very strong only at short distances we may approximate it by a delta function,

$$W(|\boldsymbol{r}-\boldsymbol{r}'|) \simeq g\delta(\boldsymbol{r}-\boldsymbol{r}') \tag{2.57}$$

where g is a constant governing the interaction strength. It can be related to the two-body s-wave scattering length a_s by $g = 4\pi a_s \hbar^2/m$. Plugging (2.57) into the interaction term of (2.56) we obtain

$$g \int \mathrm{d}^3 r\ \hat{\psi}^\dagger(\boldsymbol{r}) \underbrace{\hat{\psi}^\dagger(\boldsymbol{r})\hat{\psi}(\boldsymbol{r})}_{\hat{n}(\boldsymbol{r})} \hat{\psi}(\boldsymbol{r}) \tag{2.58}$$

so that we can write

$$\hat{H}_a = \int \mathrm{d}^3 r\ \hat{\psi}^\dagger(\boldsymbol{r}) \left(-\frac{\hbar^2}{2m}\boldsymbol{\nabla}^2 + V_{\mathrm{trap}}(\boldsymbol{r}) + gn(\boldsymbol{r}) \right) \hat{\psi}(\boldsymbol{r}), \tag{2.59}$$

which shows that the *effective* second quantized Hamiltonian is of single-particle potential type only. However, the potential depends on the density itself. Hence, for a given particle number and temperature we obtain the non-linear Schrödinger equation

$$\left(-\frac{\hbar^2}{2m}\boldsymbol{\nabla}^2 + V_{\mathrm{trap}}(\boldsymbol{r}) + gn(\boldsymbol{r}) \right) \psi_i(\boldsymbol{r}) = \epsilon_i \psi_i(\boldsymbol{r}) \tag{2.60}$$

together with

$$n(\boldsymbol{r}) = \sum_i \frac{1}{\mathrm{e}^{\beta(\epsilon_i-\mu)}-1}\ |\psi_i(\boldsymbol{r})|^2 \tag{2.61}$$

and

$$N = \int \mathrm{d}^3 r\ n(\boldsymbol{r}) = \sum_i \frac{1}{\mathrm{e}^{\beta(\epsilon_i-\mu)}-1}. \tag{2.62}$$

The last equation is used to determine the chemical potential μ. The set of equations (2.60)–(2.62) is to be solved self-consistently.[2] It is called the *Gross-Pitaevskii equations*.

[2]One could start with a guess for $n(\boldsymbol{r})$, solve (2.60) to obtain the ϵ_i and ψ_i, use (2.62) to determine μ and then (2.61) to calculate the new density. The cycle is repeated until convergence is achieved.

At $T = 0$ all atoms occupy the ground state ψ_0, i.e., $N = N_0$, and

$$n_0(\boldsymbol{r}) = N_0|\psi_0(\boldsymbol{r})|^2. \tag{2.63}$$

In this limit the self-consistent solution of the set (2.60)–(2.62) reduces to finding the ground state for the Gross-Pitaevskii equation

$$\left(-\frac{\hbar^2}{2m}\boldsymbol{\nabla}^2 + V_{\text{trap}}(\boldsymbol{r}) + gN|\psi_0|^2\right)\psi_0(\boldsymbol{r}) = \epsilon_0\psi_0(\boldsymbol{r}). \tag{2.64}$$

Because the number of atoms N is finite ($10^4 - 10^6$), we cannot strictly speak about a phase transition. However, in the experiment (and the numerical solution of the Gross-Pitaevskii equations) one observes a sudden increase in the number of atoms N_0 occupying the ground state ψ_0 at $T = T_c$, which is sufficiently sharp to clearly identify T_c.

As the ideal Bose gas is without any interaction ($g = 0$) what has been achieved experimentally with alkali metal atoms is actually not an ideal BEC. Instead, the weak interactions are responsible for the creation of a so-called *superfluid* which shows zero viscosity, persistent currents, and vortices.

BECs have been also used to demonstrate macroscopic quantum coherence, i.e., superpositions and interference of macroscopic numbers of atoms have been observed.

2.2 Superfluids

Most substances turn into solids as the temperature goes to zero. Helium is an exception. Both ^{3}He and ^{4}He remain liquid. We will see that this happens because of the weak van der Waals interaction and the low mass. Although the electronic configuration is the same for ^{3}He and ^{4}He (i.e., they are "chemically equivalent") they behave very differently at low temperatures because ^{3}He is a fermion and ^{4}He is a boson. Superfluidity sets in for ^{4}He at 2.17 K while for ^{3}He not before 2 mK, but then with more than one superfluid phase. In the following Subsections we will discuss the properties of ^{4}He and follow once more the book by J.F. Annett.[3]

2.2.1 Quantum fluids

The interaction between rare gas atoms (He, Ne, Ar, Kr, Xe) can be approximately modeled using a Lennard-Jones potential of the form

$$V(r) = E_0\left(\frac{d^{12}}{r^{12}} - 2\frac{d^6}{r^6}\right) \tag{2.65}$$

[3]James F. Annett, *Superconductivity, Superfluids and Condensates* (Oxford University Press, Oxford, 2010).

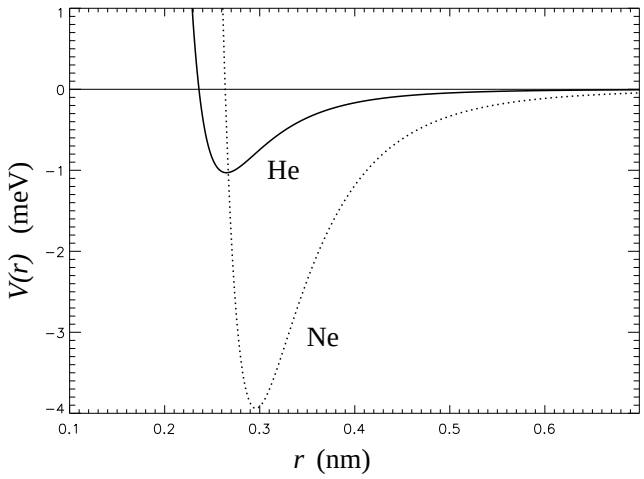

Figure 2.4: The potential (2.65) for He and Ne.

where E_0 is the potential minimum and d is its position. The values for He are $d = 0.265\,\text{nm}$, $E_0 = 1.03\,\text{meV}$. For Ne one has $d = 0.296\,\text{nm}$, $E_0 = 3.94\,\text{meV}$. The potential (2.65) for both cases is shown in Fig. 2.4.

Now we consider a He and a Ne fluid and want to understand why He is a quantum fluid and Ne is not. At normal pressure Ne becomes liquid at 27 K and freezes at 24 K. An average momentum for a given temperature is given by

$$\frac{p^2}{2m} = k_\text{B}T \qquad \Rightarrow \qquad p = \sqrt{2mk_\text{B}T}. \tag{2.66}$$

With of $p = \hbar k$ and $k = 2\pi/\lambda$ we obtain

$$\lambda = \sqrt{\frac{2\pi^2\hbar^2}{mk_\text{B}T}} = \sqrt{\pi}\lambda_\text{dB} \tag{2.67}$$

where λ_dB is by definition the thermal de Broglie wavelength. For Ne we find for the above temperatures $\lambda_\text{dB} \simeq 0.07\,\text{nm}$. As the potential minimum is at $d = 0.3\,\text{nm}$ we have $d \gg \lambda_\text{dB}$ and quantum effects are not expected to play any role. The Ne atoms are almost point-like and "sit" well-localized in the potential minima. Instead, ^{4}He becomes liquid at 4 K. The low temperature and the low mass lead to rather big $\lambda_\text{dB} = 0.4\,\text{nm} > d$. Hence, ^{4}He is a quantum fluid. The thermal de Broglie wavelength is even larger for ^{3}He but we concentrate on the bosonic ^{4}He here.

The phase diagrams of ^{4}He and Ne are shown in Fig. 2.5. In both cases the gas-liquid boundary ends at the critical point. However, for He the liquid-gas separation line never meets the liquid-solid line, which means there is no triple-point. Below a certain pressure there is no solid phase at any temperature. Moreover, there are

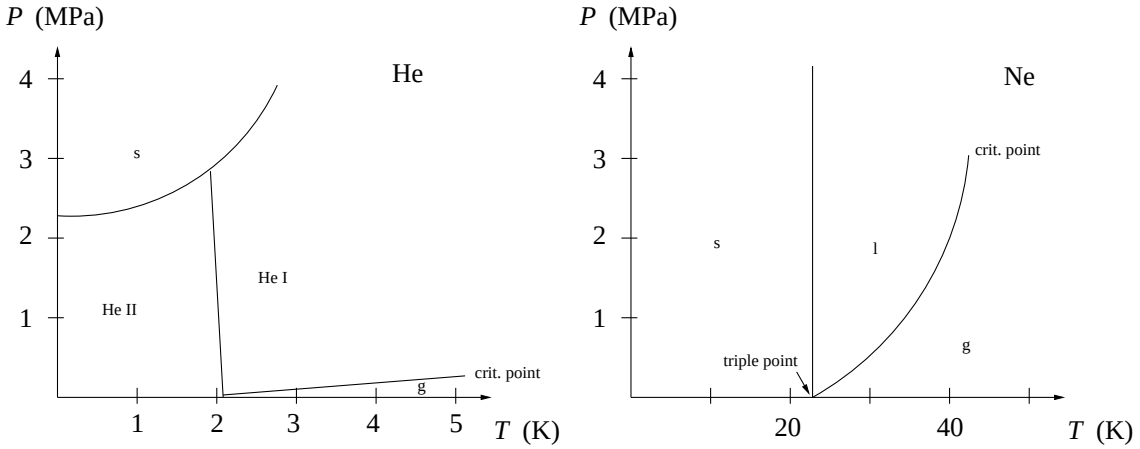

Figure 2.5: Schematic phase diagrams for He and Ne. At normal pressure He remains liquid down to $T = 0$ whereas Ne crystallizes.

two liquid phases, the "normal" He I and the superfluid He II. Both are quantum fluids.

The physical reason of why quantum fluids cannot crystallize is the zero point energy. Quantum systems have nonvanishing kinetic energy even in the ground state, i.e., at zero temperature. If the uncertainty in position is less than the lattice spacing, a substance can crystallize. On the other hand, if the uncertainty is larger than the position of the minimum in the interaction potential, the substance will not crystallize.

We consider the pair potential (2.65) and approximate it by a harmonic oscillator potential around the minimum $r = d$,

$$V(r) \simeq V(d)+V'(d)(r-d)+\frac{1}{2}V''(d)(r-d)^2+\cdots = -E_0+\underbrace{\frac{36E_0}{d^2}}_{\frac{1}{2}m\omega_0^2}(r-d)^2+\cdots . \quad (2.68)$$

From this we infer

$$\omega_0 = \sqrt{\frac{72E_0}{md^2}} \quad (2.69)$$

and the zero point energy should be of the order of[4]

$$\mathcal{E}_0 = \frac{1}{2}\hbar\omega_0. \quad (2.70)$$

For the He-parameters for E_0 and d above we obtain $\mathcal{E}_0 \simeq 1.5\,\mathrm{meV}$, i.e., similar to E_0. As $1\,\mathrm{eV}$ corresponds to a temperature $1\,\mathrm{eV}/k_\mathrm{B} = 11605\,\mathrm{K}$ we see that $1.5\,\mathrm{meV}$ corresponds to thermal motion at $17\,\mathrm{K}$. This lies even well above the temperature

[4]We just do an order of magnitude estimate here and neglect the crystal structure.

where He II forms! For Ne one finds a $\mathcal{E}_0$ well below E_0 and a temperature which indeed fits to the melting temperature.

2.2.2 Macroscopic wavefunction reloaded

In (2.1.4) we saw already that as $T \to 0$ all bosons condense in one state ψ_0. Instead of normalizing the ground state wavefunction to unity, as we did in (2.63), we may normalize it to the total number of particles in the condensed phase N_0 and write

$$n_0(\boldsymbol{r}) = |\psi_0(\boldsymbol{r})|^2, \qquad N_0 = \int \mathrm{d}^3 r\, n_0(\boldsymbol{r}). \tag{2.71}$$

We know that a wavefunction in general is complex and has a phase so that

$$\psi_0 = \sqrt{n_0}\, \mathrm{e}^{\mathrm{i}\theta} \tag{2.72}$$

where θ is real. However, (2.64) suggests that we can choose ψ_0 real. Let us imagine that the superfluid system or BEC is prepared with a macroscopic number of particles N_0 in the ground state ψ_0. Then, at later times, the quantum phase θ would evolve like $\theta(t) = -\epsilon_0 t/\hbar$. Such a purely time-dependent phase does not lead to observable effects unless a superposition of quantum states is constructed (which we want to avoid because we want to keep as much particles as possible in the ground state). However, let us suppose that the superfluid or BEC is somehow set into motion *as a whole*. We know that a particle moving with a well-defined momentum is quantum mechanically described by a plane wave $\mathrm{e}^{\mathrm{i}\boldsymbol{k}\cdot\boldsymbol{r}}/\sqrt{V}$. Hence, in order to describe a moving BEC or superfluid the phase θ must be space-dependent,

$$\theta = \theta(\boldsymbol{r}). \tag{2.73}$$

The current density is given by [suppressing all arguments $(\boldsymbol{r})$]

$$\boldsymbol{j}_0 = \frac{\hbar}{2m\mathrm{i}} \left\{\psi_0^* \boldsymbol{\nabla}\psi_0 - \psi_0 \boldsymbol{\nabla}\psi_0^*\right\}. \tag{2.74}$$

We find with $\psi_0 = \sqrt{n_0}\, \mathrm{e}^{\mathrm{i}\theta}$

$$\boldsymbol{\nabla}\psi_0 = (\boldsymbol{\nabla}\sqrt{n_0} + \sqrt{n_0}\mathrm{i}\boldsymbol{\nabla}\theta)\, \mathrm{e}^{\mathrm{i}\theta}, \qquad \boldsymbol{\nabla}\psi_0^* = (\boldsymbol{\nabla}\sqrt{n_0} - \sqrt{n_0}\mathrm{i}\boldsymbol{\nabla}\theta)\, \mathrm{e}^{-\mathrm{i}\theta}, \tag{2.75}$$

and thus

$$\boldsymbol{j}_0 = \frac{\hbar}{m} n_0 \boldsymbol{\nabla}\theta. \tag{2.76}$$

Because

$$\boldsymbol{j}_0 = n_0 \boldsymbol{v}_s \tag{2.77}$$

we infer that the *superfluid velocity* is

$$\boldsymbol{v}_s = \frac{\hbar}{m} \boldsymbol{\nabla}\theta. \tag{2.78}$$

2.2.3 Properties of He II

Experiments by Kapitsa in the 1930s showed that He II can flow without dissipation and viscosity η. This phenomenon is called *superflow*. Imagine a capillary of radius R and length L. A normal fluid flows because of a pressure difference ΔP along the capillary. From dimensional analysis one finds[5] that for a fluid flow velocity v

$$\frac{\Delta P}{L} \sim \eta \frac{v}{R^2}. \tag{2.79}$$

Kapitsa showed that for superfluid-flows below a critical velocity v_c the pressure difference ΔP is always zero, which means $\eta = 0$. Other experiments show that normal He I and superfluid He II coexist. Liquid He is thus described by a two-fluid model. The total particle density reads

$$n = n_s + n_n \tag{2.80}$$

where the index s stands for "superfluid" and n stand for "normal". For the current density we have

$$\boldsymbol{j} = \boldsymbol{j}_s + \boldsymbol{j}_n, \tag{2.81}$$

$$\boldsymbol{j}_s = n_s \boldsymbol{v}_s, \qquad \boldsymbol{j}_n = n_n \boldsymbol{v}_n. \tag{2.82}$$

Only the normal He I component n_n can carry heat and entropy. The He II component n_s is in a many-body quantum state. Remember that a "standard" quantum mechanical ground state of, e.g., an atom, has zero entropy. Hence, the heat current density is

$$\boldsymbol{Q} = T \underbrace{\frac{S}{V}}_{s} \boldsymbol{v}_n \tag{2.83}$$

with s the fluid entropy per unit volume. As a consequence there can be particle flow without heat flow if in a mixture of He I and II only He II can pass through a *superleak* connecting reservoirs of different temperatures. Consider the situation depicted in Fig. 2.6a.

Using the Gibbs free energy (free enthalpy)

$$G = U - TS + PV = \mu N \tag{2.84}$$

one has

$$\mathrm{d}G = -S\mathrm{d}T + V\mathrm{d}P. \tag{2.85}$$

Fluid flow will be such that $\mathrm{d}G = 0$, thus

$$P_2 - P_1 = s(T_2 - T_1). \tag{2.86}$$

[5]The dimension of viscosity is pressure $\times$ time.

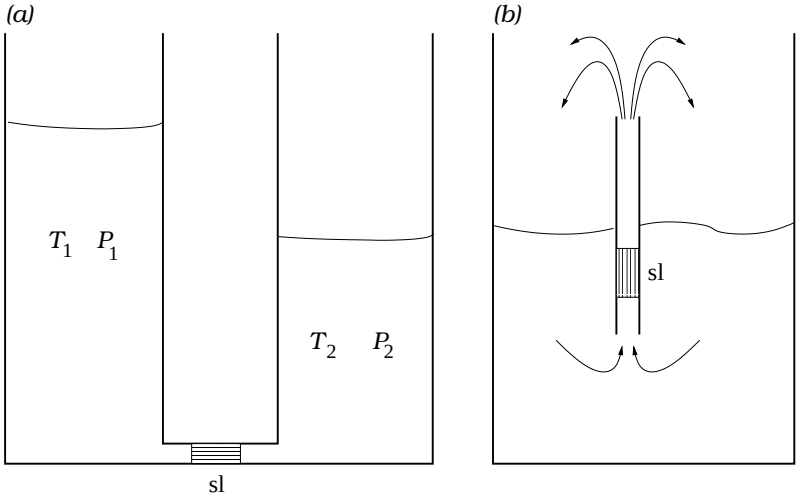

Figure 2.6: Thermo-mechanical effects due to a "superleak" sl through which only He II flows. (a) A temperature difference T_2-T_1 gives rise to a pressure gradient P_2-P_1, whiches drives a superflow. However, the superflow does not carry entropy such that the temperature difference remains despite particle transport. (b) Fountain effect. A heated superleak leads to a superflow forming a fountain above the surface.

This shows that a temperature difference will give rise to a pressure difference. The pressure difference will generate a flow. A normal fluid would—upon flowing—decrease the temperature gradient. However, since He II does not carry entropy, the temperature difference, and thus the pressure gradient, will remain ($\rightarrow$ fountain effect, Fig. 2.6b). He II has other uncommon features. It establishes a thin film at surfaces of containers and overcomes walls ($\rightarrow$ wikipedia, youtube).

2.2.4 Flow quantization

From (2.78) follows that superflow is a potential flow. Hence, it is *irrotational*,

$$\boldsymbol{\nabla} \times \boldsymbol{v}_s = \mathbf{0} \tag{2.87}$$

as long as θ is well defined. Note that if $\psi_0(\boldsymbol{r}) = 0$ somewhere, θ is not defined. Within a region where θ is defined we have from Stoke's theorem also $\oint \boldsymbol{v}_s \cdot \mathrm{d}\boldsymbol{r} = 0$.

Now we consider a flow along a tube (see Fig. 2.7). Within the tube we assume a potential flow but we allow for not defined θ outside the tube. Then the *circulation*

$$\oint \boldsymbol{v}_s \cdot \mathrm{d}\boldsymbol{r} = \kappa \tag{2.88}$$

may be different from zero (although independent from the integration path along the tube). Inserting (2.78) we have

$$\kappa = \frac{\hbar}{m} \oint \boldsymbol{\nabla}\theta \cdot \mathrm{d}\boldsymbol{r} = \frac{\hbar}{m}\Delta\theta \tag{2.89}$$

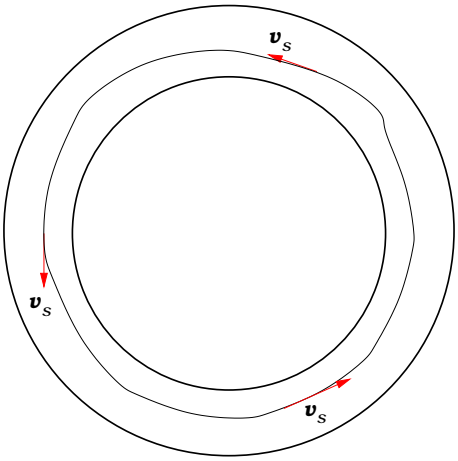

Figure 2.7: Superflow along a tube. Potential flow inside the tube. Nevertheless the circulation might be $\neq 0$.

where $\Delta\theta$ is the change in θ after going around the tube. As the wavefunction must be uniquely defined at all points inside the tube

$$\Delta\theta = 2\pi n \tag{2.90}$$

with n an integer. The circulation

$$\kappa = \frac{hn}{m} \tag{2.91}$$

is quantized, and one *quantum of circulation* is h/m. The quantum number n is also called the topological *winding number*. Flow quantization has been observed in experiments. Consider, for instance, liquid helium trapped between two rotating cylinders. The normal component has viscosity and will be set into rotation as well. The He II instead remains at rest with $\kappa = n = 0$. Now decrease the temperature so that the amount of normal He I decreases and turns into superfluid He II. Because of angular momentum conservation, the He II will start rotating too. However, it does so by sudden jumps of h/m in the circulation! Similar to the only *discrete* excitations of atoms also quantum fluids undergo discrete transitions between *macroscopic* states. In the same way, namely by transfer of angular momentum to the superfluid He I above T_c and subsequent cooling, persistent currents can be set up, since there is no mechanism that stops the superflow of He II.

Consider another setup. We start with a cylinder of liquid He. Initially the He II component is described by a wavefunction with well-defined θ everywhere so that $\boldsymbol{\nabla} \times \boldsymbol{v}_s = \mathbf{0}$, $\oint \boldsymbol{v}_s \cdot \mathrm{d}\boldsymbol{r} = 0$, i.e., there is no circulation. Then the cylinder is rotated and angular momentum may be transferred from the normal He I to He II upon cooling. In fact, one observes a bent surface due to centrifugal forces. Obviously,

the superfluid He II was excited because the parabolic shape of the surface implies an increase in energy. So where are the points of undefined θ which makes such a behavior possible?

As the curl of $\boldsymbol{v}_s = v_r\boldsymbol{e}_r + v_\phi\boldsymbol{e}_\phi + v_z\boldsymbol{e}_z$ in cylindrical coordinates reads

$$\boldsymbol{\nabla}\times\boldsymbol{v}_s = \frac{1}{r}\begin{vmatrix} \boldsymbol{e}_r & r\boldsymbol{e}_\phi & \boldsymbol{e}_z \\ \frac{\partial}{\partial r} & \frac{\partial}{\partial\phi} & \frac{\partial}{\partial z} \\ v_r & rv_\phi & v_z \end{vmatrix} \tag{2.92}$$

for a circular flow fulfilling $\boldsymbol{\nabla}\times\boldsymbol{v}_s = \boldsymbol{0}$

$$\frac{1}{r}\frac{\partial}{\partial r}(rv_\phi) = 0 \tag{2.93}$$

results. Hence,

$$\boldsymbol{v}_s = \frac{\kappa}{2\pi r}\,\boldsymbol{e}_\phi, \tag{2.94}$$

which satisfies $\boldsymbol{\nabla}\times\boldsymbol{v}_s = \boldsymbol{0}$ everywhere except at $r = 0$, the so-called *vortex core* of size $\simeq 1\,\text{Å}$. In the vortex core the wavefunction $\psi_0 = 0$, and θ is not defined.[6] The sum over all circulations of all vortices must add up to the total circulation of the He II fluid which determines the parabolic bending of the free surface. For a cylinder of radius R and angular frequency ω the total circulation is

$$\kappa = \oint \boldsymbol{v}_s\cdot\mathrm{d}\boldsymbol{r} = (2\pi R)(\omega R) = \frac{h}{m}N_v \tag{2.95}$$

where N_v is the number of vortices. The number of vortices per unit area in the rotating superfluid thus is $N_v/\pi R^2 = 2m\omega/h$. Vortices have been observed experimentally. For small rotation rates they form triangular arrays. Such vortex patterns have also been observed in BECs by rotating the (elliptically shaped) trap potential.

2.3 Clusters

Unlike gases or fluids clusters are more strongly bound aggregates of, say, 10 up to millions of atoms. Clusters bridge the gap between molecules and solids and may be categorized according to their binding:

1. metallic clusters (e.g., alkali: delocalized electrons);
2. valence clusters, semiconductor clusters (e.g., C, Si: covalent);
3. van der Waals clusters (e.g., rare gases: dispersive forces);
4. ionic clusters (e.g., $(\text{NaCl})_N$: heteropolar, difference in electro negativity);

[6] If we integrate, e.g., along a circle, $\mathrm{d}\boldsymbol{r} = r\boldsymbol{e}_\phi\,\mathrm{d}\phi$, from $\phi = 0$ to 2π we indeed obtain $\oint \boldsymbol{v}_s\cdot\mathrm{d}\boldsymbol{r} = \kappa$.

⋮

Due to their size of a few up to tens of nm the optical behavior of clusters is quite distinct from both single atoms and bulk matter. Unlike atoms clusters may display a pronounced collective behavior while their finite size distinguishes them from bulk matter. This is particularly evident in their response to radiation. However, before we study the interaction of clusters with (laser) light we need to understand their structure. On an *ab initio* level one should solve the many-particle Schrödinger equation for electrons and ions, just like in molecular physics. In fact, the theoretical *ab initio* methods applied are essentially the same in both molecular (or chemical) and cluster physics, e.g., linear combination of atomic orbitals (tight binding), Hartree-Fock, density functional theory, molecular dynamics, ..., all of them numerical in nature. Fortunately, many striking features of cluster structure and response theory can be understood in terms of simple analytical models, with which we will start now.

2.3.1 Magic numbers

Experimentally measured abundances of clusters as a function of the number of atoms N typically show high yields for particular N. Such N are called *magic numbers*. Obviously, when clusters are formed out of an initially homogeneous gas of atoms (or small molecules) such Ns are energetically more favorable than clusters with, e.g., $N \pm 1$. Such a behavior can be due to the ionic structure or due to the electronic structure. We will focus on electronic structure first.

Electronic structure of alkali metal clusters

Figure 2.8a shows the abundance of Na_N clusters under certain conditions.[7] Obviously $N = 8, 20, 40, 58, 92$-clusters are energetically favorable.

In alkali clusters the number of atoms N equals the number of valence electrons. In a first approximation we may model a neutral alkali metal cluster by N electrons that move in the potential created by the N singly charged ions. As the valence electrons in metals are delocalized we may disregard the ionic structure, assuming a smooth potential. This is the opposite of van der Waals clusters where each electron belongs to its "parent atom". We thus have to feed N electrons into a potential, a problem we know well from, e.g., atomic physics. The potential should take the interaction among the valence electrons into account, at least on a mean-field level. Let us assume we have such an effective potential $V(\boldsymbol{r})$. Because we do not know it better we assume it is spherical, $V(\boldsymbol{r}) = V(r)$.

The Schrödinger equation

$$\left(-\frac{\hbar^2}{2m}\boldsymbol{\nabla}^2 + V(r)\right)\Psi(\boldsymbol{r}) = E\Psi(\boldsymbol{r}) \tag{2.96}$$

[7] Specified in W.D. Knight *et al.*, Phys. Rev. Lett. **52**, 2141 (1984).

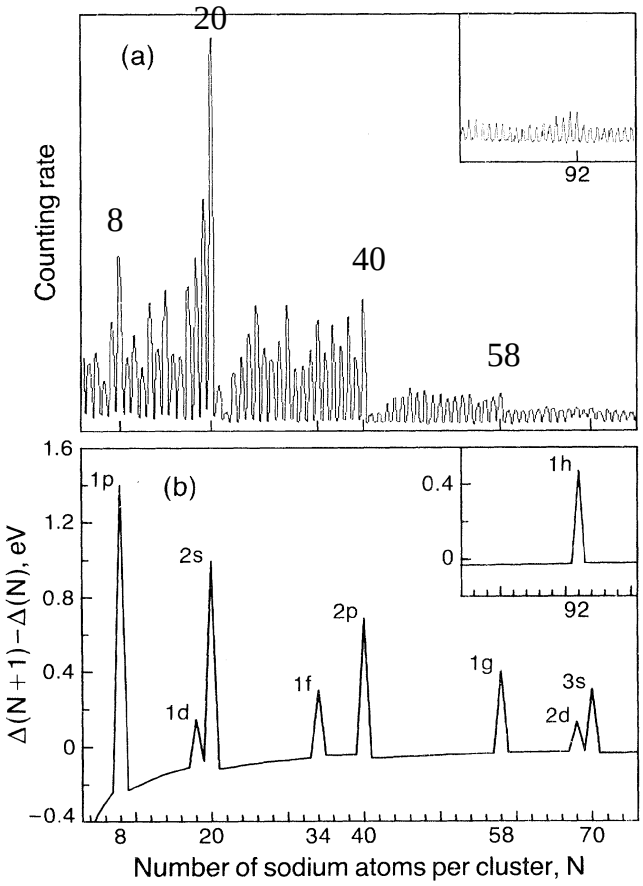

Figure 2.8: (a) Mass spectrum of Na clusters. (b) Model results for the change in the electron energy difference [from W.D. Knight *et al.*, Phys. Rev. Lett. **52**, 2141 (1984)].

separates,

$$\Psi(\boldsymbol{r}) = \frac{\phi_\ell(r)}{r} Y_\ell^m(\theta,\varphi), \quad \ell = 0,1,2,\ldots, \quad m = -\ell, -\ell+1, \ldots, \ell, \tag{2.97}$$

$$\left(-\frac{\hbar^2}{2m}\frac{\mathrm{d}^2}{\mathrm{d}r^2} + \frac{\ell(\ell+1)\hbar^2}{2mr^2} + V(r)\right)\phi_\ell(r) = E\phi_\ell(r) \tag{2.98}$$

(the magnetic quantum number m should not be confused with the electron mass $m_e = m$ here).

We know analytically the eigenenergies E for certain $V(r)$, e.g., the Coulomb potential or the 3D harmonic oscillator where

$$V(r) = \frac{1}{2}m\omega^2 r^2 \qquad \Rightarrow E_{k,\ell} = \left(2k + \ell + \frac{3}{2}\right)\hbar\omega, \quad k = 0,1,2,\ldots. \tag{2.99}$$

Note that the eigenenergies E depend on ℓ and there is no restriction to ℓ depending on the principal quantum number. This is different from the Coulomb case where $E_n \sim 1/n^2$ and $\ell < n$. Now let us see whether we can understand the magic numbers $N = 8, 20, 40, 58, 92$ from above if we model the binding potential of the cluster with a harmonic oscillator. For reasons which will become clear below we introduce a new principal quantum number

$$n = k + 1 \tag{2.100}$$

so that

$$E_{n,\ell} = \left(2(n-1) + \ell + \frac{3}{2}\right)\hbar\omega, \qquad n = 1,2,3,\ldots. \tag{2.101}$$

For a given n and ℓ the degeneracy due to the $2\ell+1$ possible m-values (and the two spin-degrees of freedom) is

$$d_\ell = 2(2\ell+1). \tag{2.102}$$

However, combinations of n and ℓ will lead to the same $E_{n,\ell}$ if

$$q = 2(n-1) + \ell \tag{2.103}$$

is equal, i.e.,

$$E_q = \left(q + \frac{3}{2}\right)\hbar\omega, \qquad q = 0,1,2,\ldots. \tag{2.104}$$

Table 2.1 shows the principal quantum numbers q for given quantum numbers n (columns) and ℓ (rows). The numbers in the square brackets indicate $2(2\ell+1)$.

We see that $q = 0$ is occupied by 2 electrons and $q = 1$ by 6. $q = 2$ occurs twice in the Table, namely for $n\ell = 20 = 2$s and $n\ell = 12 = 1$d. Hence, there are $2 + 10 = 12$ electrons in the $q = 2$-shell. Also $q = 3$ occurs twice. By filling electrons up to a level q we find the following number of valence electrons (= number of atoms) in the system:

Table 2.1: Principal quantum number q of the 3D harmonic oscillator for given quantum numbers n (columns) and ℓ (rows). The numbers in the square brackets indicate $2(2\ell+1)$. s, p, d, f, g ... refers to the usual spectroscopic notation.

ℓ $n\rightarrow$ $\downarrow$ $[2(2\ell+1)]$	1	2	3
0 s [2]	0	2	4
1 p [6]	1	3	5
2 d [10]	2	4	6
3 f [14]	3	5	7
4 g [18]	4	6	8

$q\ \rightarrow$	0	1	2	3	4
number of valence electrons in shell	2	6	12	20	30
number of valence electrons/atoms in system	2	8	20	40	70

Comparison with Fig. 2.8 shows that we are able to reproduce the magic numbers 8, 20, and 40. As we know from the rare gas atoms, closed electronic shells are particularly robust, i.e., electrons are hard to remove and chemically inert. The energy gap to the system with one electron more is particularly large. However, the higher magic numbers (although less pronounced) 58 (and also 92) are not reproduced by the 3D harmonic oscillator. Hence, the effective potential seems to be different. In fact, even if we stick to spherical potentials the magic numbers depend on the precise form of $V(r)$. Fig. 2.9 illustrates how the levels shift as one switches from the harmonic oscillator via an intermediate potential (e.g., a Woods-Saxon potential) to the spherical square well. The levels not only shift and split due to the removal of degeneracies but also cross, thus producing a level scheme for the square well potential very different from the harmonic oscillator. The numbers close to the levels indicate the number of electrons in the system up to that level. We see that the numbers 58 and 92 indeed appear, and the gaps to the next higher states are pronounced for these values.

Thomas-Fermi approach

So far we assumed the effective potential $V(r)$ being given. Now we go one step further and try to determine it self-consistently. The simplest way to do so is to apply Thomas-Fermi (TF) theory in which the electrons are described as a locally homogeneous gas. This approximation is suitable as long as the gradients of the electron density are small, i.e., the potential is sufficiently "flat".

Assume that the ionic background can be modeled by a homogeneously charged sphere of radius R. We know from electrostatics that the potential of such a sphere is harmonic inside and Coulombic outside. Now we fill electrons into this potential.

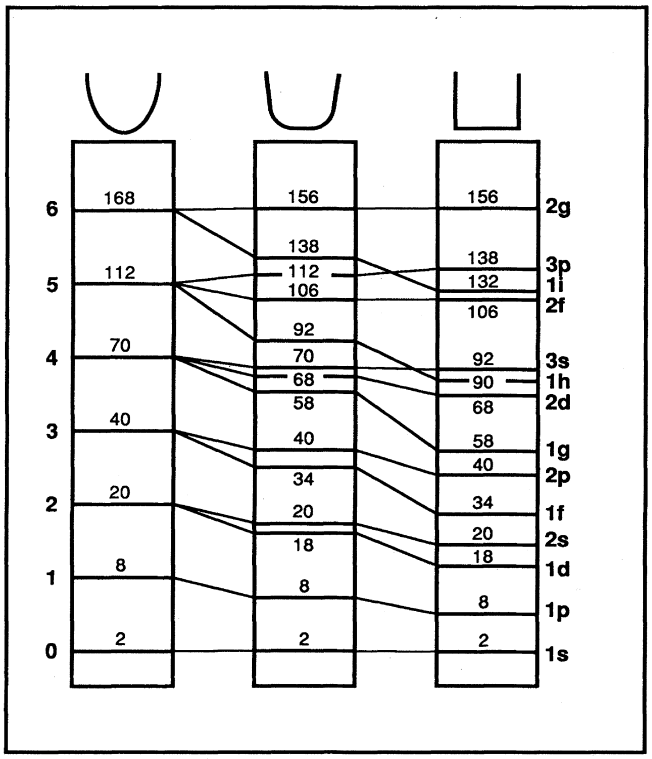

Figure 2.9: Level shifts and occupation numbers as one proceeds from the 3D harmonic oscillator (principal quantum number q indicated to the left) via an intermediate potential to the spherical square well potential (spectroscopic notation $n\ell$ to the right) [from W.A. de Heer, Rev. Mod. Phys. **65**, 611 (1993)].

The electron charge will create a potential itself, thus modifying the effective potential "seen" be subsequent electrons to be filled in. The goal is to calculate the electron density and the effective potential self-consistently.

The Wigner-Seitz radius r_s is defined via

$$N\,\frac{4}{3}\pi r_s^3 = \frac{4}{3}\pi R^3 \qquad \Rightarrow \quad R = r_s N^{1/3}, \tag{2.105}$$

i.e., each of the N atoms occupy a spherical volume of radius r_s. Each atom in the cluster contributes with v valence electrons so that the number of electrons N_e is

$$N_e = vN. \tag{2.106}$$

The charge density of the ionic background is given by

$$\rho_+(r) = \frac{veN}{\frac{4}{3}\pi R^3}\Theta(R-r) = \frac{3ve}{4\pi r_s^3}\;\Theta(R-r) = en_+(r), \tag{2.107}$$

i.e., it has a step-like profile. The electron charge density is

$$\rho_-(r) = -en(r) \tag{2.108}$$

where $n(r)$ is the electron number density, to be determined self-consistently.

From the Maxwell equation[8]

$$\boldsymbol{\nabla}\cdot\boldsymbol{E} = 4\pi\rho, \qquad \rho = \rho_+ + \rho_- \tag{2.109}$$

follows the Poisson equation

$$\boldsymbol{\nabla}^2\varphi = -4\pi\rho, \qquad \boldsymbol{E} = -\boldsymbol{\nabla}\varphi \tag{2.110}$$

with φ the potential. Hence,

$$\boldsymbol{\nabla}^2\varphi = 4\pi e(n - n_+). \tag{2.111}$$

From the theory of the homogeneous electron gas we know that for a given Fermi energy

$$E_F = \frac{\hbar^2 k_F^2}{2m} \tag{2.112}$$

the number of occupied states (and thus the number of electrons N_e) is

$$N_e = 2\;\frac{V_e\left(\frac{4}{3}\pi(\hbar k_F)^3\right)}{(2\pi\hbar)^3}. \tag{2.113}$$

[8]We use cgs-units here.

Here, the numerator is the total available phase space volume,[9] the denominator is the phase space volume occupied by one quantum state, and the factor 2 accounts for the two possible spin-degrees of freedom. The homogeneous electron density is

$$n = \frac{N_e}{V_e} = \frac{k_F^3}{3\pi^2} \qquad \Rightarrow \quad k_F = (3\pi^2 n)^{1/3}. \tag{2.114}$$

The key idea in TF theory is to treat the electrons *locally* like a homogeneous electron gas but allow the electron density (and thus also the Fermi wave number k_F) to vary slowly in space. We set

$$E_0 = \frac{\hbar^2}{2m} k_F^2(r) + V(r), \qquad V(r) = -e\varphi(r), \tag{2.115}$$

where E_0 is the total energy. The electrons fill all states up to the chemical potential μ so that $E_0 = \mu$. For a neutral cluster the chemical potential is zero so that

$$\frac{\hbar^2}{2m} k_F^2(r) = e\varphi(r), \tag{2.116}$$

giving us with (2.114) a relation between electron density and potential:

$$n(r) = \frac{k_F^3(r)}{3\pi^2} = \frac{\left(\frac{2me\varphi(r)}{\hbar^2}\right)^{3/2}}{3\pi^2} = \frac{(2me)^{3/2}}{3\pi^2\hbar^3}\varphi^{3/2}(r) \tag{2.117}$$

or

$$\varphi(r) = \left(n(r)\, \frac{3\pi^2\hbar^3}{(2me)^{3/2}} \right)^{2/3} = n^{2/3}(r)\, \frac{(3\pi^2)^{2/3}\hbar^2}{2me}. \tag{2.118}$$

We obtain from (2.111)

$$\boldsymbol{\nabla}^2 \left[\frac{(3\pi^2)^{2/3}\hbar^2}{2me} n^{2/3} \right] = 4\pi e(n - n_+).$$

So far the theory is general. Now we make use of what we expect for clusters on physical grounds. Inside the cluster the electrons will mainly compensate the positive charge so that we expect

$$n = n_+ - n^{(0)}, \qquad n^{(0)} \ll n_+. \tag{2.119}$$

Linearization then yields (→ exercise)

$$\boldsymbol{\nabla}_{\boldsymbol{x}}^2 \left(\frac{n^{(0)}}{n_+} \right) - k^2 \left(\frac{n^{(0)}}{n_+} \right) = 0 \tag{2.120}$$

[9] V_e is the volume of the box in which the homogeneous electron gas is considered.

where the dimensionless position $\boldsymbol{x} = \boldsymbol{r}/R$ is used, and

$$k = \left(\frac{12}{\pi}\right)^{1/3} \left(\frac{r_s}{a_0}\right)^{1/2} v^{1/6} N^{1/3}. \tag{2.121}$$

In cgs-units the Bohr radius is $a_0 = \hbar^2/me^2$. Because of spherical symmetry (2.120) becomes

$$\frac{1}{x}\frac{\partial^2}{\partial x^2}\left(x\frac{n^{(0)}}{n_+}\right) - k^2\left(\frac{n^{(0)}}{n_+}\right) = 0, \qquad x = \frac{r}{R} \tag{2.122}$$

a solution of which can be written in the form

$$\frac{n^{(0)}}{n_+} = 2\mathrm{e}^{-k} A\, \frac{\sinh kx}{x}, \qquad x < 1 \tag{2.123}$$

or

$$\frac{n}{n_+} = 1 - 2\mathrm{e}^{-k} A\, \frac{\sinh kx}{x}, \qquad x < 1. \tag{2.124}$$

For $x > 1$ the ionic potential is the same as if all the positive charge was located in the origin, i.e., Coulombic. As a consequence we simply obtain the standard TF equation

$$\chi'' = C\frac{\chi^{3/2}}{x^{1/2}}, \qquad \chi = x\varphi, \qquad C = \frac{2^{7/2}R^2}{3\pi a_0^{3/2} e^{1/2}}. \tag{2.125}$$

As in the atomic case the boundary condition for a neutral system is $\chi' = 0$ when $\chi = 0$ for $x \to \infty$. We expect the density to fall-off rapidly outside the ionic core. Hence we may ignore the variation of $x^{1/2}$ around the ion boundary $x = 1$ in the denominator of (2.125),

$$\chi'' \simeq C\chi^{3/2}. \tag{2.126}$$

A solution is of the form

$$\chi \sim \frac{1}{(x-D)^4}, \qquad \varphi \sim \frac{1}{x(x-D)^4}, \qquad n \sim \varphi^{3/2} \sim \frac{1}{x^{3/2}(x-D)^6}. \tag{2.127}$$

We find

$$\frac{n}{n_+} = \frac{30^3}{k^6}\, \frac{1}{x^{3/2}(x-D)^6}, \qquad x > 1 \tag{2.128}$$

and determine the constants A and D by matching the densities and their derivatives in the regions $x < 1$ (2.124) and $x > 1$ (2.128) at $x = 1$. As k given in (2.121) is $\gg 1$ for sufficiently big clusters[10] we expand

$$D = 1 - \frac{6.1}{k} - \frac{1.2}{k^2} + \cdots, \qquad A = 0.5 + \frac{0.6}{k} + \cdots. \tag{2.129}$$

[10]For Na_{20} where $r_s/a_0 = 3.9$ and $v = 1$ we have already $k = 8.4$.

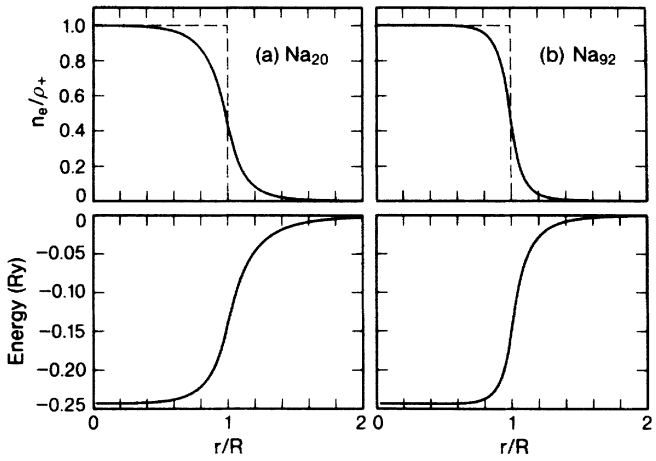

Figure 2.10: Electron densities and single-particle potentials for (a) Na_{20} and (b) Na_{92} clusters. The dashed profile indicates the positive charge density [from V. Kresin, Phys. Rev. B **38**, 3741 (1988)]. Note that n_e/ρ_+ in Kresin's paper is n/n_+ in our notation.

The potential in units of $e^2/2a_0 = 13.6\,\mathrm{eV}$ (Rydberg) can be written as

$$V = -e\varphi = -\frac{3.7}{r_s^2}\frac{e^2}{2a_0}\left(\frac{n}{n_+}\right)^{2/3}. \tag{2.130}$$

Figure 2.10 shows electron densities and single-particle potentials for Na_{20} and Na_{92} clusters. We see that the "spillout" is more pronounced for the smaller cluster, i.e., the approximation that $n \simeq n_+$ inside becomes more accurate with increasing cluster size. Also the related assumption that the electron density quickly drops around $x = 1$ is better for large clusters. As in atomic TF theory the density drops too slowly as $x \to \infty$. While the radius of the potential well and the steepness of the density at the ion surface increases with the cluster size, the depth of the potential is size-independent.

How does the simple TF result compare with more elaborate numerical simulation results? The shapes of the potentials look similar. The depths, however, are different, as is seen in in Fig. 2.11 for four Na_N-clusters. The TF potential is filled up to $E = \mu = 0$ whereas in more advanced quantum calculations the highest occupied orbital is well below the continuum threshold. The energy gap between the bottom of the potential and the highest occupied orbital is similar. Another striking difference is the oscillation of the electron density inside the cluster, which is absent in the TF result. This is also known from atoms and is due to the fact that TF theory is not formulated in terms of electronic orbitals but just in terms of the electron density. As a consequence, there is no shell structure in TF theory which could leave its fingerprints in the total density.

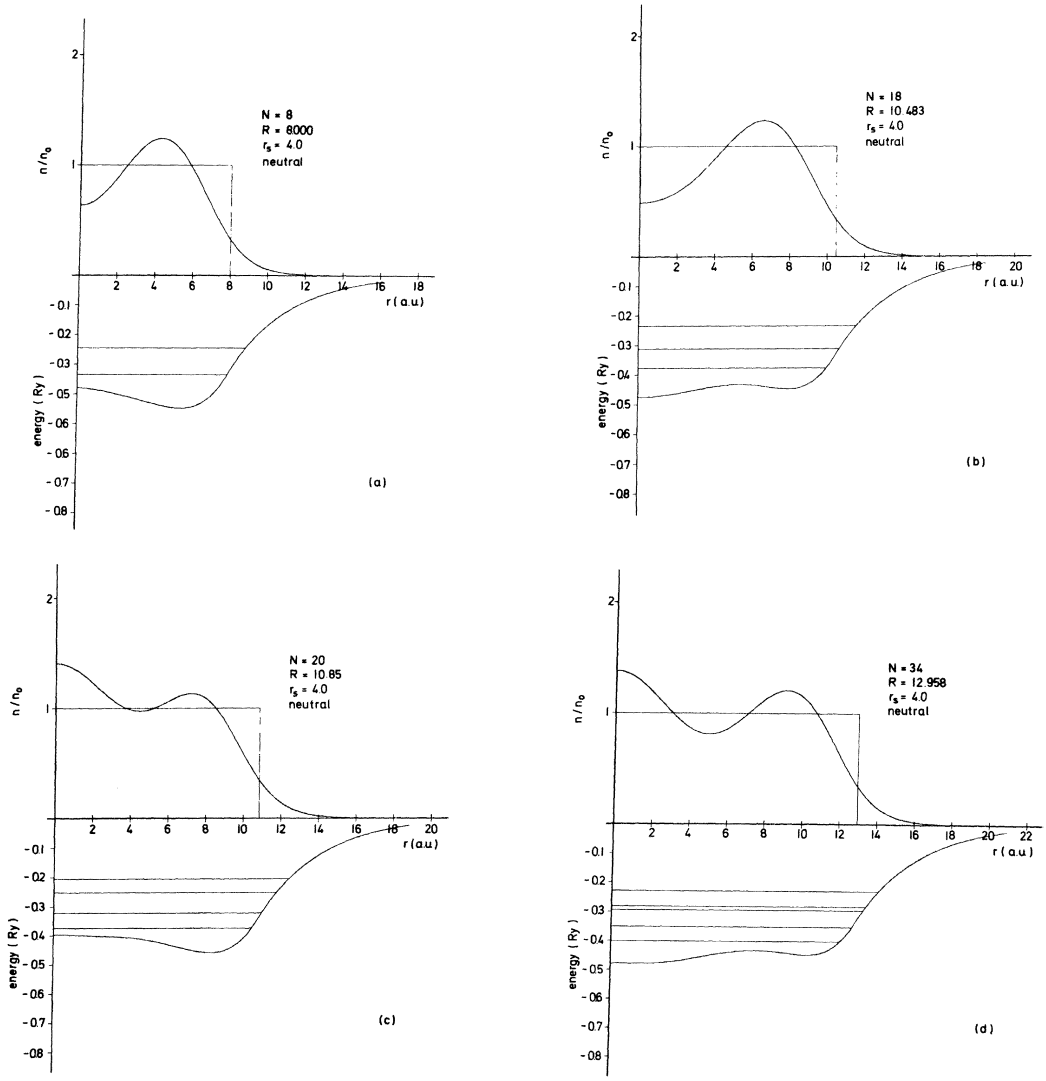

Figure 2.11: Density functional results for n/n_+ and effective potential for $N = 8, 18, 20, 34$ [from W. Ekardt, Phys. Rev. B **29**, 1558 (1984)].

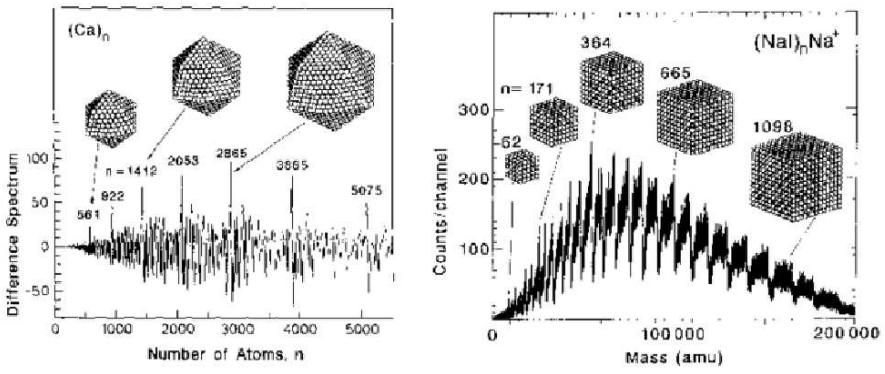

Figure 2.12: Abundances for Ca (icosahedral symmetry) and NaI clusters (cubic), indicating magic numbers and the corresponding atomic shell structures. Each oscillation in the mass spectrum of NaI clusters corresponds to the completion of one square face on a cuboid structure [from T.P. Martin, Phys. Rep. **273**, 199 (1996)].

Kresin tried to determine the magic numbers from his TF effective potentials by arguing that a shell is closed at those cluster sizes where the TF potential supports the next state of orbital angular momentum quantum number ℓ.

Atomic shell effects

So far we were able to explain the magic numbers observed by considering closures of *electronic* shells in self-consistent potentials where the ionic background was treated in the jellium approximation. This works well for metal clusters at not too low temperatures. When the temperature decreases the ion positions "freeze out". As in the bulk material the ions arrange in a particular crystal structure which minimizes the energy, also in clusters some configurations are energetically more favorable than others. While at higher temperatures there are many configurations of almost equal energy (isomers) the number reduces with decreasing temperature. Atomic configurations which minimize the total energy will thus also give rise to magic numbers (*atomic shell effect*). Compared to the magic numbers due to electronic shell closures the atomic magic numbers are much more species-dependent, as are crystal structures in solid state physics. Figure 2.12 shows mass spectra and structures for Ca and NaI clusters.

2.3.2 Theoretical approaches to the cluster many-body problem

Single atoms such as Na are already many-particle systems and thus notoriously difficult to treat on a fundamental quantum level, which would imply the solution of the Schrödinger equation (assuming relativistic and QED effects being negligible).

As clusters consist of 10-10^6 atoms the situation there is even worse, not only because the number of particles increases but also because the spherical symmetry of the binding potential is lost. It is also worse compared to the corresponding solid state system, as the finite size of clusters does not allow the imposition of periodic boundary conditions. On the other hand, the situation is similar to molecular physics, and, in fact, the methods are similar. In the following we will present the most common theoretical and numerical approaches and illustrate them with typical results.[11]

General remarks

Usually, a "computer experiment" on laser cluster interaction consists of

1. Finding the initial configuration (and the characterization of the latter, e.g., the determination of the linear response spectrum in order to know where resonances are etc.);

2. Apply a pump laser pulse in order to trigger some dynamics of electrons and/or ions;

3. Perhaps, apply a probe pulse (often of interest if comparison with experiment is made);

4. Evaluate the observables of interest;

5. Analyze the dynamics by plotting appropriate entities (not restricted to what is experimentally accessible), e.g., vs time.

In general, many runs are necessary, either because averaging over orientations or laser intensities is required for the comparison with experiment or—and this is usually the case—because new questions arise.

As in molecular physics, the time scales of electrons and ions are very different. While electrons respond to the laser field on the attosecond scale, the ions, due to their higher mass, respond on the 10-100 femtosecond scale. Hence, a full quantum description is prohibitive. Instead, methods where electrons and ions are treated on a different footing are to be applied, similar to molecular physics.

Hamiltonian

The many-body Hamiltonian reads

$$H = H_{\rm el} + H_{\rm coupl} + H_{\rm ion} + U_{\rm ext}, \tag{2.131}$$

[11] In this Section we will largely follow the book by P.-G. Reinhard and E. Suraud *Introduction to cluster dynamics* (Wiley, Weinheim, 2004).

where

$$H_{\rm el} = \sum_i \frac{p_i^2}{2m} + \frac{1}{2}\sum_{i\neq j}\frac{e^2}{|\boldsymbol{r}_i - \boldsymbol{r}_j|}, \tag{2.132}$$

$$H_{\rm coupl} = -\sum_{iI}\frac{Z_I e^2}{|\boldsymbol{r}_i - \boldsymbol{R}_I|}, \tag{2.133}$$

$$H_{\rm ion} = \sum_I \frac{P_I^2}{2M_I} + \frac{1}{2}\sum_{I\neq J}\frac{Z_I Z_J e^2}{|\boldsymbol{R}_I - \boldsymbol{R}_J|} \tag{2.134}$$

and $U_{\rm ext}$ describes the coupling to an external field (e.g., laser, projectile). The lower-case letters describe the electrons, the upper-case letters the ions. The same holds for the indices. The ionic charge states are Z_I, the masses are M_I.

Ions

Because already in atomic hydrogen $M/m \simeq 2000$ the ions are much more inert than the electrons. As in molecular physics one may apply the Born-Oppenheimer (BO) approximation,

$$\Psi(\boldsymbol{r};\boldsymbol{R}) = \psi_{\rm ion}(\boldsymbol{R})\phi_{\boldsymbol{R}}(\boldsymbol{r}), \quad \boldsymbol{R} = (\boldsymbol{R}_1, \boldsymbol{R}_2, \ldots), \quad \boldsymbol{r} = (\boldsymbol{r}_1, \boldsymbol{r}_2, \ldots). \tag{2.135}$$

The ion positions appear only as parameters in the electronic wavefunction because the electrons are assumed to be "quick enough" to follow *adiabatically* the ions. This ansatz allows (with some approximations) for a decoupling of the full Schrödinger equation into an electronic Schrödinger equation ($U_{\rm ext} = 0$ here),

$$(H_{\rm el} + H_{\rm coupl})\phi_{\boldsymbol{R}}(\boldsymbol{r}) = E_{\rm el}(\boldsymbol{R})\phi_{\boldsymbol{R}}(\boldsymbol{r}) \tag{2.136}$$

and an ionic one,

$$\begin{aligned} E\psi_{\rm ion}(\boldsymbol{R}) &= \{H_{\rm ion} + E_{\rm el}(\boldsymbol{R})\}\psi_{\rm ion}(\boldsymbol{R}) \\ &= \left\{\sum_I \frac{P_I^2}{2M_I} + V_{\rm BO}(\boldsymbol{R})\right\}\psi_{\rm ion}(\boldsymbol{R}) \end{aligned} \tag{2.137}$$

where

$$V_{\rm BO}(\boldsymbol{R}) = \frac{1}{2}\sum_{I\neq J}\frac{Z_I Z_J e^2}{|\boldsymbol{R}_I - \boldsymbol{R}_J|} + E_{\rm el}(\boldsymbol{R}) \tag{2.138}$$

is the BO potential. However, for the systems we have in mind, i.e., clusters in strong fields, we cannot assume that the electrons always adjust adiabatically to any of the electronic eigenstates so that a simple reduction to dynamics on BO surfaces is not possible. Instead, we will treat the ions classically and allow for arbitrary excitations of the electrons. Hence, the numerical demand will be very much on the electronic side because strong excitations, including ionization, require large numerical grids.

Ion-electron coupling

Because the simulation of the electron dynamics is so computationally expensive it is worthwhile thinking about which electrons will actually participate in the dynamics. Usually the inner shell electrons are so strongly bound that they may safely be considered together with the ion just as one *ionic core*. However, one has to make sure that the wavefunctions of the active electrons are sufficiently accurate. This is the idea of *pseudo potentials*. Let the orthonormalized single-particle core-electron states be denoted by $|\varphi_1\rangle, \ldots, |\varphi_{N_c}\rangle$. We assume we know them from some electronic-structure calculation (Hartree-Fock, density functional theory, ...) and they fulfill a single-particle Schrödinger equation

$$h\,|\varphi_\alpha\rangle = \epsilon_\alpha\,|\varphi_\alpha\rangle \tag{2.139}$$

where h is the single-particle Hamiltonian. The active valence electron is in the state

$$|\varphi_v\rangle\,, \qquad \langle\varphi_v|\varphi_\alpha\rangle = 0, \qquad \alpha = 1, \ldots, N_c \tag{2.140}$$

and also fulfills

$$h\,|\varphi_v\rangle = \epsilon_v\,|\varphi_v\rangle\,. \tag{2.141}$$

We now introduce an auxiliary wavefunction ψ in such a way that φ_v can be recovered by projecting out all core states,

$$|\varphi_v\rangle = |\psi\rangle - \sum_{c=1}^{N_c} |\varphi_c\rangle\,\langle\varphi_c|\psi\rangle. \tag{2.142}$$

Inserting this into (2.141) yields

$$(h + V_{\rm psp})\,|\psi\rangle = \epsilon_v\,|\psi\rangle\,, \tag{2.143}$$

i.e., an effective Schrödinger equation for ψ in which, besides h, a pseudo potential

$$V_{\rm psp} = \sum_{c=1}^{N_c} |\varphi_c\rangle\,(\epsilon_v - \epsilon_c)\langle\varphi_c| \tag{2.144}$$

appears. Note that ψ has the same single-particle energy as φ_v. The pseudo potential $V_{\rm psp}$ takes care of the repulsive force exerted by the core electrons. For practical calculations, however, a pseudo potential of the form (2.144) is inconvenient because it is *nonlocal*. Each application of $V_{\rm psp}$ to a wavefunction involves integration over whole space. To that end *local* parametrized pseudo potentials of the form

$$V_{\rm psp}(r) = \sum_{i=1}^{2} c_i\,\frac{\mathrm{erf}\,(r/\sigma_i)}{r}, \qquad c_1 + c_2 = -e^2 Z_{\rm ion} \tag{2.145}$$

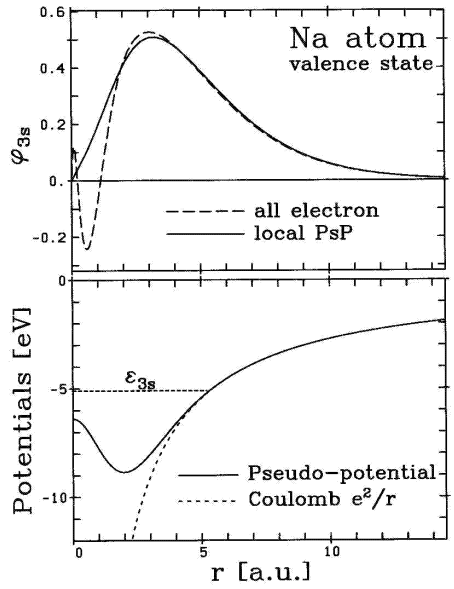

Figure 2.13: Upper panel: Comparison of the Na valence 3s wavefunction from an "all-electron calculation" (dashed) and using a pseudo potential (solid). Lower panel: the corresponding full Coulombic potential (dashed) and the local pseudo potential (2.145) for Na. The asymptotic behavior of wavefunctions and potentials match while for $r \to 0$ the full "all-electron" potential is deeper so that the 3s wavefunction in it has indeed three zeros. Instead, the 3s wavefunction from the pseudo potential treatment is actually the ground state in its pseudo potential, i.e., it has only one zero at $r = 0$ [from P.-G. Reinhard and E. Suraud *Introduction to cluster dynamics* (Wiley, Weinheim, 2004)].

are used. Here, erf is the error function, c_i are fit parameters, and $Z_{\rm ion}$ is the charge state of the ionic core (including the core electrons). Figure 2.13 shows such a pseudo potential for Na "at work".

While the asymptotic behavior of the pseudo potential wavefunction is the same as that from the "all-electron" calculation, the nodal structure at short distances differs. This difference is acceptable as long as one is just interested in electronic structure because for, e.g., chemical bonding the wiggles of the wavefunctions at short distances are not important. However, for the electron dynamics (e.g., for scattering) this might not be the case.

Polarization is also neglected if simple pseudo potentials are used. As a consequence, van der Waals interactions are swept under the rug. Moreover, local pseudo potentials of the type (2.145) can only support valence orbitals having angular momentum $\ell = 0$. Pseudo potentials for $\ell \neq 0$ have been developed but are more complicated.

Assuming that we have constructed a spherical atomic pseudo potential, the potential of the ionic background in a cluster reads

$$U_{\rm back}(\boldsymbol{r}) = \sum_I V_{\rm psp}(|\boldsymbol{r} - \boldsymbol{R}_I|). \tag{2.146}$$

$U_{\rm back}(\boldsymbol{r})$ has no symmetries if the ion configuration has none so that a full 3D treatment of the electrons in such a background potential is required. On the other hand we expect that, e.g., simple metal clusters (alkali clusters) should be well described by a spherically symmetric ionic potential. Hence, one may go one step in the approximation chain further and perform a spherical average of the total cluster pseudo potential,

$$U_{\rm back}^{\rm (SAPS)}(r) = \frac{1}{4\pi} \sum_I \int {\rm d}\Omega \; V_{\rm psp}(|r\boldsymbol{e}_r(\Omega) - \boldsymbol{R}_I|) \tag{2.147}$$

where SAPS is an acronym for *spherically averaged pseudo potential scheme* and r and $\boldsymbol{e}_r(\Omega)$, $\Omega = (\vartheta, \varphi)$ are radius and unit vector in radial direction with respect to the cluster center, and ${\rm d}\Omega$ is the solid angle element. We expect such a SAPS approach being increasingly valid with increasing cluster size. Note that the (classical) ion *dynamics* remain 3D. Only the electrons "see" a spherically averaged ion potential.

The next step in the electron-ion approximation chain amounts to introduce a pseudo potential for the cluster background in the first place. The simplest choice is the *jellium*, used already above in Sec. 2.3.1.

The number density of elementary charges e inside the cluster is

$$n_0 = \frac{N_e}{\frac{4}{3}\pi R^3} = \frac{3v}{4\pi r_s^3}. \tag{2.148}$$

In the following we will assume the valence $v = 1$ so that $N_e = N_{\text{ion}} = N$. The spherical, step-like jellium number density is

$$n(r) = n_0 \, \Theta(R - r). \tag{2.149}$$

The corresponding ion charge density (2.107) is

$$\rho_+(r) = en(r). \tag{2.150}$$

From this density follows the jellium potential

$$U_{\text{jel}}(r) = \begin{cases} -\dfrac{Ze^2}{r} & \text{for} \quad r > R \\ \dfrac{1}{2}m\omega_{\text{Mie}}^2(r^2 - R^2) - \dfrac{Ze^2}{R} & \text{for} \quad r \leq R \end{cases} . \tag{2.151}$$

Here, Ze is the total net charge of the ionic background, and

$$\omega_{\text{Mie}}^2 = \frac{4\pi e^2 n_0}{3m} \tag{2.152}$$

is the *Mie plasmon frequency*. The potential (2.151) is that of a homogeneously charged sphere: harmonic inside (with oscillator frequency ω_{Mie}) and Coulombic outside ($\rightarrow$ exercise). Hence, one expects a particularly large response of the system to perturbations with frequencies ω around ω_{Mie}. Remember that excursion, velocity etc. of a driven harmonic oscillator diverges at resonance. In reality, there are always damping mechanisms preventing the divergence, but a particularly efficient coupling to the system is observed at $\omega = \omega_{\text{Mie}}$, as will be discussed below.

The steep jellium potential typically overestimates ω_{Mie} as compared to experiment and simulations beyond jellium. One can correct for that by using a "soft jellium" potential where the ionic background does not jump step-like as in (2.149) ($\rightarrow$ Woods-Saxon potential).

Electrons

The proper simulation of the electron dynamics is the computationally most expensive part. Although the electron-electron interaction potential is known and local, the problem is notoriously difficult because *correlation* is often important. Already (time-independent) electronic structure calculations are extremely demanding because of the so-called *exponential wall*: the computational cost on a Schrödinger equation-level increases exponentially with the number of degrees of freedom. Therefore only very small systems can be treated exactly. In the other extreme, the idealized system of an *infinite homogeneous electron gas* (IHEG) is also exactly solvable. From (2.114) we know already that

$$k_F = (3\pi^2 n)^{1/3}. \tag{2.153}$$

Let us first treat the IHEG on a Hartree-Fock (HF) level where correlation is neglected but exchange is included. We assume a homogeneous ionic background compensating the direct Hartree interaction of the electronic charge density so that only kinetic and exchange energy remain:

$$\frac{\mathcal{E}_{\rm HF}}{V} = \sum_{\alpha} \langle \varphi_\alpha | \frac{p^2}{2m} | \varphi_\alpha \rangle - \frac{1}{2} \sum_{\alpha\beta} \langle \varphi_\alpha \varphi_\beta | V_{\rm C} | \varphi_\beta \varphi_\alpha \rangle \tag{2.154}$$

with $V_{\rm C}$ the Coulomb-interaction potential between two electrons. The sums run over the occupied single-particle HF orbitals. Inserting box-normalized plane waves this expression can be calculated analytically but it diverges for $N \to \infty$, which is not surprising. It is more sensible to calculate the *energy per electron*,

$$\frac{\mathcal{E}_{\rm HF}}{N} = \frac{\mathcal{E}_{\rm HF}}{nV}. \tag{2.155}$$

From the theory of the ideal Fermi gas (cf. Statistical Physics lecture) we know $\mathcal{E}_{\rm kin}/N = \frac{3}{5}\varepsilon_F$ with ε_F the Fermi energy. The exchange-part can be calculated in an analogous way. One obtains

$$\begin{aligned} \frac{\mathcal{E}_{\rm HF}}{N} &= \frac{3\hbar^2 k_F^2}{10m} - \frac{3e^2 k_F}{4\pi} \\ &= \underbrace{\frac{3(3\pi^2)^{2/3}}{10m} n^{2/3}}_{\varepsilon_{\rm kin}[n]} \underbrace{- \frac{3e^2(3\pi^2)^{1/3}}{4\pi} n^{1/3}}_{\varepsilon_{\rm x}[n]}. \end{aligned} \tag{2.156}$$

What is missing in the HF treatment is correlation, i.e., the correlation energy per electron

$$\varepsilon_{\rm c}[n] = \varepsilon_{\rm xc}[n] - \varepsilon_{\rm x}[n], \tag{2.157}$$

which has been determined numerically and then parametrized. Figure 2.14 shows the contributions $\varepsilon_{\rm kin}$, $\varepsilon_{\rm x}$, $\varepsilon_{\rm xc}$, and the total energy $\mathcal{E}/N = \mathcal{E}_{\rm HF}/N + \mathcal{E}_{\rm c}/N$.

The semi-analytical results for the IHEG have been extremely valuable, as they served not only as the starting point (or justification) for the Thomas-Fermi approach but also helped to develop *density functionals* for density functional theory, to be discussed next.

Nobel prize-winning density functional theory (DFT) is one of the most widely applied methods in molecular physics, solid-state physics, chemical physics and biophysics. It overcomes the *exponential wall*-problem by using the fact that all observables are functionals of the density $n(\boldsymbol{r})$ alone. The Hohenberg-Kohn theorem states that there is a unique mapping between the external potential and the particle density. Because the external potential defines the system under study all observables are thus functionals of the particle density alone.

The main advantages of DFT as compared to Hartree-Fock is that the effective potential is local (unlike the Fock term) and that correlation is included (in principle). The earliest and simplest version of DFT is Thomas-Fermi (TF) theory, where

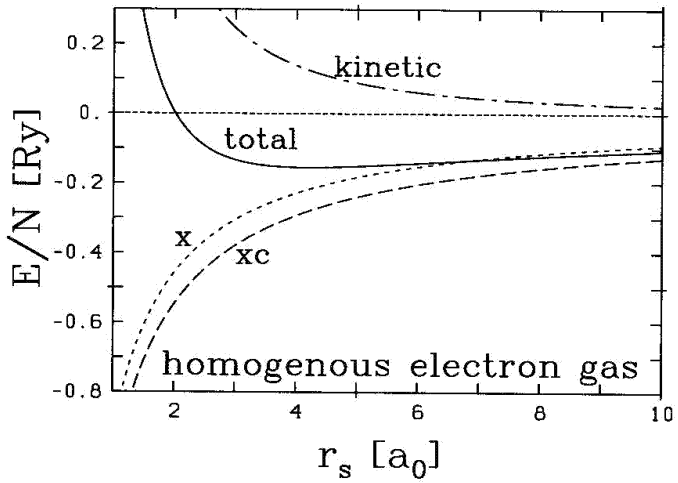

Figure 2.14: Contributions $\varepsilon_{\rm kin}$, $\varepsilon_{\rm x}$, $\varepsilon_{\rm xc}$ to the total energy per particle for the homogeneous electron gas vs the Wigner-Seitz radius r_s. In the high-density limit $r_s \to 0$ the relative importance of correlation decreases. The total energy per particle is dominated by kinetic energy and exchange in this limit. In the low-density limit correlation, exchange, and kinetic energy contribute similarly [from P.-G. Reinhard and E. Suraud *Introduction to cluster dynamics* (Wiley, Weinheim, 2004)].

even the kinetic energy of the system is written as an explicit functional of the density by employing the IHEG result for $\varepsilon_{\rm kin}$. Gradient corrections can be added to TF theory (TF-Weizsäcker, TFW) but they destroy the simple scaling behavior. As a theory should be either approximate but simple or complicated but accurate, TFW is hardly used nowadays. Moreover, TF-like theories do not produce a shell structure.

Most DFT calculations are nowadays implemented using the *Kohn-Sham* (KS) scheme. The idea behind the KS method is to introduce an auxiliary system of non-interacting particles that leads to the same particle density as the original, interacting system. This is only the case if the effective potential for these auxiliary particles is chosen accurately enough.

Starting point for DFT is an energy functional for the energy of all the electrons in the system,

$$\mathcal{E}_{\rm total,el} = \mathcal{E}_{\rm kin}[\{\varphi_\alpha\}] + \mathcal{E}_{\rm el-ion}[n, \{\boldsymbol{R}_I\}] + \mathcal{E}_{\rm C,el}[n] + \mathcal{E}_{\rm xc}[n] \tag{2.158}$$

where

$$n(\boldsymbol{r}) = \sum_\alpha \varphi_\alpha^+(\boldsymbol{r})\varphi_\alpha(\boldsymbol{r}), \tag{2.159}$$

$$\mathcal{E}_{\rm kin}[\{\varphi_\alpha\}] = \int {\rm d}^3r \sum_\alpha \varphi_\alpha^+ \frac{p^2}{2m}\varphi_\alpha, \tag{2.160}$$

$$\mathcal{E}_{\rm el-ion}[\{\varphi_\alpha\},\{\boldsymbol{R}_I\}] = \int \mathrm{d}^3r \sum_\alpha \varphi_\alpha^+ U_{\rm back}\varphi_\alpha, \tag{2.161}$$

$$\mathcal{E}_{\rm C,el}[n] = \frac{1}{2}\int \mathrm{d}^3r \int \mathrm{d}^3r' \frac{e^2 n(\boldsymbol{r}')n(\boldsymbol{r})}{|\boldsymbol{r}-\boldsymbol{r}'|}, \tag{2.162}$$

$$\mathcal{E}_{\rm xc}[n] = \int \mathrm{d}^3r\, n(\boldsymbol{r})\,\varepsilon_{\rm xc}[n(\boldsymbol{r})]. \tag{2.163}$$

Here, $\varphi_\alpha(\boldsymbol{r})$ is a single-particle two-component spinor,[12] $\mathcal{E}_{\rm el-ion}$ is the energy due to the ionic potential[13], $\mathcal{E}_{\rm C,el}$ is the Coulomb energy due to the mutual repulsion of the electrons (Hartree term), and $\mathcal{E}_{\rm xc}$ is the energy due to exchange and correlation. For the latter approximations have to be employed because there is no analytic result for $\varepsilon_{\rm c}$ even in the case of the IHEG, let alone for finite systems or systems with a structured ionic background.

Variation of the total energy (2.158) with respect to φ_α^+ leads to the KS equation ($\rightarrow$ Advanced Quantum Theory script)

$$h_{\rm KS}\varphi_\alpha = \epsilon_\alpha\varphi_\alpha, \qquad \alpha = 1,\ldots,N_e, \tag{2.164}$$

where

$$h_{\rm KS} = \frac{p^2}{2m} + U_{\rm C,el} + U_{\rm xc} + U_{\rm back}, \tag{2.165}$$

$$U_{\rm C,el} = \int \mathrm{d}^3r' \frac{e^2 n(\boldsymbol{r}')}{|\boldsymbol{r}-\boldsymbol{r}'|}, \tag{2.166}$$

$$U_{\rm xc} = \varepsilon_{\rm xc} + n\frac{\partial\varepsilon_{\rm xc}}{\partial n}. \tag{2.167}$$

The KS Hamiltonian depends on the KS orbitals, $h_{\rm KS} = h_{\rm KS}[\{\varphi_\alpha\}]$. Hence, the KS orbitals have to be determined self-consistently. The "art of DFT" is to find and use a sufficiently accurate exchange correlation potential $U_{\rm xc}$. The simplest approach is based on the IHEG where

$$\frac{\mathcal{E}_{\rm xc}}{V} = \frac{\mathcal{E}_{\rm xc}}{N}\frac{N}{V} = \varepsilon_{\rm xc}n \qquad \Rightarrow \qquad \mathcal{E}_{\rm xc} = \int \mathrm{d}^3r\, \varepsilon_{\rm xc}[n]\, n. \tag{2.168}$$

One then assumes that the IHEG concept is valid also for a space-dependent density, leading to the *local density approximation* (LDA)

$$\mathcal{E}_{\rm xc}^{\rm (LDA)} = \int \mathrm{d}^3r\, \varepsilon_{\rm xc}[n(\boldsymbol{r})]\, n(\boldsymbol{r}) \tag{2.169}$$

This seems a very crude approximation and is expected to hold only for smoothly varying densities with small gradients. In practice, it works surprisingly well in many cases.

[12] So that $\varphi_\alpha^+(\boldsymbol{r})\varphi_\alpha(\boldsymbol{r})$ amounts to a sum over the two spin-components.

[13] If the ions are modelled by a local potential the expression simplifies to $\mathcal{E}_{\rm el-ion}[n,\{\boldsymbol{R}_I\}] = \int \mathrm{d}^3r\, n(\boldsymbol{r})\, U_{\rm back}$.

The exchange-part of the LDA energy functional (2.169) is known analytically [see (2.156)],

$$\varepsilon_{\mathrm{x}}[n] = -\frac{3e^2}{4}\left(\frac{3}{\pi}\right)^{1/3} n^{1/3}. \tag{2.170}$$

The exchange potential (2.167) then is

$$U_{\mathrm{x}}^{(\mathrm{LDA})}[n(\boldsymbol{r})] = \frac{\delta \mathcal{E}_{\mathrm{x}}^{(\mathrm{LDA})}}{\delta n} = \frac{\delta}{\delta n}\int \mathrm{d}^3 r\ \varepsilon_{\mathrm{x}}[n(\boldsymbol{r})]n(\boldsymbol{r}) = -e^2\left(\frac{3}{\pi}\right)^{1/3} n^{1/3}(\boldsymbol{r}). \tag{2.171}$$

This is the so-called *Slater approximation*, used well before the formal foundation of DFT. The correlation part can be taken approximately into account by using parametrizations of the numerically determined IHEG-result for ε_{c}.

A weak point of the LDA is the self-interaction error. This can be seen most clearly in the limiting case of a one-electron system such as atomic hydrogen where electron correlation vanishes and the Hartree potential (2.166) should be *exactly* cancelled by the exchange potential U_{x}. The LDA does not do this, which leads to a wrong asymptotic behavior of the total effective KS potential. In neutral atoms, for instance, the total effective KS potential should drop asymptotically $\sim -1/r$ whereas in LDA it drops faster (exponentially). As a consequence, the LDA potential does not support a Rydberg series, and the highest occupied orbital is typically too low in energy, giving a rather erroneous ionization potential. Self-interaction corrections curing this shortcoming have been developed and can be implemented at moderate computational cost.

Note that the KS orbitals have been introduced as auxiliary entities for the sole purpose to reproduce via the noninteracting KS system the density $n(\boldsymbol{r})$ of the interacting physical system. Rigorously speaking, the KS orbitals have no physical meaning. However, in practice they prove useful for, e.g., understanding shell structure or the interpretation of linear response spectra.

Figure 2.15 shows the result of a DFT calculation for a Na_{138}-cluster (cf. figure caption for a discussion).

We only mention here in passing that DFT can be also formulated for "spin-polarized" systems with $n = n_\uparrow + n_\downarrow$ where $n_\uparrow \neq n_\downarrow$.

DFT has been extended to time-dependent problems (TDDFT). The time-dependent analogue of the Hohenberg-Kohn theorem is called *Runge-Gross theorem* and states that also a time-dependent external potential is uniquely mapped to the time-dependent density, given the initial state. As a consequence, all observables are functionals of the density again. Due to the lack of a minimization principle in the time-dependent case the proof of the Runge-Gross theorem is more involved than the proof of the Hohenberg-Kohn theorem of ground state DFT. The same is true for the derivation of the time-dependent KS equation (TDKS). However, finally it reads as expected,

$$h_{\mathrm{KS}}(t)\varphi_\alpha(\boldsymbol{r},t) = \mathrm{i}\hbar\frac{\partial}{\partial t}\varphi_\alpha(\boldsymbol{r},t) \tag{2.172}$$

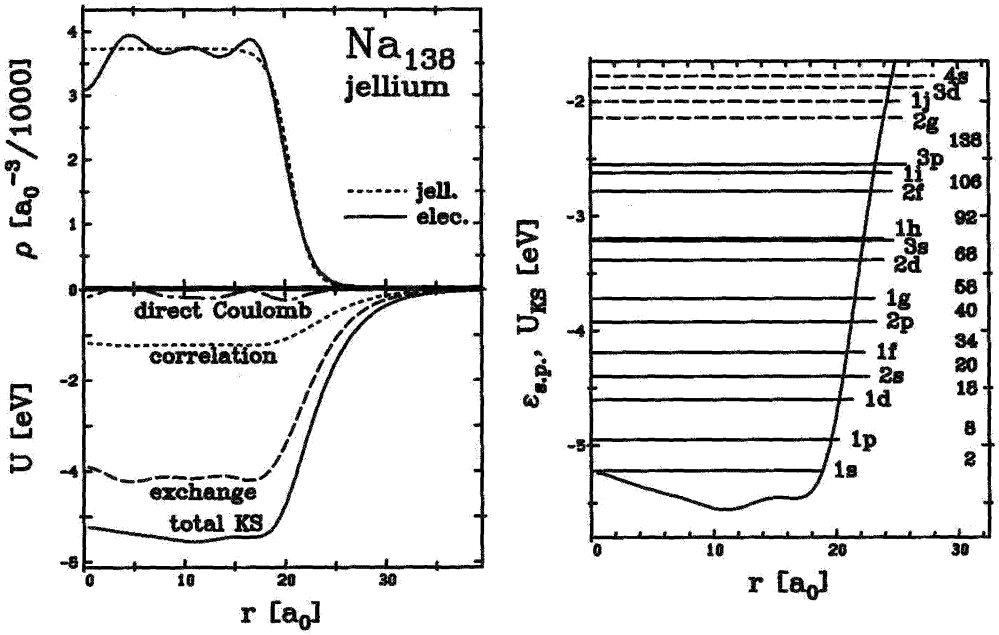

Figure 2.15: KS result for a Na_{138}-cluster, calculated with a soft-jellium ionic background. The left upper panel shows the densities (soft-jellium dashed and electron density solid). The left lower panel shows the partial contributions to the total KS potential ($U_{\rm KS} = U_{\rm C,el} + U_{\rm xc} + U_{\rm back}$, solid). $U_{\rm xc}$ is separated into exchange (long-dashed) and correlation (dashed), showing that exchange is dominating. $U_{\rm C,el}$ and $U_{\rm back}$ (the sum being denoted as "direct Coulomb", broken solid) almost cancel each other. The small fluctuations are due to the shell structure. The binding of the cluster is due to exchange and correlation. The right hand side shows the KS orbital energies ϵ_α, occupied orbitals being drawn solid, unoccupied ones dashed. The separation between the highest occupied orbital (3p) and the lowest unoccupied one (2g) is rather large. In fact, 138 is a magic number. The energy difference between the bottom of the potential and the highest occupied orbital is about 3 eV, corresponding to $k_F \simeq 0.5/a_0$ in bulk Na. This energy difference does not change with increasing cluster size. Only the level density increases in order to accommodate more electrons [from P.-G. Reinhard and E. Suraud *Introduction to cluster dynamics* (Wiley, Weinheim, 2004)].

where $h_{\rm KS}(t)$ may now contain some explicitly time-dependent external driver [e.g., the laser in dipole approximation described by the potential $e\boldsymbol{E}(t)\cdot\boldsymbol{r}$]. Usually an *adiabatic approximation* is used for $U_{\rm xc}$ in the time-dependent case,

$$U_{\rm xc}(\boldsymbol{r},t) \simeq U_{\rm xc}[n(\boldsymbol{r},t)], \tag{2.173}$$

i.e., density functionals known for DFT are evaluated with the time-dependent density. More advanced functionals (e.g., those with self-interaction correction) are orbital-dependent. In this case it is assumed that $U_{\rm xc}(\boldsymbol{r},t) \simeq U_{\rm xc}[\{\varphi_\alpha(\boldsymbol{r},t)\}]$. However, one can show that the exact $U_{\rm xc}$ in the time-dependent case has to have *memory*, i.e., it not only depends on the current time t but also on previous times $t' < t$. Exchange-correlation functionals with memory are under development but computationally more demanding. Most of the TDDFT studies are in the linear response-regime, a few go beyond linear response.[14] Highly correlated dynamical processes or resonant excitations are usually not well described by known, adiabatic $U_{\rm xc}$. How to improve the performance of TDDFT in this direction is the topic of current research.

Coupled ion and electron dynamics

We decided to treat the ions classically and the electrons quantum mechanically, e.g., via TDDFT. The electrons may be highly excited. They "see" the ions either "naked" in an all-electron simulation or as a pseudo potential, i.e.,

$$U_{\rm back}(\boldsymbol{r}) = \sum_I V_{\rm psp}(|\boldsymbol{r}-\boldsymbol{R}_I|). \tag{2.174}$$

Because of *actio = reactio* the ion I experiences the force due to the electron fluid

$$\boldsymbol{F}_{I,\rm el} = -\boldsymbol{\nabla}_{\boldsymbol{R}_I} U_{\rm el}(\boldsymbol{R}_I) \tag{2.175}$$

where

$$U_{\rm el}(\boldsymbol{R}_I) = \int \mathrm{d}^3r\; n(\boldsymbol{r})\, V_{\rm psp}(|\boldsymbol{r}-\boldsymbol{R}_I|). \tag{2.176}$$

Hence, the equations of motion for the ions read

$$\dot{\boldsymbol{P}}_I = -\boldsymbol{\nabla}_{\boldsymbol{R}_I}\left\{\frac{1}{2}\sum_{J\neq K}\frac{e^2 Z_J Z_K}{|\boldsymbol{R}_J-\boldsymbol{R}_K|} + U_{\rm el}(\boldsymbol{R}_I) + U_{\rm ext}(\boldsymbol{R}_I,t)\right\}, \tag{2.177}$$

$$\dot{\boldsymbol{R}}_I = \frac{\boldsymbol{P}_I}{M_I}. \tag{2.178}$$

Here, $U_{\rm ext}(\boldsymbol{R}_I,t)$ describes the coupling of the external driver (e.g., laser) to the ions, which can usually be neglected because of $M_I \gg m$. The driver interacts

[14] Note that the Runge-Gross theorem is not restricted to small perturbations.

only indirectly with the ions via excitation of the electrons. In the above equations we suppress the time argument unless there is an explicit time-dependence (as in the coupling to the laser in $U_{\rm ext}$). The $\boldsymbol{R}_I$ become time-dependent upon solving the system (2.177), (2.178) and enter the TDKS equation via $U_{\rm back}$. Hence, solving the coupled electron-ion system (2.172), (2.177), (2.178) poses an initial value problem. Typically a simulation starts from the ground state of the electron-ion system whose determination is already demanding. Then the $\{\boldsymbol{R}_I(t)\}$ and $\{\varphi_\alpha(\boldsymbol{r},t)\}$ are propagated. If the electrons are treated within LDA the whole procedure is called *time-dependent local density approximation molecular dynamics* (TDLDA-MD). It is still quite demanding because of the very different time scales, meaning that the electrons have to be propagated for many time steps until the ions move appreciably.

In a further step along the approximation chain one may treat the electrons semi-classically (Vlasov-Uehling-Uhlenbeck approach) and describe them by a classical distribution function $f(\boldsymbol{r},\boldsymbol{p})$ which is then sampled by test-particles of, e.g., Gaussian shape. Even simpler is a purely classical MD simulation where both ions and electrons are point-like and follow the classical equations of motion. This MD approach still scales with the square of the number of particles involved so that it is restricted to systems with less than, say, 10000 particles. If binary collisions are negligible, as they are in sufficiently hot plasmas, the so-called *particle-in-cell* (PIC) method can be applied (see below).

2.3.3 Optical properties of clusters

Once the structure of a cluster is determined on may study its *optical properties*, that is, one is interested in the effect of the cluster *on* an incoming electromagnetic wave and the effect of the electromagnetic wave *on* the cluster. In other words, the cluster will disturb the incoming wave upon *scattering* of radiation (which we studied extensively for the case of atoms in Sec. 1.3.16), and the incoming field may modify the cluster. In the simplest case the field just polarizes the cluster and a description within dielectric theory is possible. However, in intense laser fields clusters are "destroyed", which means that laser energy is converted to particle energy. The simulation of such a complicated and multi-faceted interaction between laser radiation and a many-particle system requires advanced numerical methods.

Optical response

The spectrum emitted by a laser irradiated object contains a wealth of information about the structure of the object. From the lines in absorption or emission spectra one infers the energy difference of the levels E_k, E_a involved in the dipole-allowed transition,

$$\hbar\omega_{ka} = E_k - E_a. \tag{2.179}$$

The heights of these peaks are proportional to the corresponding oscillator strengths (cf. Sec. 1.3.13) while their widths are related the decay rates of the states in-

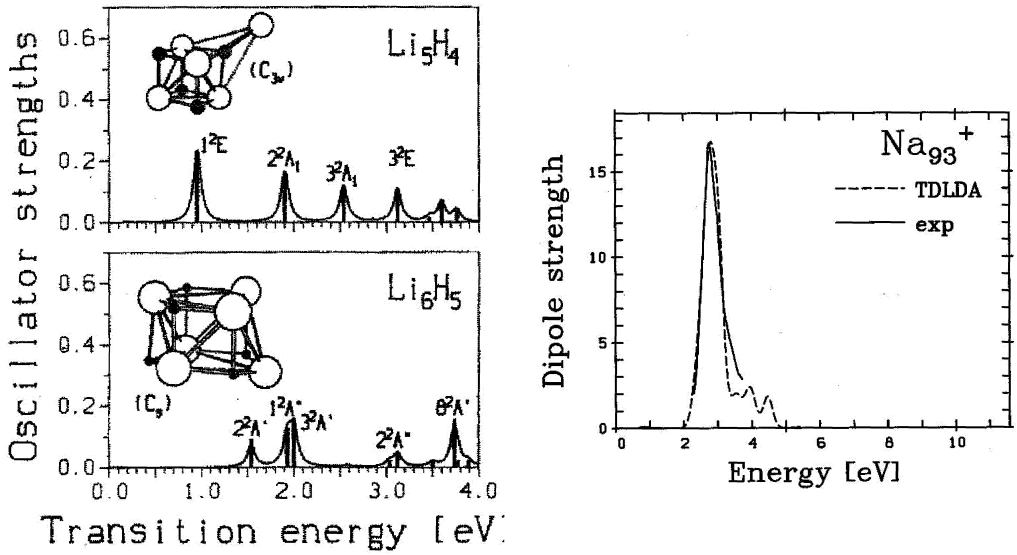

Figure 2.16: Left panel: photo absorption spectra for two Li_nH_{n-1} clusters. Right panel: spectrum for the metal cluster Na_{93}^+ [from P.-G. Reinhard and E. Suraud *Introduction to cluster dynamics* (Wiley, Weinheim, 2004)].

volved. In general, the photoabsorption spectra of small molecules are quite species-dependent as far as the positions of the spectral lines are concerned.

Now, it turns out that this is not the case for alkali metal clusters. Instead of well separated spectral lines one rather observes a broad spectral feature, called the *Mie resonance*, which hardly shifts as a function of the cluster size (see Fig 2.16).

Consider the jellium model of a simple metal cluster from above. If the electron cloud oscillates against the ion jellium background the frequency will be

$$\omega = \sqrt{\frac{C}{M}} \tag{2.180}$$

where the mass M of the electron cloud is

$$M = N_e m \tag{2.181}$$

and C is the "spring constant" due to a restoring force to be determined. The energy of the displaced electron cloud in the jellium potential reads

$$\mathcal{E}(\boldsymbol{r}) = \int \mathrm{d}^3 r'\, n(\boldsymbol{r}') U_{\mathrm{jel}}(\boldsymbol{r} - \boldsymbol{r}') \tag{2.182}$$

and U_{jel} fulfills the Poisson equation

$$\boldsymbol{\nabla}^2 U_{\mathrm{jel}} = 4\pi e^2\, n_0\, \Theta(R - r), \qquad n_0 = \frac{N_e}{\frac{4\pi}{3} R^3}. \tag{2.183}$$

We assume that there are as many positive charges in the ionic background as there are electrons.

As the potential energy stored in a spring elongated along x is $\mathcal{E} = Cx^2/2$ the spring constant governing oscillations along x is obtained as

$$C = \frac{\partial^2 \mathcal{E}}{\partial x^2}. \tag{2.184}$$

For a spherical drop the same holds for y and z. Thus we have

$$3C = \boldsymbol{\nabla}^2 \mathcal{E}|_{\boldsymbol{r}=0} = \int \mathrm{d}^3 r'\, n(\boldsymbol{r}') \boldsymbol{\nabla}^2 U_{\mathrm{jel}}(\boldsymbol{r} - \boldsymbol{r}') \Big|_{\boldsymbol{r}=0} = 4\pi e^2 \int \mathrm{d}^3 r'\, n(\boldsymbol{r}')\, n_0\, \Theta(R - r'). \tag{2.185}$$

Simplifying as much as possible, we also assume that the electron cloud assumes a step profile, i.e.,

$$n(\boldsymbol{r}) = n_0\, \Theta(R - r) \tag{2.186}$$

with the same n_0 as for the ions above. In this case

$$\int \mathrm{d}^3 r'\, n_0^2\, \Theta(R - r') = \frac{4\pi}{3} R^3 n_0^2 \tag{2.187}$$

so that

$$\omega^2 = \frac{C}{M} = \frac{\frac{4\pi e^2}{3} \frac{4\pi}{3} R^3 n_0^2}{N_e m} = \frac{\frac{4\pi e^2}{3} n_0}{m}. \tag{2.188}$$

Hence, we obtain the *Mie plasma frequency*

$$\omega_{\mathrm{Mie}} = \left(\frac{4\pi e^2 n_0}{3m} \right)^{1/2} = \frac{\omega_{\mathrm{p}}}{\sqrt{3}} \tag{2.189}$$

where ω_{p} is the bulk plasma frequency. In terms of the valence v and the Wigner-Seitz radius r_s the Mie plasma frequency assumes the form

$$\omega_{\mathrm{Mie}} = \left(\frac{e^2 v}{m r_s^3} \right)^{1/2}. \tag{2.190}$$

For sodium clusters we have $r_s = 4\, a_0$ and $v = 1$, which yields $\hbar\omega_{\mathrm{Mie}} = 3.4\,\mathrm{eV}$. The experimental spectra, as well as numerically calculated ones using, e.g., time-dependent density functional theory, have the peak at somewhat lower energies (see Fig. 2.16). One reason for this red shift is the *spillout* of electron density, which is not taken into account in (2.186). The spillout

$$\Delta N_e = 4\pi \int_R^\infty \mathrm{d}r\, r^2\, n(r) \tag{2.191}$$

leads to a red-shifted Mie frequency

$$\omega'_{\mathrm{Mie}}{}^2 = \omega_{\mathrm{Mie}}^2 \left(1 - \frac{\Delta N_e}{N_e} \right) \tag{2.192}$$

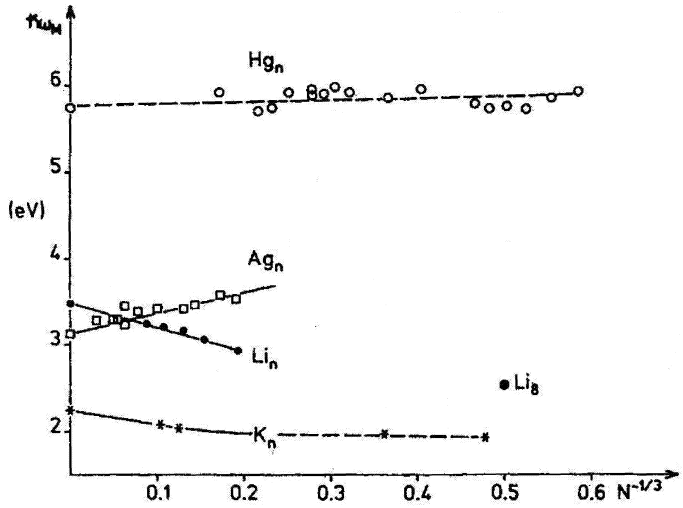

Figure 2.17: Mie plasmon energy vs inverse cluster size for K, Li, Ag, and Hg clusters [from P.-G. Reinhard and E. Suraud *Introduction to cluster dynamics* (Wiley, Weinheim, 2004)].

As the spillout ΔN_e is proportional to the surface area while N_e is proportional to the volume we have

$$\frac{\Delta N_e}{N_e} \sim \frac{R^2}{R^3} = \frac{1}{R} \sim \frac{1}{N_e^{1/3}}. \tag{2.193}$$

We therefore expect an increasing red-shift with decreasing cluster size or, in other words, a negative slope of $\omega'_{\rm Mie}$ when plotted vs $N_e^{-1/3}$. Figure 2.17 shows that this is indeed the case for alkali metal clusters Li_n and K_n. However, the slope for mercury (Hg_n) is flat and the one of Ag_n even positive. This is because of polarization of loosely bound electrons, which counter balances the spillout effect.

How is the Mie plasmon resonance built up from transitions between KS levels? After all, in a quantum description there is nothing like an electron sphere oscillating against an ionic background. Instead, there are single-particle orbitals, occupied and unoccupied levels, and transitions between them. This is illustrated in Fig. 2.18.

In Fig. 2.19d transitions are indicated as vertical lines above the frequency (or energy) axis. Taking into account the oscillator strength for such *one-particle-one-hole-transitions* (1ph) one obtains the spectrum in Fig. 2.19c. Most of the oscillator strength lies in the lowest-energy transitions. Instead, the experimental spectrum in Fig. 2.19a shows nothing there but only a broad Mie resonance. Obviously, 1ph transitions of independent KS electrons in a *frozen* effective groundstate KS potential (also called "bare" KS potential) cannot form a plasmon. On the other hand, there is a group of 1ph transitions in the energy regime where the Mie plasmon is observed, although with negligible oscillator strengths. However, a TDDFT calculation should also take into account the change of the KS potential due to

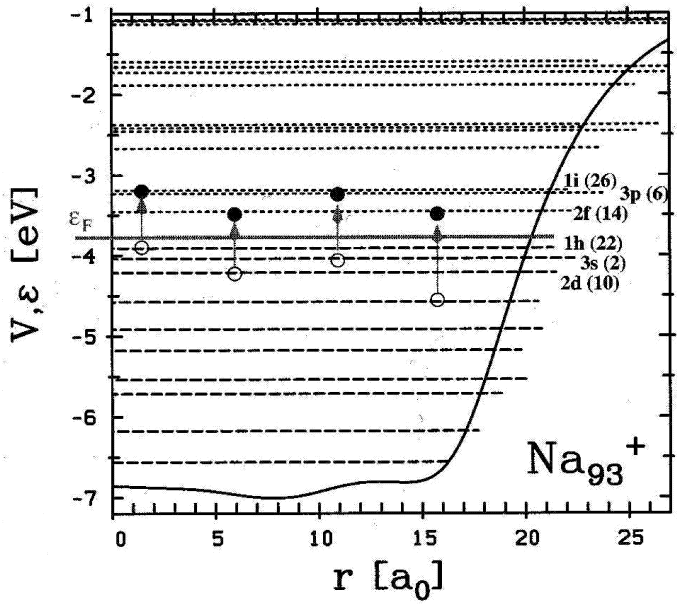

Figure 2.18: Dominant transitions between occupied and unoccupied KS levels for a Na_{93}^{+} cluster (KS potential drawn solid). The occupied levels are drawn dashed, the unoccupied ones dotted. The numbers attached indicate the spectroscopic notation of the level and the multiplicity (number of KS electrons in this level). The strongest 1ph transitions are indicated by arrows. [from P.-G. Reinhard and E. Suraud *Introduction to cluster dynamics* (Wiley, Weinheim, 2004)].

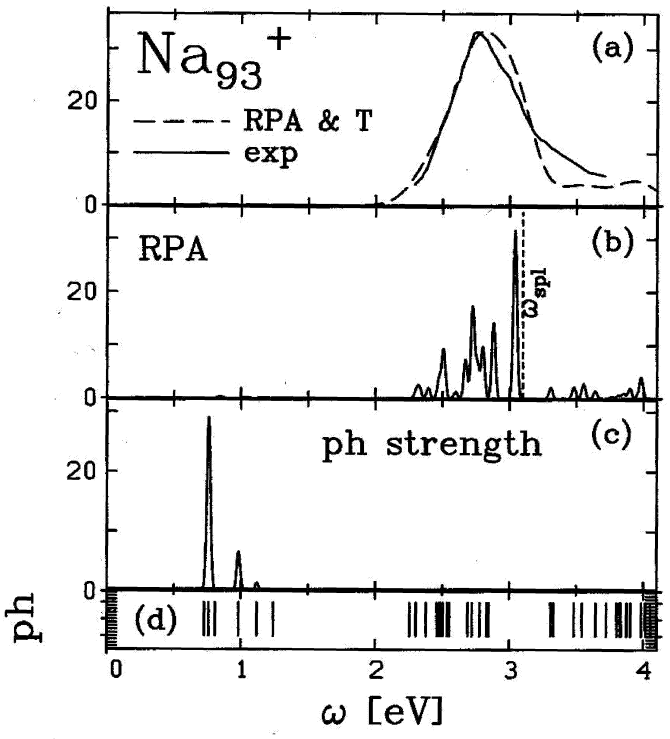

Figure 2.19: Formation of the Mie plasmon. The experimental broad Mie resonance is shown in (a). In panel (d) indicated are the 1ph transition energies, in (c) the corresponding oscillator strengths. In (c) the result of a RPA calculation (linear response) is shown, which, when convoluted with a Gaussian to account for line broadening, is in good agreement with experiment [from P.-G. Reinhard and E. Suraud *Introduction to cluster dynamics* (Wiley, Weinheim, 2004)].

the excitations. In the interacting system this amounts to taking into account the Coulomb-interaction between the electrons. This can be done by linearization of the density-dependent KS Hamiltonian, the result being equivalent to the so-called *random phase approximation* (RPA) of many-body theory. In the DFT community this is just called *linear response*. The result of such a RPA or linear response calculation is shown in Fig. 2.19b. One clearly sees that in RPA oscillator strength is shifted towards the transitions whose energies are around the classical Mie plasmon energy. Finally, thermal and other line-broadening effects can be modeled by convolution of the linear response spectrum in Fig. 2.19b with a Gaussian. The result is shown in Fig. 2.19a, in good agreement with the experimental result.

Chapter 3

Laser plasmas

At an intensity $\simeq 10^{14}\,\mathrm{Wcm}^{-2}$ the outermost electrons of the atoms the target is made of are ripped out by the electric field of the laser. As a consequence the target is quickly turned into a *plasma*, at least at the surface. This, in turn, has consequences for the further pulse propagation. If the plasma is *overdense* ($\omega_\mathrm{p} > \omega$) an electromagnetic wave of frequency ω cannot propagate in it and will be reflected. The interplay between laser pulse propagation and plasma generation is delicate and complex. Obviously, for its description methods going beyond the dipole approximation are necessary, and one has to solve both the equations of motion for the particles and Maxwell's equations self-consistently. Quantum effects are usually neglected in laser plasma simulations while—at very high intensities—relativistic effects have to be taken into account.

The first Section in this Chapter is devoted to the very first step in the interaction scenario, the plasma generation via the electric field of the laser.

3.1 Plasma generation

The Hamiltonian governing an electron moving in a Coulomb potential $-Z/r$ and a static electric field $\boldsymbol{E} = E\boldsymbol{e}_z$ reads (in atomic units, see Appendix A)

$$\hat{H} = \frac{\hat{\boldsymbol{p}}^2}{2} + V_\mathrm{eff}, \qquad V_\mathrm{eff} = -\frac{Z}{r} + Ez. \tag{3.1}$$

The effective potential V_eff describes a tilted Coulomb potential (see Fig. 3.1). A perturbative treatment of the problem can be found in almost all quantum mechanics or atomic physics text books (Stark effect). In first order (linear Stark effect) the degeneracy with respect to the angular quantum number ℓ is removed while the degeneracy in the magnetic quantum number m is maintained. The non-degenerate ground state is only affected in second order (quadratic Stark effect). It is down-shifted in energy since the potential widens in the presence of the field. In the case of the hydrogen atom ($Z = 1$) this down-shift is given by $\Delta\mathcal{E} = -9E^2/4$.

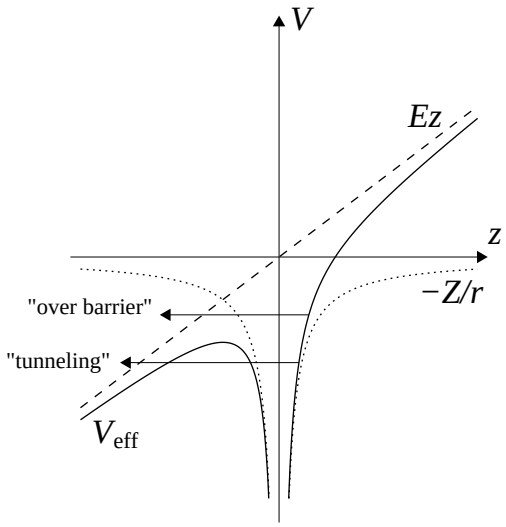

Figure 3.1: Effective potential V_{eff} in field direction. The unperturbed Coulomb potential and the field potential are also shown separately. Depending on the initial (and possibly Stark-shifted) state, the electron may either escape via tunneling or classically via "over-barrier" ionization.

Let us first point out that, strictly speaking, there exist no discrete, bound states anymore even for the tiniest electric field. This is because even a very small field gives rise to a potential barrier (see Fig. 3.1) through which the initially bound electron may tunnel. The electric field couples all bound states to the continuum and thus all discrete states become resonances with a finite line width. Mathematically speaking, the Hamiltonian (3.1) has only a continuous spectrum, and the eigenfunctions are no longer square-integrable. However, since the barrier for small fields is far out, the probability for tunneling is extremely low (note that the tunneling probability decreases exponentially with the distance to be tunneled, as will be shown below) and the states are "quasi-discrete".

A strong increase in the ionization probability is expected when the electron can even escape classically, that is, when the distance to be tunneled shrinks to zero. In a first approximation this so-called "critical field" E_{crit} may be estimated as follows: neglecting the Stark effect, classical over-barrier ionization sets in when the barrier maximum coincides with the energy level of the electron. The position of the barrier is (for $E > 0$) located at

$$z_{\text{barr}} = -\sqrt{\frac{Z}{E}} \tag{3.2}$$

and the energy at the barrier maximum is

$$V_{\text{barr}} = -2\sqrt{ZE}. \tag{3.3}$$

Hence, if we restrict ourselves to the ground state of hydrogen-like ions, we require that

$$\mathcal{E} = -\frac{Z^2}{2} \stackrel{!}{=} -2\sqrt{ZE_{\rm crit}} \tag{3.4}$$

so that

$$E_{\rm crit} = \frac{Z^3}{16}. \tag{3.5}$$

Because of the strong Z-dependence of the critical field even with the most intense lasers available today it is not possible to fully strip heavy elements. In fact, using the above formulas one easily estimates that "naked" ions only up to $Z = 20$ can be achieved even at $10^{22}\,\mathrm{Wcm}^{-2}$.[1] For a hydrogen-like ion of $Z = 20$ the ground state energy is in the 5-keV range, meaning that at 800 nm around 3500 photons must be absorbed in order to remove the last electron. It is obvious that perturbation theory is neither feasible nor adequate in this regime.

3.1.1 *Landau tunneling rate

Going one step beyond a classical over-barrier analysis amounts to take tunneling into account. This can be done in a semi-classical way. Note that the Schrödinger equation with the Hamiltonian (3.1) separates in parabolic coordinates (ξ, η, φ),

$$\xi = r + z, \quad \eta = r - z, \qquad r = \frac{1}{2}(\xi + \eta), \quad z = \frac{1}{2}(\xi - \eta), \qquad 0 \le \xi, \eta. \tag{3.6}$$

Here, r is the radial coordinate, and φ is the azimuthal angle (as in spherical, polar or cylindrical coordinates). Cuts of contours of constant ξ and η in the xz-plane are shown in Fig. 3.2. The Hamiltonian in parabolic coordinates reads

$$\hat{H} = -\frac{2}{\xi + \eta}\left[\partial_\xi(\xi\partial_\xi) + \partial_\eta(\eta\partial_\eta)\right] - \frac{1}{2\xi\eta}\partial_\varphi^2 - \frac{2Z}{\xi + \eta} + E\frac{\xi - \eta}{2}. \tag{3.7}$$

Plugging the ansatz

$$\Psi = f_1(\xi) f_2(\eta) \mathrm{e}^{\mathrm{i}m\varphi} \tag{3.8}$$

into the Schrödinger equation $\mathcal{E}\Psi = \hat{H}\Psi$ and multiplying by $(\xi + \eta)/2$ leads to an equation that can be decoupled into

$$\frac{\mathrm{d}}{\mathrm{d}\xi}\left(\xi\frac{\mathrm{d}f_1}{\mathrm{d}\xi}\right) + \left(\frac{\mathcal{E}}{2}\xi - \frac{m^2}{4\xi} - \frac{E}{4}\xi^2\right) f_1 + Z_1 f_1 = 0, \tag{3.9}$$

$$\frac{\mathrm{d}}{\mathrm{d}\eta}\left(\eta\frac{\mathrm{d}f_2}{\mathrm{d}\eta}\right) + \left(\frac{\mathcal{E}}{2}\eta - \frac{m^2}{4\eta} + \frac{E}{4}\eta^2\right) f_2 + Z_2 f_2 = 0 \tag{3.10}$$

[1] Note that other ionization mechanisms (e.g., collisional ionization or the ionization by electric fields generated in a plasma) may assist in achieving higher charge states than expected from the laser field alone.

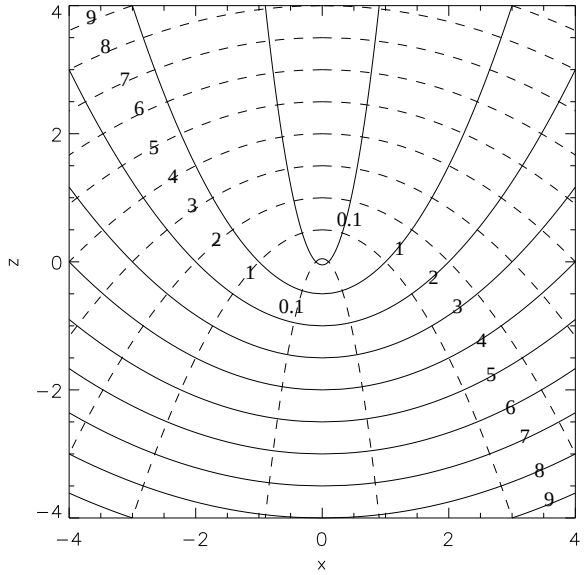

Figure 3.2: Illustration of parabolic coordinates. Cuts of contours $\xi = \text{const}$ (dashed, values given next to the lines) and $\eta = \text{const}$ (solid) in the xz-plane (azimuthal symmetry with respect to the z-axis).

where Z_1, Z_2 are separation constants fulfilling

$$Z_1 + Z_2 = Z. \tag{3.11}$$

Division by 2ξ and 2η, respectively, yields the two Schrödinger equations

$$\left[-\frac{1}{2}\left(\frac{\mathrm{d}^2}{\mathrm{d}\xi^2} + \frac{1}{\xi}\frac{\mathrm{d}}{\mathrm{d}\xi} - \frac{m^2}{4\xi^2}\right) - \frac{Z_1}{2\xi} + \frac{E}{8}\xi\right] f_1 = \frac{\mathcal{E}}{4} f_1, \tag{3.12}$$

$$\left[-\frac{1}{2}\left(\frac{\mathrm{d}^2}{\mathrm{d}\eta^2} + \frac{1}{\eta}\frac{\mathrm{d}}{\mathrm{d}\eta} - \frac{m^2}{4\eta^2}\right) - \frac{Z_2}{2\eta} - \frac{E}{8}\eta\right] f_2 = \frac{\mathcal{E}}{4} f_2 \tag{3.13}$$

which have the same shape as two Schrödinger equations in cylindrical coordinates for the potentials

$$V_\xi = -\frac{Z_1}{2\xi} + \frac{E}{8}\xi, \qquad V_\eta = -\frac{Z_2}{2\eta} - \frac{E}{8}\eta. \tag{3.14}$$

Both potentials have a Coulombic part and a linear contribution, like V_{eff} in (3.1). However, because $\xi, \eta \geq 0$, the potential V_ξ has only bound states (we assume without loss of generality $E > 0$). The potential V_η instead displays a barrier. Hence, in parabolic coordinates ionization happens with respect to the η coordinate while the electron remains confined in ξ. The consequences of this in Cartesian coordinates can be understood with the help of Fig. 3.2: confinement to a region $\xi < \xi_{\max}$ implies preferred electron emission towards negative z with a lateral spread

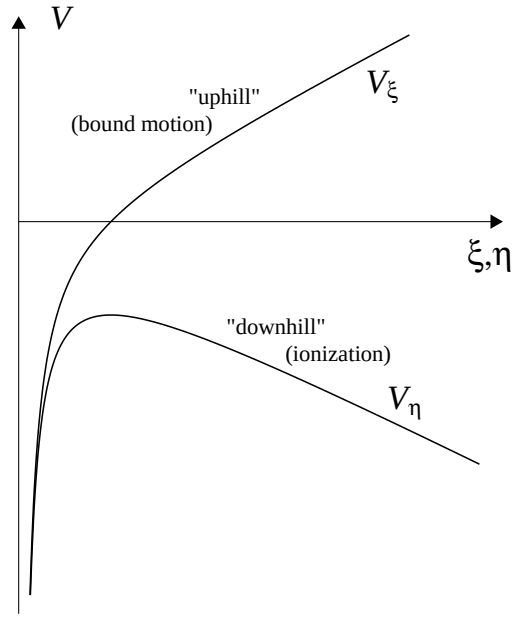

Figure 3.3: Illustration of the potentials V_ξ and V_η [Eqs. (3.14)]. The "uphill potential" V_ξ (for $E > 0$) supports only bound states while the "downhill potential" V_η displays a barrier through which the electron may tunnel.

that can be estimated by the confining contour $\xi_{\max}$. The potentials V_ξ and V_η are called "uphill" and "downhill potential," respectively. They are illustrated in Fig. 3.3. Given an energy $\mathcal{E}$ one finds a sequence of Z_1 for which the solution of the Schrödinger equation in ξ, Eq. (3.12), leads to normalizable bound states. This sequence can be labeled by the number of nodes in f_1 for $\xi > 0$, $n_1 = 0, 1, 2, \ldots$ (note that $Z_1 < 0$ is also possible). The second equation (3.13) has to be solved for $Z_2 = Z - Z_1$ and the same energy $\mathcal{E}$. This is possible because the corresponding Hamiltonian $\hat{H}_\eta$ [i.e., the square bracket in (3.13)] has a continuous spectrum and is neither bound from below nor from above.

In the field-free case $E = 0$ the two Schrödinger equations (3.12) and (3.13) are identical, and the relation between the "usual" principal quantum number n and the parabolic quantum numbers n_1, n_2 is given by

$$n_i + \frac{|m| + 1}{2} = n\frac{Z_i}{Z}, \qquad n_1 + n_2 + |m| + 1 = n, \qquad i = 1, 2. \tag{3.15}$$

Let us consider the tunneling of the electron in atomic hydrogen through the barrier of the "downhill potential" in Fig. 3.3. We assume that the electron is initially in the 1s ground state. The Schrödinger equation (3.13) for $m = 0$, $Z_2 = 1/2$, $\mathcal{E} = -1/2$ reads

$$\left[-\frac{1}{2}\left(\frac{\mathrm{d}^2}{\mathrm{d}\eta^2} + \frac{1}{\eta}\frac{\mathrm{d}}{\mathrm{d}\eta}\right) - \frac{1}{4\eta} - \frac{E}{8}\eta\right] f_2(\eta) \;=\; -\frac{1}{8} f_2(\eta). \tag{3.16}$$

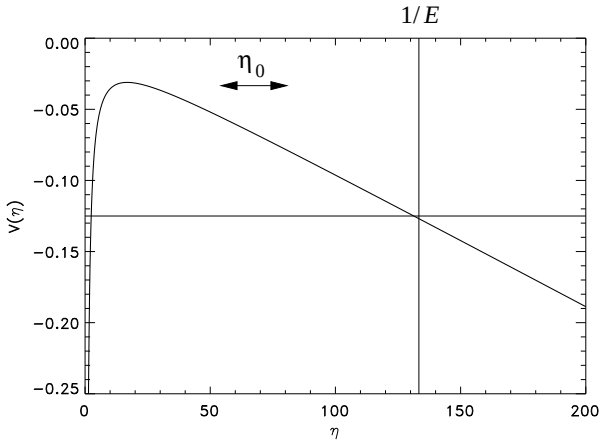

Figure 3.4: Plot of the potential $V(\eta)$ [Eq. (3.19)] for $E = 0.0075$. The tunnel "exit" η_1 for sufficiently low fields E is in good approximation given by $\eta_1 \simeq 1/E$. The matching point η_0 is located inside the barrier where $1 \ll \eta_0 \ll 1/E$ holds.

Substituting $\chi(\eta) = \sqrt{\eta} f_2(\eta)$ yields

$$\frac{\mathrm{d}^2\chi}{\mathrm{d}\eta^2} + \left(-\frac{1}{4} + \frac{1}{2\eta} + \frac{1}{4\eta^2} + \frac{1}{4}E\eta\right)\chi = 0. \tag{3.17}$$

Comparison with

$$-\frac{1}{2}\frac{\mathrm{d}^2\chi}{\mathrm{d}\eta^2} + V(\eta)\chi = \epsilon\chi \tag{3.18}$$

shows that we effectively deal with one-dimensional motion of an electron in the potential

$$V(\eta) = -\frac{1}{2}\left(\frac{1}{2\eta} + \frac{1}{4\eta^2} + \frac{1}{4}E\eta\right) \tag{3.19}$$

with total energy $\epsilon = -1/8$. The potential $V(\eta)$ is of the form depicted in Fig. 3.4. We now match at a position η_0 inside the barrier,

$$1 \ll \eta_0 \ll 1/E \tag{3.20}$$

the "left" quasi-classical wave function

$$\chi_{\mathrm{left}}(\eta) = -\frac{\mathrm{i}C}{\sqrt{|p|}} \exp\left(\left|\int_{\eta_0}^{\eta} p(\eta')\,\mathrm{d}\eta'\right|\right) \tag{3.21}$$

with the "right" quasi-classical outgoing wave function

$$\chi_{\mathrm{right}}(\eta) = \frac{C}{\sqrt{p}} \exp\left(\mathrm{i}\int_{\eta_0}^{\eta} p(\eta')\,\mathrm{d}\eta' + \mathrm{i}\pi/4\right) \tag{3.22}$$

where

$$p(\eta) = \sqrt{2[\epsilon - V(\eta)]} = \sqrt{-\frac{1}{4} + \frac{1}{2\eta} + \frac{1}{4\eta^2} + \frac{1}{4}E\eta}. \tag{3.23}$$

The semi-classical approximation breaks down at the classical turning point $\eta_1 \simeq 1/E$ since $p(\eta_1) = 0$. In general, semi-classical wave functions are accurate as long as the de Broglie wave length $2\pi\hbar/p$ is small compared to the length scale characterizing changes in the potential (i.e., the potential should be sufficiently "flat"). For vanishing momentum p the de Broglie wave length is infinite so that the semi-classical approximation necessarily breaks down. However, for the calculation of the probability flux out of the potential the disagreement between the semi-classical wave function and the exact wave function in a narrow region around the classical turning point η_1 plays no role.

For the determination of the normalization constant C we set the left wave function at position η_0 equal to the unperturbed wave function so that

$$-\frac{\mathrm{i}C}{\sqrt{|p_0|}} = \sqrt{\eta_0}\frac{1}{\sqrt{\pi}}\mathrm{e}^{-(\xi+\eta_0)/2} \tag{3.24}$$

with $p_0 = p(\eta_0)$. The "uphill" coordinate ξ appears as a parameter here which will be integrated out later on; in other words: the wave function is assumed to retain its ground state shape with respect to ξ (i.e., the Stark effect is neglected). We obtain for the right wave function

$$\chi_{\mathrm{right}}(\eta,\xi) = \mathrm{i}\sqrt{\frac{\eta_0|p_0|}{\pi p(\eta)}}\mathrm{e}^{-(\xi+\eta_0)/2}\exp\left(\mathrm{i}\int_{\eta_0}^{\eta} p(\eta')\,\mathrm{d}\eta' + \mathrm{i}\pi/4\right) \tag{3.25}$$

so that

$$|\chi_{\mathrm{right}}(\eta,\xi)|^2 = \frac{\eta_0|p_0|}{\pi p(\eta)}\exp\left(-\xi - \eta_0 + 2\Re\left[\mathrm{i}\int_{\eta_0}^{\eta} p(\eta')\,\mathrm{d}\eta'\right]\right) \tag{3.26}$$

where $\Re$ denotes the real part. Because of (3.20) we can expand $p(\eta)$ in $\varepsilon = 1/\eta$,

$$p(\eta) = \begin{cases} \frac{1}{2}\left(\sqrt{E\eta - 1} + \frac{1}{\eta\sqrt{E\eta-1}} + \cdots\right) & \text{outside barrier, } \eta > \eta_1 \\ \frac{1}{2}\left(\mathrm{i}\sqrt{1 - E\eta} + \frac{1}{\mathrm{i}\eta\sqrt{1-E\eta}} + \cdots\right) & \text{inside barrier, } \eta < \eta_1 \end{cases}. \tag{3.27}$$

Since $E\eta_0 \ll 1$, it is sufficient to take $|p_0| = 1/2$. In order to keep the leading terms dependent on E in the prefactor as well as in the exponent, we set in the denominator of the prefactor in (3.26) $p(\eta) = (\sqrt{E\eta - 1})/2$. In the exponent we integrate inside the barrier and have to keep both terms in the expansion (3.27). We thus obtain

$$\begin{aligned} |\chi_{\mathrm{right}}(\eta,\xi)|^2 &= \frac{\eta_0}{\pi\sqrt{E\eta-1}}\mathrm{e}^{-(\xi+\eta_0)} \\ &\quad \times \exp\left(-\int_{\eta_0}^{\eta_1}\left[\sqrt{E\eta-1} - \frac{1}{\eta\sqrt{E\eta-1}}\right]\mathrm{d}\eta\right). \end{aligned} \tag{3.28}$$

The integral can be solved. Using $\eta_1 \simeq 1/E$ and $\eta_0 E \ll 1$ we obtain for the probability density outside the barrier

$$|\chi_{\text{right}}(\eta,\xi)|^2 = \frac{4\,\mathrm{e}^{-\xi}}{\pi E\sqrt{E\eta-1}}\,\mathrm{e}^{-2/(3E)}. \tag{3.29}$$

The total probability current through a plane perpendicular to the z-axis is

$$\Gamma = \int_0^\infty |f_1(\xi)f_2(\eta)|^2 v_z 2\pi\rho\,\mathrm{d}\rho \tag{3.30}$$

where $f_1(\xi)$, $f_2(\eta)$ are the wave functions introduced in (3.8), v_z is the velocity in z-direction and ρ is the radial cylindrical coordinate. The ξ-dependent part $|f_1|^2$ is included in $|\chi_{\text{right}}(\eta,\xi)|^2$ so that

$$\Gamma = \int_0^\infty \frac{|\chi_{\text{right}}(\eta,\xi)|^2}{\eta} v_z 2\pi\rho\,\mathrm{d}\rho. \tag{3.31}$$

With $z = (\xi-\eta)/2 \simeq -\eta/2$ for small ξ and large η, we estimate for v_z

$$-\frac{1}{2} = \frac{1}{2}v_z^2 + Ez \simeq \frac{1}{2}v_z^2 - \frac{1}{2}E\eta \qquad \Rightarrow \qquad v_z \simeq \sqrt{E\eta-1} \tag{3.32}$$

so that

$$\Gamma = \int_0^\infty \frac{|\chi_{\text{right}}(\eta,\xi)|^2}{\eta}\sqrt{E\eta-1}\;2\pi\rho\,\mathrm{d}\rho. \tag{3.33}$$

Finally, with

$$\rho = \sqrt{\xi\eta} \qquad \Rightarrow \qquad \mathrm{d}\rho = \mathrm{d}\sqrt{\xi\eta} = \frac{1}{2}\frac{\eta}{\sqrt{\xi\eta}}\mathrm{d}\xi + \frac{1}{2}\frac{\xi}{\sqrt{\xi\eta}}\mathrm{d}\eta \simeq \frac{1}{2}\sqrt{\frac{\eta}{\xi}}\,\mathrm{d}\xi \tag{3.34}$$

(where the last step again follows from $\eta \gg \xi$) we arrive at

$$\Gamma = \int_0^\infty \frac{|\chi_{\text{right}}(\eta,\xi)|^2}{\eta}\sqrt{E\eta-1}\;2\pi\sqrt{\xi\eta}\frac{1}{2}\sqrt{\frac{\eta}{\xi}}\,\mathrm{d}\xi = \int_0^\infty \frac{4}{E}\,\mathrm{e}^{-2/(3E)}\,\mathrm{e}^{-\xi}\mathrm{d}\xi$$

so that

$$\Gamma = \frac{4}{E}\,\mathrm{e}^{-2/(3E)}. \tag{3.35}$$

This is the Landau-rate for tunneling ionization of atomic hydrogen from the ground state. The Landau-rate is exact in the limit of low field strengths E while it overestimates ionization as the over-barrier field strength is approached. Figure 3.5 shows the rate Γ vs the field strength E.

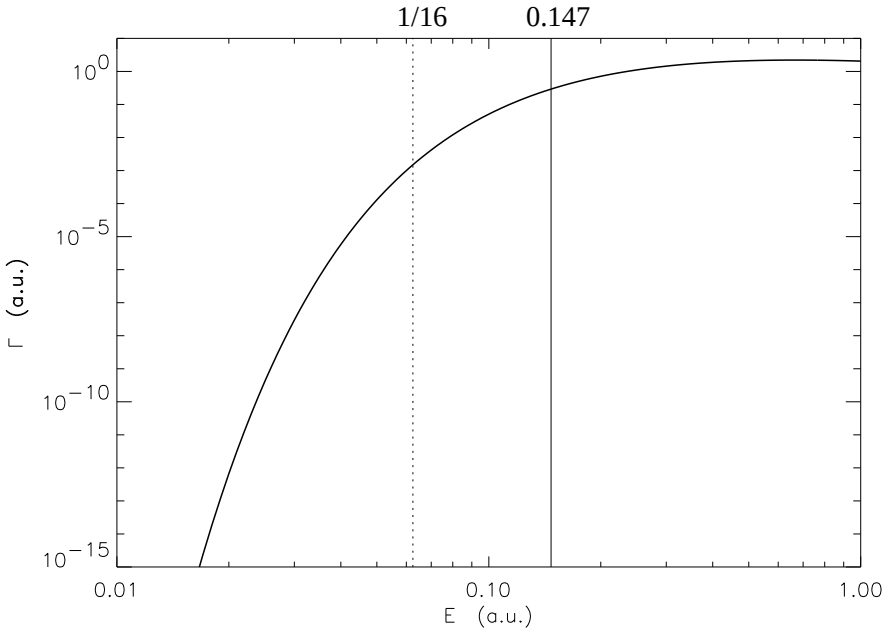

Figure 3.5: The Landau-rate (3.35) vs field strength E. The vertical dashed line indicates the over-barrier field strength (3.5).

3.1.2 *Tunneling *vs* multiphoton ionization

There are at least three different energy scales (and the related time scales) in the physics of atoms in strong laser fields: (i) the ionization potential $\mathcal{E}_{\rm ip} = |\mathcal{E}|$, (ii) the photon energy ω, and (iii) the ponderomotive energy $U_{\rm p}$. The pulse duration may introduce an additional laser-related time-scale while the energy spectrum of the atom, through typical transitions, could introduce an additional species-related time-scale. If one ignores the two latter parameters, the atomic species enter through $\mathcal{E}_{\rm ip}$ only.

In case $\omega > \mathcal{E}_{\rm ip} \gg U_{\rm p}$ or $\mathcal{E}_{\rm ip} > \omega \gg U_{\rm p}$ perturbation theory in lowest nonvanishing order (LOPT) can be applied. In contrast, when with the increasing laser intensity the regime $\mathcal{E}_{\rm ip} > U_{\rm p} > \omega$ is reached, non-perturbative effects such as above-threshold ionization (ATI) and channel-closings take place. This regime is commonly referred to as (nonperturbative) multiphoton ionization (MPI). Finally, increasing the intensity further (or decreasing the photon energy) one arrives at $U_{\rm p} > \mathcal{E}_{\rm ip} > \omega$. Translated into the time-domain this implies that both the inner-atomic time-scale and the ionization dynamics are fast with respect to a laser period. If this is the case, a quasi static field ionization picture may be applied where, at the instant of ionization t', the electron moves in an effective potential which is the sum of the Coulomb (or effective core) potential and the instantaneous potential of the laser, as depicted in Fig. 3.1. If the field reaches the critical field estimated above, the electron may escape even classically over the barrier.

*Keldysh parameter

The Keldysh parameter γ can be interpreted as the ratio of the "tunneling time" and the laser period. In semi-classical WKB theory and a simplified 1D-point-of-view where one considers only the tunneling along the polarization axis the time to tunnel through a static Coulomb barrier is

$$T_{\text{tunnel}} \simeq \int_0^{z_{\text{exit}}} \frac{\mathrm{d}z}{|p(z)|} = \int_0^{\kappa^2/2E} \frac{\mathrm{d}z}{\sqrt{\kappa^2 - 2Ez}} = \frac{\kappa}{E} \tag{3.36}$$

with $\kappa = \sqrt{2\mathcal{E}_{\text{ip}}}$.

The Keldysh parameter is

$$\gamma = \omega T_{\text{tunnel}} = \frac{\omega\kappa}{E} = \sqrt{\frac{\mathcal{E}_{\text{ip}}}{2U_{\text{p}}}} \tag{3.37}$$

and, hence, indicates whether the tunneling process is fast on the inneratomic time scale ($\gamma < 1$, tunneling ionization) or the laser field reverses sign before the tunneling is completed ($\gamma > 1$, MPI). Besides $\gamma < 1$ also $\mathcal{E}_{\text{ip}}/\omega \gg 1$ must be satisfied (i.e., very many photons are involved in the tunneling process) to render the semi-classical tunneling approach applicable. Moreover, for higher and higher field amplitude (and thus decreasing γ) one sooner or later enters the BSI regime. Extrapolating tunneling rate formulas to the BSI usually overestimates the ionization rate. By increasing the field strength or decreasing the laser frequency one also approaches the relativistic regime where $U_{\text{p}} \simeq mc^2$ or greater. However, just because the laser driven *free* electron dynamics is relativistic does not mean that relativistic corrections are already important for the *tunneling* dynamics. Relativistic and QED corrections to the binding energy $\mathcal{E}$ because of a high nuclear charge Z have to be taken into account, of course.

Numerous strong laser-atom experiments operate around $\gamma \simeq 1$ or at $\gamma > 1$ and are thus not in the tunneling domain. Taking, for instance, the case of atomic hydrogen in an 800 nm and $10^{14}\,\text{W/cm}^2$ laser pulse one finds $\gamma \simeq 1.1$. This is a typical value for ATI measurements.

What are the differences between the ionization dynamics in the MPI and in the tunneling domain? Since in the tunneling regime the process is fast compared to a laser period, significant ionization occurs during a single half laser cycle, predominantly around the electric field maximum because the barrier is lowest then. Furthermore, in tunneling ionization the quiver amplitude E/ω^2 of the freed electron in the laser field is large compared to the atomic dimension, unlike in MPI. This has consequences for the rescattering dynamics that is responsible for various effects, such as the ATI plateau, high-harmonic generation, and nonsequential ionization.

Appendix A

Atomic units

One atomic unit of		Value
mass	m_e	$9.1094 \cdot 10^{-31}\mathrm{kg}$
length	$\frac{\hbar^2 4\pi\varepsilon_0}{e^2 m_\mathrm{e}} = a_0$	$0.5292 \cdot 10^{-10}\mathrm{m}$
time	$\frac{\hbar^3 (4\pi\varepsilon_0)^2}{m_\mathrm{e} e^4}$	$2.4189 \cdot 10^{-17}\mathrm{s}$
charge	e	$1.6022 \cdot 10^{-19}\mathrm{C}$
action	$\hbar$	$1.0546 \cdot 10^{-34}\mathrm{J}$
permittivity	$4\pi\varepsilon_0$	$4\pi \cdot 8.8542 \cdot 10^{-12}\mathrm{CV^{-1}m^{-1}}$
energy	$\frac{m_\mathrm{e} e^4}{\hbar^2 (4\pi\varepsilon_0)^2}$	$4.3598 \cdot 10^{-19}\mathrm{J} = 27.21\,\mathrm{eV}$
velocity	$\frac{e^2}{\hbar 4\pi\varepsilon_0}$	$2.1877 \cdot 10^{6}\mathrm{ms^{-1}} = \alpha c$
el. field	$\frac{m_\mathrm{e}^2 e^5}{\hbar^4 (4\pi\varepsilon_0)^3}$	$5.1422 \cdot 10^{11}\mathrm{Vm^{-1}}$
magn. flux density	$\frac{m_\mathrm{e}^2 e^3}{\hbar^3 (4\pi\varepsilon_0)^2}$	$2.3505 \cdot 10^{5}\mathrm{T}$
laser intensity	$\frac{e^{12} m_\mathrm{e}^4}{8\pi\alpha\hbar^9 (4\pi\varepsilon_0)^6}$	$3.5095 \cdot 10^{20}\mathrm{Wm^{-2}}$